

ULTRASOUND-TRIGGERED DRUG DELIVERY USING ACOUSTIC DROPLET VAPORIZATION

by

Mario Leonardo Fabilli

A dissertation submitted in partial fulfillment
of the requirements for the degree of
Doctor of Philosophy
(Biomedical Engineering)
in The University of Michigan
2010

Doctoral Committee:

Professor J. Brian Fowlkes, Chair
Professor Paul L. Carson
Associate Professor Joseph L. Bull
Assistant Professor Omolola Eniola-Adefeso
Research Assistant Professor Oliver D. Kripfgans

Brick walls are there for a reason. The brick walls are not there to keep us out. The brick walls are there to give us a chance to show how badly we want something. Because the brick walls are there to stop the people who don't want it badly enough.

RANDY PAUSCH (1960-2008)

© Mario Leonardo Fabilli

All rights reserved
2010

For my family

ACKNOWLEDGMENTS

To quote one of my favorite literary giants, Dave Barry¹:

There are a number of people without whom I could not have written this [dissertation], but I hope you don't hold that against them. They are all fine people, and they had no idea how it would turn out.

But on a more serious note, I am grateful to my doctoral committee - Drs. Brian Fowlkes, Paul Carson, Oliver Kripfgans, Joe Bull, and Lola Eniola-Adefeso - for their scientific guidance, advice, and criticism. I am especially thankful for my mentors within the Basic Radiological Sciences (BRS) Ultrasound group, who wholeheartedly (and without the blink of an eye) welcomed me back into the lab when I decided to return for my doctorate. Dr. Fowlkes, my advisor, has been an outstanding mentor who has deepened my scientific thinking with his pragmatic and reductionist approach to the most complicated problems. His *modus operandi*, the 'get your ducks in a row' attitude, is powerfully simple yet effective in solving technical and non-technical challenges. His knowledge, support, and leadership - coupled with his passion for scientific research - made my doctoral journey truly enjoyable. I would like to thank Dr. Carson for his visionary and unconventional outlook within the research landscape. His ability to form new, cross-disciplinary ideas is inspirational and his perspective on life is refreshing. I am also fortunate for Dr. Kripfgans, whose research captivated me as a sophomore undergraduate student. His motivation, encouragement, willingness to devote his time at a moment's notice, and his endless

¹D. Barry, *Dave Barry Does Japan*. New York, NY: The Random House Ballantine Publishing Group, 1992.

supply of occasionally funny jokes are thankfully appreciated.

There are many other individuals within the BRS group that have been instrumental during my studies and who are integral parts of the BRS family. I would like to thank Dr. Jerry LeCarpentier for his many thought-provoking, philosophical, and feline-related discussions, as well as Dr. Scott Swanson for providing invaluable feedback and guidance concerning matters of chemistry. Drs. Douglas Miller and Chunyan Dou patiently taught me the meticulous methods involved in culturing cells. My former labmate, Dr. Kevin Haworth, was such a great person to work with and a huge help when tackling experiments and theory. Based on our ability to pack up the lab during our move from the Kresge III building to the Medical Sciences I building, we will always have fallback careers if needed. I would also like to thank Drs. Michael Richards, Man Zhang, Frederic Padilla, and Xueding Wang for their helpful support and many conversations during my studies. I am also thankful for Dr. Sumedha Sinha's wit, not to mention her constant supply of chocolates, and Fong Ming Hooi's cheerful optimism. Dr. Kim Ives has been an indispensable member of our scientific team during *in vivo* experiments. Carol Cribbins and Sharon Karahan have provided excellent administrative support. I am thankful for the opportunity to mentor and teach undergraduate students who have worked in our lab - Ian Sebastian, Nasir Fakhri, and James Lee. Hopefully they aren't too traumatized to pursue additional research opportunities in the future.

I would like to thank collaborators outside of the BRS group, such as Drs. Jonathan Rubin and William Roberts, who provided much clinical, scientific, and mathematical insight with my work. Dr. Xiao Shao was very supportive and accommodating during the organic synthesis reactions. Dr. Morand Piert, who served on my committee during my qualifying exam, and Dr. Phillip Sherman were pivotal in furthering the drug release studies *in vivo*. I appreciated Dr. Tim Hall's advice on the mental aspects of completing a doctorate. Furthermore, I am grateful

for the partnerships that have developed with the members of Dr. Bull's group: Dr. Stan Samuel, David Lee, Robinson Seda, and Harm Nieuwstadt. A big *thank you* to Maria Steele in the Department of Biomedical Engineering for facilitating my entry into the doctoral program and providing prompt administrative support throughout my studies. I am also thankful for the outstanding and motivating mentors I had while working at Pfizer, especially Drs. Steve Arrivo, Fred LaPlant, and Michael Pelletier. I learned a great deal from them.

Finally, I would like to thank my family for their love, support, craziness, and endless supply of delicious food. Most especially, I would like to thank my parents, Franca and Leonardo, for being my first teachers. Their loving encouragement means everything to me and my life's successes would have been impossible without them. I am grateful for Franco, my brother, who has been a close friend to me throughout my entire life, not to mention a chemistry and materials science consulting source. I would like to thank my furry friends, Lucy and Oscar, for instilling a sense of sanity and peace in my life. Lastly, I am extremely blessed to have my wife, Marta. She has been with me through all of the joys and frustrations of this doctoral journey, and more importantly, through all of life's ups and downs. She is a source of strength and motivation for me

Ann Arbor, Michigan

September 2010

TABLE OF CONTENTS

DEDICATION	ii
ACKNOWLEDGMENTS	iii
LIST OF FIGURES	ix
LIST OF TABLES	xvi
LIST OF ACRONYMS	xviii
LIST OF SYMBOLS	xx
ABSTRACT	xxi
CHAPTER	
I. Introduction	1
1.1 The Magic Bullet	1
1.2 An Overview of Targeted Drug Delivery	2
1.2.1 Pharmaceutical Approaches	3
1.2.2 Ultrasound Modulated Systems	5
1.3 Colloids used in Diagnostic and Therapeutic Ultrasound	7
1.3.1 Microbubble Agents	7
1.3.2 Perfluorocarbon Emulsions	10
1.3.3 Acoustic Droplet Vaporization	12
1.4 Overview of Dissertation	14
II. The Role of Inertial Cavitation in Acoustic Droplet Vaporization	25
2.1 Introduction	25
2.2 Materials and Methods	28
2.2.1 PFC Droplets	28
2.2.2 Experimental Setup	29
2.2.3 ADV and IC Data Analysis	31
2.2.4 ADV and IC Threshold Determination	35
2.3 Results and Discussion	37

2.3.1	Bulk Fluid Parameters	37
2.3.2	Droplet Parameters	39
2.3.3	Acoustic Parameters	44
2.4	Conclusions	47
2.5	Acknowledgments	50
III.	Delivery of Chlorambucil using an Acoustically-Triggered, Perfluoropentane Emulsion	55
3.1	Introduction	55
3.2	Materials and Methods	57
3.2.1	Emulsion preparation	57
3.2.2	Optical characterization of the emulsions	58
3.2.3	ADV threshold measurements	58
3.2.4	Evaluation of CHL loading in emulsion	59
3.2.5	Cytotoxicity of CHL in solution	60
3.2.6	Ultrasound triggering of CHL-loaded emulsion	61
3.2.7	ADV efficiency	64
3.3	Results	64
3.3.1	Emulsion characterization	64
3.3.2	CHL cytotoxicity on CHO cells	69
3.3.3	Ultrasound triggering of the CHL-loaded emulsion	70
3.3.4	ADV efficiency	74
3.4	Discussion	76
3.5	Conclusions	80
3.6	Acknowledgments	80
IV.	Delivery of Water-Soluble Drugs using Acoustically-Triggered, Perfluorocarbon Double Emulsions	86
4.1	Introduction	86
4.2	Materials and Methods	89
4.2.1	Fluorosurfactant synthesis	89
4.2.2	Fluorescein emulsion preparation	90
4.2.3	Thrombin emulsion preparation	91
4.2.4	Physical characterization of emulsions	92
4.2.5	Encapsulation efficiency of fluorescein emulsions	93
4.2.6	<i>In vitro</i> fluorescein release	93
4.2.7	Encapsulation efficiency and stability of thrombin emulsions	95
4.2.8	<i>In vitro</i> thrombin release	95
4.2.9	Statistical analysis	97
4.3	Results	98
4.3.1	Physiochemical characterization of fluorescein emulsions	98
4.3.2	<i>In vitro</i> release of fluorescein	98
4.3.3	Physiochemical characterization of thrombin emulsions	100
4.3.4	Formulation parameters affecting thrombin activity	101
4.3.5	<i>In vitro</i> release of thrombin	103

4.4	Discussion	106
4.5	Conclusions	110
4.6	Acknowledgments	111
V.	Conclusions and Future Work	119
5.1	Introduction	119
5.2	Experimental Conclusion	120
5.2.1	The Role of Inertial Cavitation in Acoustic Droplet Vaporization	120
5.2.2	Delivery of Chlorambucil using an Acoustically-Triggered, Perfluoropentane Emulsion	122
5.2.3	Delivery of Water-Soluble Drugs using Acoustically-Triggered, Perfluorocarbon Double Emulsions	123
5.3	Summary of Contributions	125
5.4	Future Work	126
5.4.1	Optimization of PFC Loading in Emulsions	126
5.4.2	PFC Emulsion Bioeffects	131
5.4.3	ADV Bioeffects	135
5.4.4	The Mechanism of Drug Release during ADV	137
5.4.5	Shell Modifications	139
5.4.6	Further Formulation Studies	140
5.4.7	<i>In vivo</i> Demonstration	144
5.4.8	Delivery of Prodrugs	145
5.5	Acknowledgments	146

LIST OF FIGURES

Figure	
1.1	Drug loading strategies for a lipid-coated, PFC microbubble. 10
2.1	Side (left) and top (right) views of the <i>in vitro</i> setup used for measuring ADV and IC in flow. A 3.5 MHz single element transducer vaporized the flowing droplets while a 10 MHz linear array recorded cine-loops; IC noise was simultaneously detected using the hydrophone. 30
2.2	Left: MEP as a function of time for four different regions: US off (region 1); US on but no bubbles in the linear array field of view (FOV) (region 2); US on and the initial wave of bubbles appears in the linear array FOV, prior to achieving a steady state (region 3); US on with a steady state number of bubbles in the linear array FOV (region 4). Right: B-mode frames (compressed intensity scale) of a flow tube in region 1 (top) and region 4 (bottom). The exterior boundary of the region of interest used to calculate the MEP is denoted as a white, dashed circle. 33
2.3	Left: RF data of a segment with and without IC. Right: Fourier transforms of RF data from left, showing the large spectral differences between a segment with and without IC. The following conditions were used: degassed water at 37°C with albumin-coated PFP droplets, 83 Hz PRF, 13 cycles, and 6.2 MPa. 34
2.4	The effect of varying the number of standard deviations - $\sigma(IFT_{degas,P})$ - on the calculated peak rarefactional pressure IC threshold. Refer to Eq. 2.3 for the criterion used to determine the presence of IC in an RF segment. The average (n = 3) IC thresholds, plotted with the respective standard deviations, are from the following experimental conditions: degassed water at 37°C with albumin-coated PFP droplets, 83 Hz PRF, and 13 cycles. 35

2.5	Mean ($n = 6$) normalized MEP and IC data plotted along with the respective sigmoidal curve fits and standard deviation at each data point. The raw MEP data was normalized - vertically shifted by 10^{-4} and scaled by 10^5 - to facilitate display on this plot. The threshold for each curve is denoted by an asterisk (*). The following conditions were used: degassed water at 37°C with albumin-coated PFP droplets, 83 Hz PRF, and 13 cycles.	36
2.6	Mean ($n = 5$) ADV and IC thresholds, plotted with standard deviations, for PFP and PFH droplets as a function of degree of superheat. The points denoted with asterisks (*) are cases where IC was measured 11°C or 19°C below the boiling point of PFP or PFH, respectively - though no corresponding increase in MEP was recorded. The following conditions were used: degassed water with albumin-coated droplets, 83 Hz PRF, and 13 cycles.	41
2.7	Left: Mean ($n = 3$) ADV thresholds and IC thresholds, plotted with standard deviations, for albumin-coated PFP droplets of various mean diameters. The points denoted with an asterisk (*) are lipid-coated droplets, whereas the other points are albumin-coated droplets. The following conditions were used: degassed water at 37°C , 83 Hz PRF, and 13 cycles. Right: Increase in mean droplet diameter over time (i.e. since day of manufacturing) for albumin-coated PFP droplets. All droplets used in this study were manufactured on the same day and stored at 5°C throughout the study. Each data point, plotted with the standard deviation, is the average of three vials.	43
2.8	Mean ($n = 5$) ADV and IC threshold, plotted with standard deviations, for various PRFs. The following conditions were used: degassed water at 37°C and 13 cycles. By comparison, the rate at which a new volume of fluid crossed the -6 dB beam width of the single-element transducer, based on the average flow velocity, was 25 Hz (middle dotted line). Therefore, each fluid volume was exposed to only a single acoustic pulse from the single element transducer for PRFs less than 25 Hz. The left and right dotted lines display the slowest and fastest rates, respectively, at which a fluid volume passes the single element US beam width, based on the experimental data.	46
2.9	Mean ($n = 3$) ADV thresholds and IC threshold (right), plotted with standard deviations, for various pulse widths at two different PRFs (10 Hz and 83 Hz). The following conditions were used: degassed water at 37°C and albumin-coated PFP droplets.	47
3.1	Left: Experimental setup used to perform ADV experiments with OptiCells TM . Right: Exposure conditions utilized during experiments. The emulsion was added to the chamber containing adherent CHO cells and subsequently exposed to US to cause ADV of the introduced droplets.	63

3.2	A visible image (left) and its corresponding fluorescent image (right) of the dual-phase emulsion containing PFP and soybean oil stained with a fluorescent dye. The spacing between the two horizontal lines on the hemacytometer is 200 μm . A 20 μm scale is included in each image. Although large droplets appear in this figure, droplets larger than 10 μm in diameter account for only 4.9% (by number) of total droplets. Refer to Fig. 3.4 for a size distribution, obtained via Coulter counter, for the emulsion.	65
3.3	Left: For $n = 338$ droplets, the ratio of the inner to outer droplet diameter is plotted as a function of the outer droplet diameter. The raw data is plotted using open, gray circles and the averaged, binned (1 μm) data is presented as closed, black circles. Right: A histogram of the raw data.	66
3.4	The emulsion size distribution, obtained using a Coulter counter, plotted as the number percent of total droplets. The 50 μm aperture enables the sizing of particles whose diameters are between 1 and 30 μm . The mean droplet diameter is $3.06 \pm 0.21 \mu\text{m}$ with 4.9% (by number) of the droplets larger than 10 μm in diameter. The CHL loading in the droplets is $3.12 \pm 0.01 \text{ mg/mL}$ emulsion.	67
3.5	A comparison of the mean ($n = 3$) ADV thresholds, plotted with standard deviations, for single-phase and dual-phase droplets as a function of average droplet diameter. The single-phase ADV thresholds are taken from a previous study [33]. The dual-phase droplets with a mean diameter of 6.96 μm were obtained by centrifuging the emulsion. The data labeled ‘dual-phase (shifted)’ has been corrected for the estimated mean PFP core diameter, using Fig. 3.3. The horizontal error bars were obtained based on the standard deviation in Fig. 3.3 (right). The following experimental conditions were used: degassed water at 37°C, 3.5 MHz single element transducer, 83 Hz pulse repetition frequency, and 13 cycles.	68
3.6	Left: Cytotoxicity of CHL initially dissolved in DMSO on CHO cells for 15 and 60-minute exposures. Right: The mean CHO cell diameter as a function of the GI. For both the left and right plots, each data point is the average of six wells, from three independent experiments. Additionally, error bars are standard deviations of the means.	70
3.7	Mean ($n = 5$) percent GI and standard deviation for each of the eight experimental groups. The presence (+) or absence (–) of each parameter - droplets, CHL, and US - is indicated above each group number. The same exposure procedure, acoustic parameters, droplet concentration, and CHL concentration (100 μM whether in DMSO or emulsified) was used for all groups.	71

3.8	Mean ($n = 5$) cell diameter and standard deviation for each of the eight experimental groups. The presence (+) or absence (-) of each parameter - droplets, CHL, and US - is indicated above each group number. The same exposure procedure, acoustic parameters, droplet concentration, and CHL concentration ($100 \mu\text{M}$ whether in DMSO or emulsified) was used for all groups.	74
3.9	The number and volume weighted distributions for the dual-phase droplets are plotted along with the mean ($n = 3$) fraction of droplets vaporized, as a function of droplet size, for different number of exposure passes by the US array. The standard deviation is plotted for the single pass case, with similarly sized standard deviations obtained for the 2 and 5 pass cases. The small decrease in efficiency between 1 and $2 \mu\text{m}$ is due to the subtraction errors between the treated (with US) and untreated (without US) cases.	75
4.1	The Kyttox 157 FSL is first converted into an acid chloride and then reacted with PEG-diamine to form a copolymer via amide linkages. .	90
4.2	Micrographs of a $W_1/\text{PFC}/W_2$ emulsion containing fluorescein in the W_1 phase. The left image is an overlay of both visible and fluorescent micrographs. The scale bar is $8 \mu\text{m}$. The structure of the $W_1/\text{PFC}/W_2$ emulsion - water droplets containing fluorescein within a globule of PFC - can be clearly seen in the right image, which displays a $100 \mu\text{m}$ diameter globule.	98
4.3	<i>In vitro</i> release profiles of PFP (left) and PFH (right) double emulsions containing fluorescein at 37°C . In each case, the release profiles obtained from the emulsion, with and without ADV, are compared to a solution of fluorescein of equal concentration. The fluorescein concentration for the PFP and PFH emulsions are 0.6 mg/mL and 0.3 mg/mL , respectively.	100
4.4	Reference curve displaying the activated clotting time (ACT) for canine blood, stored with citrate-phosphate-dextrose (CPD) solution, as a function of thrombin concentration.	102
4.5	Anticoagulative effect of the Krytox-PEG copolymer used in the thrombin emulsions. A blank emulsion, containing copolymer was mixed with thrombin solution. An aliquot of the resulting mixture, containing 1 IU thrombin, was added to blood containing CPD. Points marked with an asterisk (*) indicate copolymer levels that are not statistically different than control case (i.e. without copolymer). . .	104
4.6	The effect of ADV (3.5 MHz , $3.7 \mu\text{s}$ pulse duration, 10 ms PRP , 4.7 MPa peak rarefactional pressure, 11.3 MPa peak compressional pressure, 5 minute exposure) on the ACT for five different thrombin formulations. Cases where the ACT was statistically different after ADV are denoted by an asterisk (*).	105

5.1	Left: Distribution of human lung capillaries [12] and the associated probability that a particle of a given diameter will pass through the capillaries [13]. Right: Percent of particles retained in the lungs, relative to the total number of particles injected, one-hour after intravenous administration of particles. Five different <i>in vivo</i> studies are shown: radiolabeled, polystyrene divinylbenzene microspheres in canines [16; 17]; radiolabeled, terbutaline sulfate loaded albumin microspheres in mice [18]; radiolabeled microbubbles in mice [19]; and fluorescent polystyrene microparticles in rats [20]. Since albumin microspheres can undergo biodegradation within the lungs due to the presence of proteolytic enzymes [18], the percent of albumin microspheres retained in the lungs is lower compared to non-degradable, non-deformable particles of similar sizes [16].	127
5.2	Time activity curves of standardized uptake values (SUV) for ^{18}F -FDG solution (left) and ^{18}F -FDG contained in the W_1 phase of a $W_1/\text{PFC}/W_2$ emulsion (right) post tail vein injection in Fischer 344 rats. PFP was used as the PFC phase. The rats were inoculated with 9L gliosarcoma tumors in the bilateral forearms. The sonicated emulsion displayed a similar size distribution as seen in Fig. 5.3. Greater uptake of ^{18}F -FDG occurs in both tumors and the brain with the ^{18}F -FDG solution, compared to the $W_1/\text{PFC}/W_2$ emulsion (see Table 5.2 for integrated SUV data) due to ^{18}F -FDG encapsulation within the droplets. Accumulation of droplets in the liver and minimal lung uptake are also evident.	128
5.3	Number (left) and volume (right) weighted distributions of BSA stabilized PFP droplets. The emulsions are labeled according to the emulsification method used. The sonicated droplets possess a smaller mean diameter ($1.7\ \mu\text{m}$ versus $2.0\ \mu\text{m}$) and a lower fraction of droplets that are greater than $8\ \mu\text{m}$ in diameter (0.01% versus 2.2% based on number or 4.5% versus 74.6% based on volume) compared to the shaken droplets.	130
5.4	Micrographs of microfluidic channels, fabricated in PDMS using soft lithography, exhibiting two different flow focusing geometries. In each image, the PFC phase flows through the central channel while an aqueous solution of surfactant flows through two channels focused onto the PFC stream, thereby shearing droplets of PFC. Besides PDMS, which is hydrophobic, microchannels can be made using glass, which is hydrophilic, but can be made hydrophobic via siliconization or silanization [28].	132

5.5	Left: Micrograph of monodispersed, BSA-stabilized PFH-in-water droplets obtained using the microchannel in Fig. 5.4 (left). Right: Number weighted distributions of BSA-stabilized PFH-in-water droplets produced using the microchannel geometry in Fig. 5.4 (right). The channel with a 20 μm orifice produced PFH droplets with a mean diameter of 13.2 μm and 5.8% coefficient of variance (CV) at a rate of 290 Hz. The channel with a 35 μm orifice produced PFH droplets with a mean diameter of 22.1 μm and 3.7% CV at a rate of 128 Hz. These distributions display the ability of microchannels to produce monodisperse droplets (i.e. low CV), though a smaller orifice is needed in order to produce droplets that are transpulmonary. . . .	132
5.6	Arterial blood gas tensions (left) as well as arterial pH and respiration rate (right) in a canine (26 kg) before and after IV injections of lipid-stabilized, PFP droplets. Oxygen was used as the carrier of isoflurane, the inhaled anesthetic. A laparotomy was performed on the animal to expose the left kidney. Each injection, denoted by a vertical dotted line, contained 375 μL PFP and consisted of 2.4×10^{10} droplets (9.2×10^8 droplets/kg). ADV was performed in the renal artery subsequent to each injection. During the course of the experiment, the pO_2 and pH decreased and the pCO_2 and respiration rate increased in response to the injection of PFP droplets. Respiratory acidosis was suspected in this case. Based on the emulsion size distribution and the lung filtration function in Fig. 5.1 (left), 1% and 54% of the droplets by number and volume, respectively, are estimated to remain in the lung capillaries upon a single pass through the pulmonary circulation. This data is associated with a previously published study [3].	135
5.7	Left: The vaporization temperature of PFP droplets, as a function of droplet diameter, for two surface tension values, 30 mN/m and 50 mN/m [8]. Right: The surface tension required to stabilize PFP droplets at 37°C as a function of droplet diameter. At a given surface tension, droplets whose diameters lie to the right of the line are superheated. Individual data points represent interfacial tensions of PFP against water or phosphate buffered saline (PBS) [68]. The type of surfactant used is indicated in parentheses: BSA, polyethylene oxide- <i>co</i> -poly- ϵ -caprolactone (PEO-PCL), polyethylene oxide- <i>co</i> -polylactic acid (PEO-PLA), and cetyl trimethyl ammonium bromide (CTAB). The interfacial tension was measured at a surfactant concentration greater than critical micelle concentration for each surfactant type.	141

5.8 Left: The cytotoxicity of different CHL emulsion formulations (PFP-in-oil-in-water) on Chinese hamster ovary cells at various concentrations for 60 minute exposures. The data is overlaid onto the cytotoxicity results obtained from CHL in DMSO for 15 and 60 minute exposures (Fig. 3.6). Lipid droplets were prepared using a modified thin-film method using different ratios of L- α -phosphatidylcholine and cholesterol. The amount of total lipids per mL of emulsion, as well as the percent of lipids that is cholesterol, is indicated in the parentheses. BSA stabilized droplets, used in chapter III, are displayed as well. Right: The data from the left plot is expressed as the fraction of CHL released, based on estimating the amount of CHL released, from the %GI, using the CHL in DMSO data (Fig. 3.6). This drug release is due to CHL partitioning outward from the soybean oil. For both the left and right plots, each data point is the average of six wells from three independent experiments. Additionally, error bars are standard deviations of the means. 143

LIST OF TABLES

Table

1.1	Examples of clinically-used, targeted chemotherapy agents	4
1.2	Three generations of US contrast agents	8
1.3	Published drug delivery studies using ADV	14
2.1	Boiling points (T_b) of PFCs used to make emulsions and average droplet diameters, including standard deviations of the means, of the resulting emulsions. The emulsions were sized one day after their formulation so no significant Ostwald ripening has occurred. The average number density, including the standard deviation of the mean, is listed for the undiluted emulsions.	29
2.2	The effect of bulk fluid gas saturation, surface tension, and viscosity on the mean ($n = 5$) ADV and IC thresholds. All fluids were heated to 37°C and contained albumin-coated, PFP droplets at a concentration of 9×10^4 droplets per mL. The IC threshold of gas-saturated water without droplets, tested under the same conditions, was 5.6 ± 0.2 MPa while no IC was observed for degassed water without droplets. . . .	38
2.3	Summary of the effects of the various bulk fluid, droplet, and acoustic properties on the ADV and IC thresholds. Refer to Table 2.2 and Figs. 2.6 through 2.9 for each parameter and its corresponding ADV/IC data.	49
3.1	Groups used in the OptiCell TM experiments. For each group, the positive (+) and negative (−) symbols indicate the presence or absence, respectively, of each parameter. In the case of group 5 or 8, the CHL is present within the dispersed phase of the emulsion.	64
3.2	Results of Tukey’s test on percent GI (upper right triangle) and mean diameter (lower left triangle) data. An ‘x’ indicates groups that are not statistically different at a 0.01 or 0.05 level. Statistically significant differences at a 0.01 or 0.05 level are indicated by ‘0.01’ and ‘0.05’, respectively.	71
3.3	The fraction of total droplets vaporized, expressed in terms of number and volume fraction. The data without volume correction is the fraction of droplets vaporized, based on Fig. 3.9. The volume corrected data uses the relationship between the inner and outer droplet diameters (Fig. 3.3) to estimate the fraction of oil released.	80

4.1	Summary of fluorescein and thrombin emulsions used for studies. In all cases, the primary emulsion was formed using sonication.	91
4.2	Characterization of fluorescein and thrombin emulsions. Thrombin precipitation, during the second emulsification step, and subsequent inactivation of thrombin during ADV was suspected in T2.	99
4.3	The thrombin concentration in blood, estimated from the regression in Fig. 4.4 and the data from Fig. 4.6. The thrombin concentration, assuming the complete release of thrombin from the emulsion and no inactivation, should have been 46.3 IU/mL.	105
5.1	Blood vessels in the adult human lung [25]. By comparison, the average number of alveoli in the adult human lung is 4.8×10^8 [26]. .	129
5.2	Integrated standardized uptake value (SUV) data (0 - 35 minutes), from Fig. 5.2, for a solution of ^{18}F -FDG and ^{18}F -FDG encapsulated in the W_1 phase of a $W_1/\text{PFC}/W_2$ emulsion.	133
5.3	The composition and characterization of CHL loading in various PFP-in-oil-in-water emulsions. The mean ($n = 3$ vials) and standard deviation of each value is presented. The CHL loading was obtained using high performance liquid chromatography (see chapter III for method). The percent of CHL encapsulated within the emulsion dispersed phase (i.e. encapsulation %) was determined using ultrafiltration [73]. For the lipid stabilized emulsions, the CHL loading was substantially lower than the BSA-stabilized droplets. Micrographs of the lipid and BSA stabilized droplets confirmed a much thicker oil phase for the latter type of emulsion.	142

LIST OF ACRONYMS

AALs	acoustically active lipospheres
ACT	activated clotting time
ADV	acoustic droplet vaporization
ANOVA	analysis of variance
BSA	bovine serum albumin
CAS	chemical abstract service
CHL	chlorambucil
CHO	Chinese hamster ovary
CI	confidence interval
CPD	citrate-phosphate-dextrose
CTAB	cetyl trimethyl ammonium bromide
CV	coefficient of variance
DMSO	dimethyl sulfoxide
DPBS	Dulbecco's phosphate buffered saline
DPPA	1,2-dipalmitoyl- <i>sn</i> -glycero-3-phosphate monosodium salt
DPPC	1,2-dipalmitoyl- <i>sn</i> -glycero-3-phosphocholine
ED ₅₀	median effective dose
EDTA	ethylenediaminetetraacetic acid
¹⁸ F-FAZA	¹⁸ F-fluoroazomycin arabinoside
¹⁸ F-FDG	¹⁸ F-fluorodeoxyglucose
FOV	field of view
GI	growth inhibition
H-PFB	1H-nonafluorobutane (C ₄ HF ₉)
HNCL	hyperinflated non-collapsible lungs
HPLC	high performance liquid chromatography
IC	inertial cavitation
IC ₅₀	half maximal inhibitory concentration
ICAM-1	intercellular adhesion molecule-1
IFT	integrated Fourier transform
IU	international units
IV	intravenous
L-DOPA	L-3,4-dihydroxyphenylalanine
LD ₅₀	median lethal dose

MEA	mean echo amplitude
MEP	mean echo power
MI	mechanical index
NA	not applicable
NMR	nuclear magnetic resonance
PBS	phosphate buffered saline
PDMS	poly(dimethylsiloxane)
PEG	polyethylene glycol
PEO-PCL	polyethylene oxide- <i>co</i> -poly- ϵ -caprolactone
PEO-PLA	polyethylene oxide- <i>co</i> -polylactic acid
PET	positron emission tomography
PFB	perfluoro-n-butane (C ₄ F ₁₀)
PFC	perfluorocarbon
PFC/O/W	perfluorocarbon-in-oil-in-water
PFC/W	perfluorocarbon-in-water
PFDCO	perfluorodichlorooctane (C ₈ Cl ₂ F ₁₆)
PFH	perfluoro-n-hexane (C ₆ F ₁₄)
PFO	perfluoro-n-octane (C ₈ F ₁₈)
PFOB	perfluorooctylbromide (C ₈ BrF ₁₇)
PFP	perfluoro-n-pentane (C ₅ F ₁₂)
PGT	pulmonary gas trapping
PLGA	poly(lactic- <i>co</i> -glycolic acid)
PRF	pulse repetition frequency
PRP	pulse repetition period
RES	reticuloendothelial system
RF	radiofrequency
SDD	superheated drop detector
SUV	standardized uptake value
TI	therapeutic index
UCUCA	university committee on the use and care of animals
UNIFAC	universal functional activity coefficient
US	ultrasound
VEGFR	vascular endothelial growth factor receptor
W ₁ /PFC/W ₂	water-in-perfluorocarbon-in-water

LIST OF SYMBOLS

κ	medium compressibility
κ_s	particle compressibility
ρ	medium density
ρ_s	particle density
Σ_s	scattering cross section of a particle
σ	surface tension (chapter I) or standard deviation (chapter II)
A	amplitude
d	bubble/droplet diameter
k	wave number
ΔP	pressure difference across bubble/droplet interface
P_i	pressure inside a bubble/droplet
P_o	pressure outside a bubble/droplet
$Prob_N$	percentage probability
R	correlation coefficient
r	bubble/droplet radius
T_b	boiling point

ABSTRACT

ULTRASOUND-TRIGGERED DRUG DELIVERY USING ACOUSTIC DROPLET VAPORIZATION

by

Mario Leonardo Fabiilli

Chair: J. Brian Fowlkes

The goal of targeted drug delivery is the spatial and temporal localization of a therapeutic agent and its associated bioeffects. One method of drug localization is acoustic droplet vaporization (ADV), whereby drug-laden perfluorocarbon (PFC) emulsions are vaporized into gas bubbles using ultrasound, thereby releasing drug locally. Transpulmonary droplets are converted into bubbles that occlude capillaries, sequestering the released drug within an organ or tumor. This research investigates the relationship between the ADV and inertial cavitation (IC) thresholds - relevant for drug delivery due to the bioeffects generated by IC - and explores the delivery of lipophilic and hydrophilic compounds using PFC double emulsions.

IC can positively and negatively affect ultrasound mediated drug delivery. The ADV and IC thresholds were determined for various bulk fluid, droplet, and acoustic parameters. At 3.5 MHz, the ADV threshold occurred at a lower rarefactional pressure than the IC threshold. The results suggest that ADV is a distinct

phenomenon from IC, the ADV nucleus is internal to the droplet, and the IC nucleus is the bubble generated by ADV.

The ADV triggered release of a lipophilic chemotherapeutic agent, chlorambucil (CHL), from a PFC-in-oil-in-water emulsion was explored using plated cells. Cells exposed to a CHL-loaded emulsion, without ADV, displayed 44% less growth inhibition than cells exposed to an equal concentration of CHL in solution. Upon ADV of the CHL-loaded emulsion, the growth inhibition increased to the same level as cells exposed to CHL in solution.

A triblock copolymer was synthesized which enabled the formulation of stable water-in-PFC-in-water (W_1 /PFC/ W_2) emulsions. The encapsulation of fluorescein in the W_1 phase significantly decreased the mass flux of fluorescein; ADV was shown to completely release the fluorescein from the emulsions. ADV was also shown to release thrombin, dissolved in the W_1 phase, which could be used *in vivo* to extend synergistically the duration of ADV-generated, microbubble-based embolizations.

Overall, the results suggest that PFC double emulsions can be used as an ultrasound-triggered drug delivery system. Compared to traditional drug delivery systems, ADV could be used to increase the therapeutic efficacy and decrease the systemic toxicity of drug therapy.

CHAPTER I

Introduction

1.1 The Magic Bullet

In 1908, the German scientist, Paul Ehrlich - who coined the term *chemotherapy* - received the Nobel Prize for Physiology or Medicine based on his landmark insights in the field of immunology. Earlier in his career, Ehrlich observed that certain histological dyes selectively concentrated in specific biological structures, which caused him to postulate that such specificity could be used therapeutically [1]. Additionally, based on his seminal studies in immunology, Ehrlich hypothesized that antigens were recognized via their binding of *side chains*, later termed *receptors*, associated with cells [2]. These findings caused Ehrlich to develop the concept of a *magic bullet* - a chemical agent that possesses a high affinity to the causative agent of disease [3]. Thus, the vision of magic bullets form the basis of modern, targeted medicine and its seemingly simplistic yet challenging goal: treating pathogens or diseased tissue while remaining systemically harmless.

Despite the passage of more than a century since Ehrlich's magic bullet concept, the development of therapeutic agents that behave as magic bullets has been confounded by the biochemical and physiological complexity of the human body. Arguably, most disease states do not possess a magic bullet. The focus of this dissertation is the development of one type of technology - liquid droplets activated with ultrasound (US) - that may have the potential to be a magic bullet for multiple

diseases. This chapter presents an overview of targeted drug delivery, including the use of US and colloids in modulated (i.e. externally controlled) delivery. The proposed drug delivery mechanism, acoustic droplet vaporization (ADV), will also be presented.

1.2 An Overview of Targeted Drug Delivery

The paradigm of targeted drug delivery is the localization and subsequent action of a therapeutic agent only at the target within a suitable time window. The target is defined as a level of biological structure such as an organ or tissue type, a specific cell type within an organ or tissue, or an intracellular compartment within a specific cell type [4]. Comparatively, traditional drug delivery systems - such as immediate release capsules or intravenous infusions - which still form the predominant administration routes of drugs, are unable to effectively control the rate of drug delivery or the target area of administration. With these traditional delivery systems, non-selective drug uptake occurs by cells, tissues, or organs throughout the body due to the lack of spatial and temporal selectivity of the administered drug.

Targeted delivery systems provide numerous advantages over traditional systems including: use of less total drug, reduction in local or systemic side effects, increase in bioavailability for some drugs, and improvement in treatment efficiency. These advantages are especially important in the clinical use of drugs that possess a low therapeutic index (TI^1), which is defined in Eq. 1.1 as the ratio of the lethal dose required to kill 50% of the population, LD_{50} , to the effective (i.e. therapeutic) dose for 50% of the population, ED_{50} . The TI of a drug is not completely dependent on its inherent physiochemical properties but also a function of the manner in which the drug is formulated (ex. solution versus emulsion) and thus presented to the body

¹ TI is also commonly used in the field of ultrasound as an abbreviation for *thermal index*.

[5].

$$TI = \frac{LD_{50}}{ED_{50}} \quad (1.1)$$

The notion that the presentation of a drug contributes to its performance evolved during the 1960s [6] and contrasted with the historical role that drug delivery systems and formulations were relegated to: a “do no harm” capacity [7]. Many of the initial targeted delivery strategies included implantable macroscopic or microscopic devices that released drugs via zero order kinetics (i.e. constant rate). Some examples, both manufactured by the Alza Corporation, include Progestasert, an intrauterine device that releases progesterone, and Ocusert, an ophthalmic insert that releases the anti-glaucoma drug pilocarpine. Additionally, one of the most obvious ways of achieving targeted delivery is the direct administration of drugs into an organ or tissue. Examples include the intra-articular injection of hyaluronic acid for the treatment of knee osteoarthritis [8] or the hepatic arterial administration of chemotherapy agents in the treatment of hepatocellular carcinoma [9; 10]. However, the implantation of a drug delivery device or the at-site administration of a drug is both invasive and impractical in the treatments of disease states which are deeply situated in the body or dispersed in nature (ex. highly metastatic cancer).

1.2.1 Pharmaceutical Approaches

Three pharmaceutical strategies have been used in targeted drug delivery: site specific drug molecules, therapeutic agents that are activated at the target site (i.e. prodrugs), or the use of carrier systems that direct the drug to the target [11]. The first strategy is largely dependent on the upregulation or downregulation of specific proteins, genes, or signaling molecules that are involved in pathogenesis. Identifying drug-like molecules that selectively interact with the molecular cause of a disease, if known, is only part of this strategy. High molecular affinity and specificity does not

necessarily translate into a molecule that will possess appropriate physiochemical properties such that the molecule can be readily absorbed, escape extensive hepatic metabolism, distribute sufficiently in the target tissue, and avoid rapid excretion. Examples of these site-specific molecules in the area of chemotherapeutics are listed in Table 1.1.

Table 1.1: Examples of clinically-used, targeted chemotherapy agents

Compound	Tradename	Company	Structure	Target
Bevacuzimab	Avastin	Genentech/Roche	monoclonal antibody	vascular endothelial growth factor A
Imatinib	Gleevac	Novartis	small molecule	receptor tyrosine kinase
Sunitinib	Sutent	Pfizer	small molecule	receptor tyrosine kinase
Trastuzumab	Herceptin	Genentech	monoclonal antibody	human epidermal growth factor receptor 2

The second strategy - prodrugs - can be used to overcome physiochemical (e.g. solubility, chemical instability) or biopharmaceutical problems (e.g. bioavailability, toxicity) associated with the active form of a drug [12]. An example of this is L-3,4-dihydroxyphenylalanine (L-DOPA), the prodrug of the neurotransmitter dopamine; in this case, L-DOPA can cross the blood-brain barrier, unlike dopamine, where it is then converted into dopamine in the corpus striatum. The efficacy of a prodrug approach is dependent on the ability of the prodrug to access the target receptor and the specificity of the activating mechanism, usually an enzyme such as an esterase or amidase, at the target. Additional activation mechanisms utilized in targeted delivery of anticancer prodrugs include low extracellular pH and hypoxia within the tumor core [13].

The third strategy - carrier systems - is based on the physical inclusion or chemical attachment of a drug to a carrier. Due to the association between the drug and the carrier, the distribution of the drug is governed by the physiochemical properties of the carrier, not the drug. Carrier-based systems can be divided into two main categories: soluble macromolecules and particulates. The former

includes conjugating drugs to proteins (e.g. antibodies, albumin, glycoproteins), genetic material, or polymers (e.g. dextran, N-(2-hydroxypropyl)methacrylamide). An example is gemtuzumab ozogamicin (Mylotarg, Wyeth), a conjugate of a recombinant humanized monoclonal antibody and calicheamicin, which is used in the treatment of acute myelogenous leukemia. The cytotoxic antibiotic portion of the conjugate (calicheamicin) is targeted to CD33, a surface glycoprotein expressed on myeloid leukemia cells, via the antibody. Particulate-based carriers include colloids, liposomes, lipoproteins, niosomes, and activated carbon as well as cells (ex. erythrocytes, leukocytes, platelets, fibroblasts, and hepatocytes) . Colloids, specifically emulsions, were used in this work and will be discussed in a latter section.

1.2.2 Ultrasound Modulated Systems

An alternative approach for targeted drug delivery is the use of devices or delivery systems that release drugs in response to an external stimulus. These stimuli include magnetism [14], electricity [15], light [16], temperature [17], pH [18], or ultrasound - the focus of this work and discussed subsequently. The goal of stimulus-based delivery is to increase the spatial and temporal selectivity of drug delivery. Rather than the zero order kinetics desired by the initial developers of drug delivery systems, stimulus-triggered delivery enables the delivery of drug when or where the body needs it. In many cases, stimulus-based delivery builds upon the previously described pharmaceutical approaches to targeted drug delivery. Stimulus-based systems can be considered either open or closed-loop control systems depending on whether the rate of drug delivery is automatically adjusted based on a measured variable, such as pH [19].

Ultrasound (US) is widely used in the field of medicine both diagnostically and therapeutically. US is especially suited for drug delivery since it can be non-invasively transmitted and focused onto deeply located sites within the body with millimeter precision. There are three types of US-triggered delivery: device or depot enhanced

delivery, sonophoresis, and colloidal based delivery. The former two will be discussed here while the last type will be highlighted in the next section.

The first method, device or depot enhanced delivery, utilizes US to increase the release rate of a drug that is embedded into a polymer matrix. When exposed to US (75 kHz, 50% duty cycle, 5 W/cm²), the release rates of *p*-nitroaniline, *p*-aminohippuric acid, bovine serum albumin, and insulin were shown to dramatically increase, in a reversible manner, from both bioerodible and nonerodible matrices [20]. Similar results were obtained when polymer matrices, containing insulin, were implanted into diabetic rats and then exposed to US (1 MHz, 5 W/cm²) for 30 minutes; a dramatic decrease in blood glucose level, post US exposure, was observed [21]. In depot-enhanced delivery, acoustic cavitation is the main mechanism driving the matrix degradation and increase in drug release, similar to thrombolysis using pulsed US [22].

The second method, sonophoresis (phonophoresis), utilizes US to increase the transdermal delivery of therapeutic agents applied to the skin. Similar to other transdermal drug delivery applications, sonophoresis bypasses first-pass hepatic metabolism, thereby increasing the therapeutic efficacy of the applied drug. Recent comprehensive reviews [23; 24] detail the types of drugs used in *in vitro* and *in vivo* sonophoretic studies. Clinical studies with three non-steroidal anti-inflammatory drugs - diclofenac [25], ibuprofen [26], and ketoprofen [27] - demonstrate the efficacy of sonophoresis with 1 MHz US. Overall, low frequency US (20-100 kHz) enhances transdermal drug transport 1000 times more than high frequency US (1-3 MHz) [28; 29]. This difference is due to the increased likelihood of inertial cavitation, one of the driving mechanisms, at lower frequencies. Inertial cavitation is hypothesized to generate bilayer disordering within the stratum corneum, the major barrier to transdermal drug delivery. The next section will discuss colloids used in US-triggered drug delivery.

1.3 Colloids used in Diagnostic and Therapeutic Ultrasound

A colloid is a type of dispersed system where an internal (dispersed) phase is distributed within an external (continuous) phase. Common examples of colloids utilized in pharmaceutical formulations include emulsions (liquid-in-liquid), suspensions (solid-in-liquid), foams or microbubbles (gas-in-liquid), and aerosols (either liquid-in-gas or solid-in-gas). Colloidal particles range in diameter from approximately 1 nm to 1 μm . Larger particles (diameters $> 1 \mu\text{m}$) can generally be considered colloidal, especially in cases where the dispersed system is heterogeneous in particle size. In order to minimize the surface energy of the particles, surfactants are used to reduce the interfacial tension in the colloid, especially for emulsions or microbubbles, thereby stabilizing the particles from phase separation. Compared to a solid formulation (i.e. tablet, capsule), the surface area of a colloid is typically much larger, due to the small particle size, thereby leading to a higher dissolution rate and a potential increase in bioavailability of a colloidal drug formulation. Additionally, drugs that are insoluble in aqueous media can be formulated as colloids. Two types of US-activated colloids - microbubbles and emulsions - will be discussed next.

1.3.1 Microbubble Agents

First published by Gramiak and Shah in 1968 [30], the most commonly utilized colloids in medical US applications are microbubble-based contrast agents, which are approved for clinical, diagnostic use. Upon intravascular administration, these compressible blood pool agents increase the scattering and reflection of US waves by several orders of magnitude relative to blood. In order for microbubbles to be clinically useful in diagnostic US imaging, the contrast agent must not dissolve too quickly due to gas diffusion enhanced by the Laplace and arterial pressures. Thus, as can be seen in Table 1.2, contrast agent formulations evolved over various

generations in an effort to maximize their utility. First generation contrast agents, essentially air bubbles, are not surfactant stabilized and therefore only persist for seconds upon injection. Additionally, these first generation agents are too large to pass through capillaries and thus are used primarily in imaging the left side of the heart [31]. Second generation agents, transcapillary in size, are stabilized by a shell (2 to 500 nm thick) of protein, lipid, or polymer that enables the microbubbles to persist for up to 5 minutes after injection. The stability afforded by the shell can be explained in terms of the Laplace equation (Eq. 1.2), where ΔP is the pressure difference between the inside (P_i) and outside (P_o) of a bubble of radius r in a liquid with surface tension σ . The shell reduces the surface tension which reduces the pressure inside the bubble and thus increases the microbubble lifespan. Furthermore, the shell provides a resistance to gas permeation into or out of the microbubble [32].

$$\Delta P = P_i - P_o = \frac{2\sigma}{r} \tag{1.2}$$

Table 1.2: Three generations of US contrast agents

Generation	Gas core	Shell	Example(s)
First	Air	None	Echovist (Schering AG)
Second	Air	Protein, polymer, or lipid	Levovist (Schering AG) Albunex (Molecular Biosystems)
Third	C ₃ F ₈ , C ₄ F ₁₀ , C ₅ F ₁₂ C ₆ F ₁₄ , SF ₆	Protein, polymer, or lipid	Optison (GE Healthcare) Definity (Bristol-Myers Squibb)

Additionally, Eq. 1.2 highlights the importance of the shell in stabilizing the microbubble as the radius decreases. Besides hindering microbubble gas loss, dissolution, and coalescence, the shell enables the formation of more controlled size distributions [33]. The shell composition can affect how resistant the microbubbles are to rupture when exposed to US and hydrodynamic conditions *in vivo*. For example, lipid shells (1 to 2 nm thick) are highly compliant, rendering lipid-coated microbubbles more stable than those possessing relatively rigid albumin shells (10 to 15 nm thick) [34]. The shell can also be modified to contain polyethylene glycol

(PEG), thereby masking the contrast agent from the immune system, or targeting ligands - cell membrane receptor antibodies, peptides, or small molecules - which enables active targeting of microbubbles [35; 36]. Third generation agents, also shell stabilized, contain gases whose solubilities in blood and diffusion coefficients are significantly less than air. The use of inert, higher molecular weight gases, such as perfluorocarbons (PFCs), prolong the lifespan of microbubbles upon injection. For example, using the modified Epstein-Plesset equation [32; 37], a 5 μm diameter, lipid-coated bubble is predicted to exist for 1 second if the gas core consists of air versus 10^5 seconds (27.8 hrs) if the microbubble contains perfluorobutane [38]. In reality, third generation agents persist longer in the circulation (> 5 min), though not nearly the lifespan predicted by the aforementioned model which does not account for flow dynamics.

The use of microbubbles in targeted drug delivery is attractive due to the possibility of combining diagnostic feedback with therapy and relies upon the interaction between microbubbles and US. The resonance frequency of transpulmonary bubbles fortuitously lies in the medical imaging frequency range. Microbubbles can also oscillate in a nonlinear manner when insonified and microbubble destruction can occur at higher amplitude US. Acting as cavitation nuclei, microbubbles can generate microstream swirling, micro-jetting, and hydrodynamic shock waves during oscillations [39] that can cause bioeffects such as cellular erosion or lysis, molecular degradation, and free radical formation [40]. Alternatively, these bioeffects can be used in the enhancement of drug delivery via sonoporation, whereby insonified microbubbles adjacent to cells create a transient increase in membranes permeability. The pores generated during this process range in size from 30 to 100 nm up to a few microns and reseal over the span of seconds or minutes [41]. Thus contrast agent destruction can be used as an adjuvant for therapeutic agents not coupled to microbubbles. This is clearly seen in an *in*

vitro study where increased uptake of plasmids coding for green fluorescent protein occurred as a result of sonoporation [42].

Despite the benefits of co-administering microbubbles and therapeutic agents, there are distinct advantages of incorporating the agents within the microbubbles such as: localizing the effect of the agent at the insonation site, reducing the required dose of agent, and improving the therapeutic efficacy of the agent when dosed in a colloidal formulation. The incorporation of the drug or gene is typically accomplished using one of the following methods (Fig. 1.1): attachment (covalent or non-covalent) to the shell either directly or using a secondary carrier, such as a liposome or nanoparticle [43; 44]; intercalation within the shell [45; 46]; or incorporation within a fluid inside the shell. With the last technique, it is possible to include either an oil [47; 48] or aqueous layer within the microbubble [49].

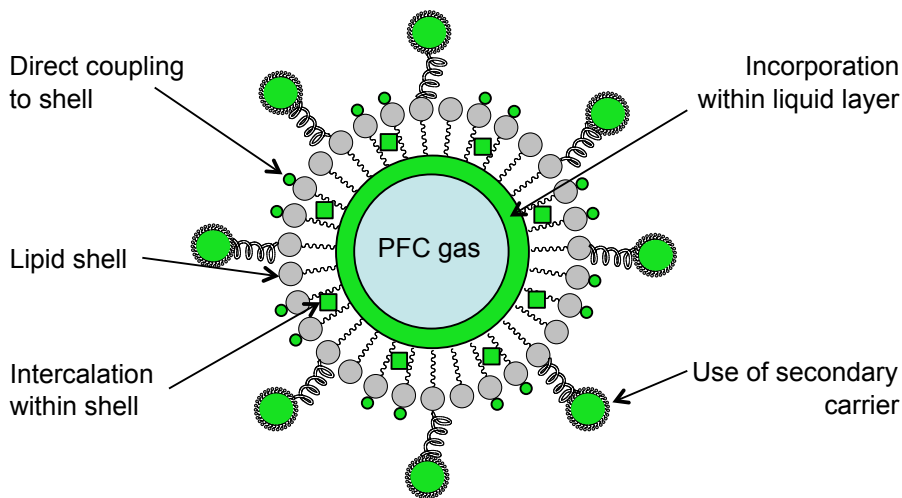


Figure 1.1: Drug loading strategies for a lipid-coated, PFC microbubble.

1.3.2 Perfluorocarbon Emulsions

Similar to PFC microbubbles, PFC emulsions (i.e. PFC-in-water) are being studied in diagnostic and therapeutic US applications as well as for *in vivo* oxygen delivery (blood substitutes) [50]. The latter application, *in vivo* oxygen delivery, utilizes higher molecular weight (i.e. higher boiling point) PFCs than the former

US applications, which is the focus of this work. PFCs possess ideal properties for biomedical applications, such as inertness and biocompatibility, and unique properties (hydrophobicity, lipophobicity, and high gas solubility) stemming from the carbon-fluorine bonds within the molecules [51]. Compared to PFC microbubbles, PFC emulsions possess a longer circulation half-life [52] and a larger payload fraction. Emulsions, however, are less echogenic than microbubbles, as can be seen in Eq. 1.3 (Born approximation) where Σ_s is the scattering cross section of a particle, r is the particle radius, k is the wave number, κ_s is the particle compressibility, κ is the medium compressibility, ρ_s is the particle density, and ρ is the medium density [53]. Thus, the scattering cross section of a droplet is less than that of an equally sized microbubble, even without including the mechanical resonance of a microbubble, due to the incompressible nature of the droplet combined with the increase in dispersed phase density.

$$\Sigma_s = \frac{4\pi}{9} k^4 r^6 \left[\left(\frac{\kappa_s - \kappa}{\kappa} \right)^2 + \frac{1}{3} \left(\frac{3\rho_s - 3\rho}{2\rho_s - \rho} \right)^2 \right] \quad (1.3)$$

In early US studies, liquid PFC - perfluorooctylbromide (PFOB) - was administered orally as a diagnostic contrast medium for gastroenterography [54]. Later, PFOB was formulated as an emulsion for intravascular injection during US imaging of rabbit livers *in vivo* [55]. Sonus Pharmaceuticals developed EchoGen, an US contrast agent consisting of a perfluoropentane (PFP) emulsion. Upon injection into the body (37°C), the PFP (29°C boiling point) droplets vaporized into microbubbles; subsequently, it was published that hypobaric activation of the emulsion prior to injection yielded more microbubbles than thermal activation alone [56]. Contrast studies with perfluorohexane (PFH) emulsions have shown that US can be used to monitor the uptake of the droplets by macrophages [57]. PFP emulsions have also been used as cavitation nucleation agents, which can promote *in vivo* gene transfer during shock wave lithotripsy [58; 59]. Additionally, nanoemulsions using

perfluorodichlorooctane (PFDCO) or PFOB have been formulated for contrast studies [60; 61]. These PFC emulsions can extravasate in the microvasculature of tumors, though the echogenicity of these colloids, relative to micron-sized PFC emulsions, is less since the scattering cross section scales according to sixth power of the particle radius (Eq. 1.3). However, the layering or accumulation of PFC nanodroplets, which can form a specular reflector, can increase the acoustic reflectivity (i.e. echogenicity) of the nanoemulsion [52].

1.3.3 Acoustic Droplet Vaporization

US triggered drug delivery can occur from PFC emulsions via a process known as acoustic droplet vaporization (ADV). ADV is a mechanism whereby an emulsion is converted into gas bubbles using ultrasound. The dispersed phase of the emulsion, typically a PFC, is usually superheated, meaning that the dispersed phase is a liquid that exists at a temperature and pressure corresponding to the vapor region in the phase diagram. The origin of ADV can be traced to Donald Glaser's development of the bubble chamber that was filled with a superheated liquid and used extensively in radiation dosimetry [62]. The passage of ionizing radiation through the chamber causes vaporization of the superheated fluid, which can be observed as tracks of bubbles. This is analogous to the cloud (Wilson) chamber, filled with a supercooled vapor, developed in 1911-1912 [63]; in this case, the passage of ionizing radiation through the chamber causes tracks of condensation in the supercooled vapor. For both chambers, the metastable state is fragile and relatively short-lived due to the high number of potential nucleation sites within the medium.

In 1979, Robert Apfel described a new type of radiation dosimeter - a superheated drop detector (SDD) - which was obtained by emulsifying a superheated fluid with an immiscible fluid, thereby fractionating the superheated fluid into many subdivisions [64]. This fractionation ensures that some droplets are free of nucleating impurities and that triggering of one droplet by radiation would not trigger all of the droplets.

Additionally, unlike a bubble chamber which is only transiently superheated upon a decrease in chamber pressure, a SDD is constantly superheated, thereby making the latter constantly sensitive to radiation. Apfel patented the SDD technology in 1998 [65] for use in three proposed applications: diagnostic contrast agent, vascular occlusion, and localized drug delivery; the sensitivity of the SDD to acoustic radiation (i.e. ultrasound) was also described in the patent. Kripfgans *et al.*, who termed the ADV acronym, demonstrated the feasibility of using medically relevant ultrasound to produce ADV with micron-sized emulsions [66]. The physical mechanisms governing the ADV process are not as well understood as the interaction between microbubbles and US. However, published works delve into the effects of acoustic, emulsion, and bulk fluid properties on the ADV process, specifically the ADV threshold [66–73]. Additionally, a theoretical model explores the effect of droplet size, gas nucleus size, bulk fluid viscosity, and bulk fluid surface tension on bubble growth during ADV [74].

ADV has been studied in four applications: aberration correction [75; 76], occlusion therapy [74; 75; 77–81], microbubble-enhanced high intensity focused US [82–84], and drug delivery. Table 1.3 lists publications focused on ADV-triggered drug delivery. Due to the hydrophobicity and lipophobicity of the dispersed PFC phase, similar formulation approaches, which were described previously for microbubbles, are utilized for PFC emulsions. Thus upon ADV, each drug-laden droplet will release its therapeutic payload when the PFC phase is vaporized. The procedure would be minimally invasive since the emulsion would be administered intravenously, and the US would be applied transcutaneously. Additionally, ADV-triggered delivery can be potentially coupled to other ADV-induced phenomenon, such as vascular occlusion, to produce therapeutic synergisms.

Table 1.3: Published drug delivery studies using ADV

Reference	Drug	PFC
Fang <i>et al.</i> 2007 [85]	resveratrol	PFP, PFH
Rapoport <i>et al.</i> 2007 [86]	doxorubicin	PFP
Fang <i>et al.</i> 2009 [87]	camptothecin	PFP, PFH
Hwang <i>et al.</i> 2009 [88]	apomorphine	PFP
Rapoport <i>et al.</i> 2009, 2010 [89–91]	paclitaxel	PFP
Fabiilli <i>et al.</i> 2010 [67]	chlorambucil	PFP
Fabiilli <i>et al.</i> 2010 [92]	fluorescein/thrombin	PFP, PFH

1.4 Overview of Dissertation

The following chapters will explore ADV and its use in drug delivery using micron-sized PFC emulsions. Each chapter contains an introductory section thereby providing the necessary background material so that each chapter can be read independently. A detailed outline of the dissertation is described below.

Chapter II investigates the relationship between ADV and inertial cavitation (IC), specifically the thresholds of each, possibly interrelated, phenomenon. This work was motivated by previous studies that focused on elucidating the mechanisms involved in ADV [68; 70; 72; 75]. IC, which occurs when a bubble is exposed to US above a certain threshold, can produce phenomena such as extravasation, sonoporation, or molecular degradation that could potentially affect ADV-triggered drug delivery. It was determined - for various bulk fluid, droplet, and acoustic properties - that the ADV threshold occurred at a lower rarefactional pressure than the IC threshold. Thus, ADV appears to be a mechanism that is separable from IC. Appropriate citations for material in this chapter include:

- M.L. Fabiilli, K.J. Haworth, O.D. Kripfgans, P.L. Carson, and J.B. Fowlkes. “The role of inertial cavitation in acoustic droplet vaporization.” *Proceedings of the IEEE International Ultrasonics Symposium*, pp. 768-771, 2008.
- M.L. Fabiilli, K.J. Haworth, N.H. Fakhri, O.D. Kripfgans, P.L. Carson, and J.B. Fowlkes, “The role of inertial cavitation in acoustic droplet vaporization.”

IEEE Transactions on Ultrasonics, Ferroelectrics, and Frequency Control, vol. 56, no. 5, pp. 1006-1017, 2009.

Chapter III provides a proof-of-concept study for drug delivery using ADV. A double emulsion (PFC-in-oil-in-water) containing chlorambucil, a lipophilic chemotherapy agent, was formulated. The ability of ADV to selectively release chlorambucil from the emulsion was tested in a plated cell model by measuring the growth inhibition of Chinese hamster ovary cells. The ADV threshold of the double emulsion and the ADV efficiency - the fraction of droplets that vaporize - were measured as a function of droplet diameter. Appropriate citations for material in this chapter include:

- M.L. Fabiilli, I.E. Sebastian, K.J. Haworth, O.D. Kripfgans, P.L. Carson, and J.B. Fowlkes. “Ultrasonic delivery of a chemotherapeutic agent using acoustic droplet vaporization (ADV).” *Proceedings of the IEEE International Ultrasonics Symposium*, 2009.
- M.L. Fabiilli, I.E. Sebastian, and J.B. Fowlkes. “Development of an acoustic droplet vaporization, ultrasound drug delivery emulsion.” *Proceedings of the International Symposium on Therapeutic Ultrasound*, pp. 295-298, 2009.
- M.L. Fabiilli, K.J. Haworth, I.E. Sebastian, O.D. Kripfgans, P.L. Carson, and J.B. Fowlkes. “Delivery of chlorambucil using acoustically-triggered, perfluoropentane emulsions.” *Ultrasound in Medicine and Biology*, vol. 36, no. 8, pp. 1364-1375, 2010.

Chapter IV describes the development of double emulsions that can contain a water-soluble therapeutic agent (water-in-PFC-in-water). Previous to the work described in chapter IV, other ADV-triggered drug delivery studies focused on the delivery of lipophilic compounds. ADV was shown to significantly increase the

mass flux of fluorescein, encapsulated within the emulsions, compared to conditions without ADV. Additionally, emulsions containing thrombin were formulated, which could be potentially used to increase the duration of ADV-generated embolizations. ADV was shown to decrease the clotting time of blood *in vitro*, indicating the release of thrombin via ADV. Appropriate citations for material in this chapter include:

- M.L. Fabiilli, J.A. Lee, O.D. Kripfgans, P.L. Carson, and J.B. Fowlkes. “Ultrasonically-activatable, perfluorocarbon double emulsions containing an aqueous payload for drug delivery.” *Proceedings of the International Symposium on Therapeutic Ultrasound*, 2010.
- M.L. Fabiilli, J.A. Lee, O.D. Kripfgans, P.L. Carson, and J.B. Fowlkes. “The release of thrombin, using acoustic droplet vaporization (ADV), from perfluoropentane double emulsions.” *Proceedings of the IEEE International Ultrasonics Symposium*, 2010.
- M.L. Fabiilli, J.A. Lee, O.D. Kripfgans, P.L. Carson, and J.B. Fowlkes. “Delivery of water-soluble drugs using acoustically-triggered, perfluorocarbon double emulsions.” *Pharmaceutical Research*, accepted September 2010.

Chapter V provides a summary of results described in the previous chapters. Based on the completed work, future studies are presented which could further the development of ADV-triggered drug delivery.

REFERENCES

- [1] M. C. Perry, ed., *The Chemotherapy Source Book*. Philadelphia, PA: Lippincott Williams and Wilkins, 4th ed., 2008.
- [2] K. Strebhardt and A. Ullrich, “Paul Ehrlich’s magic bullet concept: 100 years of progress,” *Nature Reviews Cancer*, vol. 8, no. 6, pp. 473–480, 2008.
- [3] F. Winau, O. Westphal, and R. Winau, “Paul Erlich - in search of the magic bullet,” *Microbes and Infection*, vol. 6, no. 8, pp. 786–789, 2004.
- [4] G. Poste and R. Kirsch, “Site-specific (targeted) drug delivery in cancer-therapy,” *Biotechnology*, vol. 1, no. 10, pp. 869–878, 1983.
- [5] S. MacDiarmid, B. W. Sandage, and B. K. Malhotra, “The effects of reformulation: improved therapeutic index,” *Current Urology Reports*, vol. 9, no. 6, pp. 465–471, 2008.
- [6] A. S. Hoffman, “The origins and evolution of “controlled” drug delivery systems,” *Journal of Controlled Release*, vol. 132, no. 3, pp. 153–163, 2008.
- [7] J. R. Robinson, “Controlled drug delivery - past, present, future,” in *Controlled Drug Delivery: Challenges and Strategies* (K. Park, ed.), Washington, DC: American Chemical Society, 1997.
- [8] D. Y. Wen, “Intra-articular hyaluronic acid injections for knee osteoarthritis,” *American Family Physician*, vol. 62, no. 3, pp. 565–570, 2000.
- [9] S. Higashi, N. Tabata, K.-H. Kono, Y. Maeda, M. Shimizu, T. Nakashima, and T. Setoguchi, “Size of lipid microdroplets effects results of hepatic arterial chemotherapy with an anticancer agent in water-in-oil-in-water emulsion to hepatocellular carcinoma,” *The Journal of Pharmacology and Experimental Therapeutics*, vol. 289, no. 2, pp. 816–819, 1999.
- [10] L. A. Dawson, C. J. McGinn, D. Normolle, R. K. T. Haken, S. Walker, W. Ensminger, and T. S. Lawrence, “Escalated focal liver radiation and concurrent hepatic artery fluorodeoxyuridine for unresectable intrahepatic malignancies,” *Journal of Clinical Oncology*, vol. 18, no. 11, pp. 2210–2218, 2000.

- [11] V. Kumar and G. S. Banker, "Target-oriented drug-delivery systems," in *Modern Pharmaceutics* (G. S. Banker and C. T. Rhodes, eds.), Marcel Dekker, Inc., 4th ed., 2002.
- [12] V. J. Stella, "Prodrug strategies for improving drug-like properties," in *Optimizing the "drug-like" properties of leads in drug discovery* (R. T. Borchardt, E. H. Kerns, M. J. Hageman, D. R. Thakker, and J. L. Stevens, eds.), Springer, 2006.
- [13] Y. Singh, M. Palombo, and P. J. Sinko, "Recent trends in targeted anticancer prodrug and conjugate design," *Current Medicinal Chemistry*, vol. 15, no. 18, pp. 1802–1826, 2008.
- [14] R. A. Frimpong, S. Fraser, and J. Z. Hilt, "Synthesis and temperature response analysis of magnetic-hydrogel nanocomposites," *Journal of Biomedical Materials Research Part A*, vol. 80A, no. 1, pp. 1–6, 2007.
- [15] R. Kulkarni and S. Biswanath, "Electrically responsive smart hydrogels in drug delivery: a review," *Journal of Applied Biomaterials and Biomechanics*, vol. 5, no. 3, pp. 125–139, 2007.
- [16] C. Wu, C. Chen, J. Lai, X. Mu, J. Zheng, and Y. Zhao, "Molecule-scale controlled-release system based on light-responsive silica nanoparticles," *Chemical Communications*, vol. 23, pp. 2662–2664, 2008.
- [17] M. D. Lavigne, S. S. Pennadam, J. Ellis, L. L. Yates, C. Alexander, and D. C. Gorecki, "Enhanced gene expression through temperature profile-induced variations in molecular architecture of thermoresponsive polymer vectors," *The Journal of Gene Medicine*, vol. 9, no. 1, pp. 44–54, 2007.
- [18] D. Schmaljohann, "Thermo- and pH-responsive polymers in drug delivery," *Advanced Drug Delivery Reviews*, vol. 58, no. 15, pp. 1655–1670, 2006.
- [19] J. Kost, "Intelligent drug delivery systems," in *Encyclopedia of Controlled Drug Delivery* (E. Mathiowitz, ed.), vol. 1, John Wiley & Sons, Inc., 1999.
- [20] J. Kost, K. Leong, and R. Langer, "Ultrasound-enhanced polymer degradation and release of incorporated substances - (controlled release drug delivery systems)," *Proceedings of the National Academy of Sciences of the United States of America*, vol. 86, no. 20, pp. 7663–7666, 1989.
- [21] S. Miyazaki, C. Yokouchi, and M. Takada, "External control of drug release - controlled release of insulin from a hydrophilic polymer implant by ultrasound irradiation in diabetic rats," *Journal of Pharmacy and Pharmacology*, vol. 40, no. 10, pp. 716–717, 1988.
- [22] A. D. Maxwell, C. A. Cain, A. P. Duryea, L. Yuan, H. S. Gurm, and Z. Xu, "Noninvasive thrombolysis using pulsed ultrasound cavitation therapy - histotripsy," *Ultrasound in Medicine and Biology*, vol. 35, no. 12, pp. 1982–1994, 2009.

- [23] N. B. Smith, "Perspectives on transdermal ultrasound mediated drug delivery," *International Journal of Nanomedicine*, vol. 2, no. 4, pp. 585–594, 2007.
- [24] R. Rao and S. Nanda, "Sonophoresis: recent advancements and future trends," *Journal of Pharmacy and Pharmacology*, vol. 61, no. 6, pp. 689–705, 2009.
- [25] G. C. Rosim, C. H. Barbieri, F. M. Lancas, and N. Mazzer, "Diclofenac phonophoresis in human volunteers," *Ultrasound in Medicine and Biology*, vol. 31, no. 3, pp. 337–343, 2005.
- [26] E. Kozanoglu, S. Basaran, R. Guzel, and F. Guler-Uysal, "Short term efficacy of ibuprofen phonophoresis versus continuous ultrasound therapy in knee osteoarthritis," *Swiss Medical Weekly*, vol. 133, no. 23-24, pp. 333–338, 2003.
- [27] B. Cagnie, E. Vinck, S. Rimbaut, and G. Vanderstraeten, "Phonophoresis versus topical application of ketoprofen: comparison between tissue and plasma levels," *Physical Therapy*, vol. 83, no. 8, pp. 707–712, 2003.
- [28] S. Mitragotri, D. Blankschtein, and R. Langer, "Transdermal drug delivery using low-frequency sonophoresis," *Pharmaceutical Research*, vol. 13, no. 3, pp. 411–420, 1996.
- [29] M. A. Cooper, *Pulsed cavitation ultrasound effects on tissue erosion and fluid transport*. PhD thesis, University of Michigan, Ann Arbor, MI, 2006.
- [30] R. Gramiak and P. M. Shah, "Echocardiography of the aortic root," *Investigative Radiology*, vol. 3, no. 5, pp. 356–366, 1968.
- [31] R. Diaz-Lopez, N. Tsapis, and E. Fattal, "Liquid perfluorocarbons as contrast agents for ultrasonography and ^{19}F -MRI," *Pharmaceutical Research*, vol. 27, no. 1, pp. 1–16, 2010.
- [32] M. A. Borden and M. L. Longo, "Dissolution behavior of lipid monolayer-coated, air-filled microbubbles: effect of lipid hydrophobic chain length," *Langmuir*, vol. 18, no. 24, pp. 9225–9233, 2002.
- [33] S. Hernot and A. L. Klibanov, "Microbubbles in ultrasound-triggered drug and gene delivery," *Advanced Drug Delivery Reviews*, vol. 60, no. 10, pp. 1153–1166, 2008.
- [34] J. E. Chomas, P. Dayton, J. Allen, K. Morgan, and K. W. Ferrara, "Mechanisms of contrast agent destruction," *IEEE Transactions on Ultrasonics, Ferroelectrics, and Frequency Control*, vol. 48, no. 1, pp. 232–248, 2001.
- [35] P. A. Dayton and J. J. Rychak, "Molecular ultrasound imaging using microbubble contrast agents," *Frontiers in Bioscience*, vol. 12, pp. 5124–5142, 2007.

- [36] A. L. Klibanov, “Ultrasound molecular imaging with targeted microbubble contrast agents,” *Journal of Nuclear Cardiology*, vol. 14, no. 6, pp. 876–884, 2007.
- [37] P. Epstein and M. Plesset, “On the stability of gas bubbles in liquid-gas solutions,” *Journal of Chemical Physics*, vol. 18, pp. 1505–1509, November 1950.
- [38] K. W. Ferrara, R. Pollard, and M. A. Borden, “Ultrasound microbubble contrast agents: fundamentals and application to gene and drug delivery,” *Annual Review of Biomedical Engineering*, vol. 9, pp. 425–447, 2007.
- [39] S. Tinkov, R. Bekeredjian, G. Winter, and C. Coester, “Microbubbles as ultrasound triggered drug carriers,” *Journal of Pharmaceutical Sciences*, vol. 98, no. 6, pp. 1935–1961, 2009.
- [40] D. Dalecki, “Mechanical bioeffects of ultrasound,” *Annual Review of Biomedical Engineering*, vol. 6, no. 1, pp. 229–248, 2004.
- [41] R. K. Schlicher, H. Radhakrishna, T. P. Tolentino, R. P. Apkarian, V. Zarnitsyn, and M. P. Prausnitz, “Mechanism of intracellular delivery by acoustic cavitation,” *Ultrasound in Medicine and Biology*, vol. 32, no. 6, pp. 915–924, 2006.
- [42] D. L. Miller, C. Dou, and J. Song, “DNA transfer and cell killing in epidermoid cells by diagnostic ultrasound activation of contrast agent gas bodies *in vitro*,” *Ultrasound in Medicine and Biology*, vol. 29, no. 4, pp. 601–607, 2003.
- [43] A. Kheirloom, P. A. Dayton, A. F. Lum, E. Little, E. E. Paoli, H. Zheng, and K. W. Ferrara, “Acoustically-active microbubbles conjugated to liposomes: characterization of a proposed drug delivery vehicle,” *Journal of Controlled Release*, vol. 118, no. 3, pp. 275–284, 2007.
- [44] I. Lentacker, B. G. D. Geest, R. E. Vandenroucke, L. Peeters, J. Demeester, S. C. D. Smedt, and N. N. Sanders, “Ultrasound-responsive polymer-coated microbubbles that bind and protect DNA,” *Langmuir*, vol. 22, no. 17, pp. 7273–7278, 2006.
- [45] M. A. Borden, C. F. Caskey, E. Little, R. J. Gillies, and K. W. Ferrara, “DNA and polylysine adsorption and multilayer construction onto cationic lipid-coated microbubbles,” *Langmuir*, vol. 23, no. 18, pp. 9401–9408, 2007.
- [46] J. Eisenbrey, P. Huang, J. Hsu, and M. Wheatley, “Ultrasound triggered cell death *in vitro* with doxorubicin loaded poly lactic-acid contrast agents,” *Ultrasonics*, vol. 49, no. 8, pp. 628–633, 2009.
- [47] M. S. Tartis, J. McCallan, A. F. Lum, R. LaBell, S. M. Stieger, T. O. Matsunaga, and K. W. Ferrara, “Therapeutic effects of paclitaxel-containing ultrasound contrast agents,” *Ultrasound in Medicine and Biology*, vol. 32, no. 11, pp. 1771–1780, 2006.

- [48] E. Unger, T. McCreery, R. Sweitzer, V. Caldwell, and Y. Wu, “Acoustically active lipospheres containing paclitaxel - a new therapeutic contrast agent,” *Investigative Radiology*, vol. 33, no. 12, pp. 886–892, 1998.
- [49] J. A. Kopechek, T. M. Abruzzo, B. Wang, S. M. Chrzanowski, D. A. Smith, P. H. Kee, S. Huang, J. H. Collier, D. D. McPherson, and C. K. Holland, “Ultrasound-mediated release of hydrophilic and lipophilic agents from echogenic liposomes,” *Journal of Ultrasound in Medicine*, vol. 27, no. 11, pp. 1597–1606, 2008.
- [50] M. P. Krafft, A. Chittofrati, and J. G. Riess, “Emulsions and microemulsions with a fluorocarbon phase,” *Current Opinion in Colloid and Interface Science*, vol. 8, no. 3, pp. 251–258, 2003.
- [51] J. G. Riess, “Oxygen carriers (“blood substitutes”) - raison d’etre, chemistry, and some physiology,” *Chemical Reviews*, vol. 101, no. 9, pp. 2797–2919, 2001.
- [52] G. M. Lanza and S. A. Wickline, “Targeted ultrasonic contrast agents for molecular imaging and therapy,” *Progress in Cardiovascular Diseases*, vol. 44, no. 1, pp. 13–31, 2001.
- [53] P. M. Morse and K. U. Ingard, *Theoretical Acoustics*. New York: McGraw-Hill, Inc., 1968.
- [54] M. Liu and D. Long, “Perfluorooctylbromide as a diagnostic contrast-medium in gastroenterography,” *Radiology*, vol. 122, no. 1, pp. 71–76, 1977.
- [55] R. Mattrey, F. Scheible, B. Gosink, G. Leopold, D. Long, and C. Higgins, “Perfluorooctylbromide: a liver/spleen-specific and tumor-imaging ultrasound contrast material,” *Radiology*, vol. 145, no. 3, pp. 759–762, 1982.
- [56] F. Forsberg, R. Roy, D. A. Merton, N. M. Rawool, J.-B. Liu, M. Huang, D. Kessler, and B. B. Goldberg, “Conventional and hypobaric activation of an ultrasound contrast agent,” *Ultrasound in Medicine and Biology*, vol. 24, no. 8, pp. 1143–1150, 1998.
- [57] L. M. Kornmann, D. M. Curfs, E. Hermeling, I. van der Made, M. P. de Winther, R. S. Reneman, K. D. Reesink, and A. P. Hoeks, “Perfluorohexane-loaded macrophages as a novel ultrasound contrast agent: a feasibility study,” *Molecular Imaging and Biology*, vol. 10, no. 5, pp. 264–270, 2008.
- [58] D. L. Miller, O. D. Kripfgans, J. B. Fowlkes, and P. L. Carson, “Cavitation nucleation agents for nonthermal ultrasound therapy,” *Journal of the Acoustical Society of America*, vol. 107, no. 6, pp. 3480–3486, 2000.
- [59] D. L. Miller and J. Song, “Lithotripter shock waves with cavitation nucleation agents produce tumor growth reduction and gene transfer *in vivo*,” *Ultrasound in Medicine and Biology*, vol. 28, no. 10, pp. 1343–1348, 2002.

- [60] G. Lanza, K. Wallace, M. Scott, W. Cacheris, D. Abendschein, D. Christy, A. Sharkley, J. Miller, P. Gaffney, and S. Wickline, “A novel site-targeted ultrasonic contrast agent with broad biomedical application,” *Circulation*, vol. 94, no. 12, pp. 3334–3340, 1996.
- [61] N. Soman, J. Marsh, G. Lanza, and S. Wickline, “New mechanisms for non-porative ultrasound stimulation of cargo delivery to cell cytosol with targeted perfluorocarbon nanoparticles,” *Nanotechnology*, vol. 19, no. 18, 2008.
- [62] D. Glaser, “Some effects of ionizing radiation on the formation of bubbles in liquids,” *Physical Review*, vol. 87, no. 4, p. 665, 1952.
- [63] M. Leone and N. Robotti, “A note on the Wilson cloud chamber (1912),” *European Journal of Physics*, vol. 25, no. 6, pp. 781–791, 2004.
- [64] R. E. Apfel, “Superheated drop detector,” *Nuclear Instruments and Methods*, vol. 162, no. 1-3, pp. 603–608, 1979.
- [65] R. E. Apfel, “Activatable infusible dispersions containing drops of a superheated liquid for methods of therapy and diagnosis,” Patent 5,840,276, Apfel Enterprises, Inc., November 1998.
- [66] O. D. Kripfgans, J. B. Fowlkes, D. L. Miller, O. P. Eldevik, and P. L. Carson, “Acoustic droplet vaporization for therapeutic and diagnostic applications,” *Ultrasound in Medicine and Biology*, vol. 26, no. 7, pp. 1177–1189, 2000.
- [67] M. L. Fabiilli, K. J. Haworth, I. E. Sebastian, O. D. Kripfgans, P. L. Carson, and J. B. Fowlkes, “Delivery of chlorambucil using an acoustically-triggered, perfluoropentane emulsion,” *Ultrasound in Medicine and Biology*, vol. 36, no. 8, pp. 1364–1375, 2010.
- [68] T. Giesecke and K. Hynynen, “Ultrasound-mediated cavitation thresholds of liquid perfluorocarbon droplets *in vitro*,” *Ultrasound in Medicine and Biology*, vol. 29, no. 9, pp. 1359–1365, 2003.
- [69] K.-I. Kawabata, N. Sugita, H. Yoshikawa, T. Azuma, and S.-I. Umemura, “Nanoparticles with multiple perfluorocarbons for controllable ultrasonically induced phase shifting,” *Japanese Journal of Applied Physics*, vol. 44, no. 6B, pp. 4548–4552, 2005.
- [70] O. D. Kripfgans, M. L. Fabiilli, P. L. Carson, and J. B. Fowlkes, “On the acoustic vaporization of micrometer-sized droplets,” *Journal of the Acoustical Society of America*, vol. 116, no. 1, pp. 272–281, 2004.
- [71] A. H. Lo, O. D. Kripfgans, P. L. Carson, and J. B. Fowlkes, “Spatial control of gas bubbles and their effects on acoustic fields,” *Ultrasound in Medicine and Biology*, vol. 32, no. 1, pp. 95–106, 2006.

- [72] A. H. Lo, O. D. Kripfgans, P. L. Carson, E. D. Rothman, and J. B. Fowlkes, “Acoustic droplet vaporization: effects of pulse duration and contrast agent,” *IEEE Transactions on Ultrasonics, Ferroelectrics, and Frequency Control*, vol. 54, pp. 933–946, May 2007.
- [73] N. Rapoport, D. A. Christensen, A. M. Kennedy, and K.-H. Nam, “Cavitation properties of block copolymer stabilized phase-shift nanoemulsions used as drug carriers,” *Ultrasound in Medicine and Biology*, vol. 36, no. 3, pp. 419–429, 2010.
- [74] A. Qamar, Z. Z. Wong, J. B. Fowlkes, and J. L. Bull, “Dynamics of acoustic droplet vaporization in gas embolotherapy,” *Applied Physics Letters*, vol. 96, no. 14, 2010.
- [75] O. D. Kripfgans, J. B. Fowlkes, M. Woydt, O. P. Eldevik, and P. L. Carson, “*In vivo* droplet vaporization for occlusion therapy and phase aberration correction,” *IEEE Transactions on Ultrasonics, Ferroelectrics, and Frequency Control*, vol. 49, no. 2, pp. 726–738, 2002.
- [76] K. J. Haworth, J. B. Fowlkes, P. L. Carson, and O. D. Kripfgans, “Towards aberration correction of transcranial ultrasound using acoustic droplet vaporization,” *Ultrasound in Medicine and Biology*, vol. 34, pp. 435–445, March 2008.
- [77] O. D. Kripfgans, C. M. Orifici, P. L. Carson, K. A. Ives, O. P. Eldevik, and J. B. Fowlkes, “Acoustic droplet vaporization for temporal and spatial control of tissue occlusion: a kidney study,” *IEEE Transactions on Ultrasonics, Ferroelectrics, and Frequency Control*, vol. 52, pp. 1101–1110, July 2005.
- [78] M. Zhang, M. L. Fabiilli, K. J. Haworth, J. B. Fowlkes, O. D. Kripfgans, W. Roberts, K. A. Ives, and P. L. Carson, “Initial investigation of acoustic droplet vaporization for occlusion in canine kidney,” *Ultrasound in Medicine and Biology*, vol. 36, no. 10, pp. 1691–1703, 2010.
- [79] A. Calderón, J. B. Fowlkes, and J. L. Bull, “Bubble splitting in bifurcating tubes: a model study of cardiovascular gas emboli transport,” *Journal of Applied Physiology*, vol. 99, no. 2, pp. 479–487, 2005.
- [80] B. Eshpuniyani, J. B. Fowlkes, and J. L. Bull, “A boundary element model of microbubble sticking and sliding in the microcirculation,” *International Journal of Heat and Mass Transfer*, vol. 51, no. 23-24, pp. 5700–5711, 2008.
- [81] T. Ye and J. L. Bull, “Direct numerical simulations of micro-bubble expansion in gas embolotherapy,” *Journal of Biomechanical Engineering*, vol. 126, no. 6, pp. 745–759, 2004.
- [82] K.-I. Kawabata, R. Asami, T. Azuma, H. Yoshikawa, and S.-I. Umemura, “Cavitation assisted HIFU with phase-change nano droplet,” *IEEE Ultrasonics Symposium*, vol. 1-4, pp. 780–783, 2008.

- [83] M. Zhang, M. L. Fabiilli, P. L. Carson, F. R. Padilla, S. D. Swanson, O. D. Kripfgans, and J. B. Fowlkes, “Acoustic droplet vaporization for the enhancement of ultrasound thermal therapy,” *IEEE International Ultrasonics Symposium*, 2010.
- [84] P. Zhang and T. Porter, “Ultrasound-induced thermal lesion formation with phase shift emulsion,” *8th International Symposium on Therapeutic Ultrasound*, September 2008.
- [85] J. Y. Fang, C. F. Hung, M. H. Liao, and C. C. Chien, “A study of the formulation design of acoustically active lipospheres as carriers for drug delivery,” *European Journal of Pharmaceutics and Biopharmaceutics*, vol. 67, no. 1, pp. 67–75, 2007.
- [86] N. Rapoport, Z. Gao, and A. Kennedy, “Multifunctional nanoparticles for combining ultrasonic tumor imaging and targeted chemotherapy,” *Journal of the National Cancer Institute*, vol. 99, no. 14, pp. 1095–1106, 2007.
- [87] J. Y. Fang, C. F. Hung, S. C. Hua, and T. L. Hwang, “Acoustically active perfluorocarbon nanoemulsions as drug delivery carriers for camptothecin: drug release and cytotoxicity against cancer cells,” *Ultrasonics*, vol. 49, no. 1, pp. 39–46, 2009.
- [88] T. L. Hwang, Y. J. Lin, C. H. Chi, T. H. Huang, and J. Y. Fang, “Development and evaluation of perfluorocarbon nanobubbles for apomorphine delivery,” *Journal of Pharmaceutical Sciences*, vol. 98, no. 10, pp. 3735–3747, 2009.
- [89] N. Y. Rapoport, A. M. Kennedy, J. E. Shea, C. L. Scaife, and K.-H. Nam, “Controlled and targeted tumor chemotherapy by ultrasound-activated nanoemulsions/microbubbles,” *Journal of Controlled Release*, vol. 138, no. 2, pp. 268–276, 2009.
- [90] N. Rapoport, K. Nam, Z. Gao, and A. Kennedy, “Application of ultrasound for targeted nanotherapy of malignant tumors,” *Acoustical Physics*, vol. 55, no. 4-5, pp. 586–593, 2009.
- [91] N. Rapoport, A. M. Kennedy, J. E. Shea, C. L. Scaife, and K.-H. Nam, “Ultrasonic nanotherapy of pancreatic cancer: lessons from ultrasound imaging,” *Molecular Pharmaceutics*, vol. 7, no. 1, pp. 22–31, 2010.
- [92] M. L. Fabiilli, J. A. Lee, O. D. Kripfgans, P. L. Carson, and J. B. Fowlkes, “Delivery of water-soluble drugs using acoustically-triggered, perfluorocarbon double emulsions,” *Pharmaceutical Research*, accepted September 2010.

CHAPTER II

The Role of Inertial Cavitation in Acoustic Droplet Vaporization

2.1 Introduction

Emulsions containing micron and nanometer-sized perfluorocarbon (PFC) droplets are being studied in diagnostic and therapeutic applications of ultrasound (US). For example, the use of PFC nanodroplets has been explored in US molecular imaging and the targeted delivery of therapeutic agents [1–4]. Another research area is acoustic droplet vaporization (ADV), where a superheated, micron-sized liquid droplet - stabilized by a surfactant shell - is phase-transitioned into a gas bubble using US. The superheated liquid is a straight-chain PFC, which belongs to a class of compounds that are inert, hydrophobic, lipophobic, and biocompatible [5]. The therapeutic potentials of ADV were described by Apfel [6] and Kripfgans *et al.* [7] in applications such as embolotherapy and drug delivery. Additional applications of ADV include its use in phase aberration correction [8; 9].

Micron-sized PFC droplets can be systemically administered - either intra-arterially or intravenously - and greater than 95% (by number) of the droplets are small enough to pass through capillaries without producing obstructions [10]. Upon ADV, the generated bubbles grow to typically five to six times that of the original droplet diameter [7]. Therefore, upon vaporization, the bubbles can become lodged within capillaries, thus selectively occluding blood flow to targeted tissues or organs.

The use of ADV in occlusion therapy has been successfully demonstrated *in vivo* in canine [8] and lepus [11] models to reduce cerebral and renal perfusion, respectively. The *in vitro* ADV of nanometer-sized PFC droplets has also been demonstrated [12].

The physical mechanisms involved in ADV are not clearly understood. The optimization of ADV for therapeutic applications can be potentially enhanced by elucidating the mechanisms involved in the ADV process. One proposed mechanism is acoustic cavitation, which can be defined as the creation, growth, and/or collapse of a bubble or cavity within a fluid when the fluid is exposed to an acoustic pressure field [13]. It has been found that the tensile strength of a liquid is much lower than the theoretical tensile strength due to the presence of cavitation nuclei within the fluid [14]. Two general types of cavitation exist - stable and inertial [15] - although there has been considerable debate about the terminology used. Stable cavitation is the oscillation, both linear or non-linear, of a bubble about an equilibrium size. The oscillation can continue for many cycles of acoustic pressure. Inertial cavitation (IC) occurs when the bubble diameter grows to at least twice its original diameter, generally during a single cycle of acoustic pressure [13]. The bubble then collapses violently, driven by the inertia of the fluid, potentially fragmenting into many smaller bubbles. Such cavitation can occur repetitively and even within a single bubble. The bioeffects of IC, which stem from the generated high temperatures, pressures, and velocities (i.e. shock wave and liquid jet formation), include cellular erosion or lysis, molecular degradation, and the formation of free radicals [15; 16]. In the case of embolotherapy, the minimization of these bioeffects may be important to prevent the extravasation of blood components, which could reduce the efficacy of ADV-induced embolotherapy. Alternatively, these bioeffects could enhance drug delivery via sonoporation, as highlighted in a recent review [17].

The cavitation process is started by nucleation, either within the fluid itself due to thermal motion, termed *homogeneous*, or at a boundary between the fluid and

another surface, termed *heterogeneous*. In most practical situations, heterogeneous nucleation is more common since homogeneous nucleation tends to require higher rarefactional pressures. However, the body contains few, if any, cavitation nuclei that can be activated by diagnostic US pulses [18], and the probability of homogenous nucleation within the body using diagnostic US is expected to be rare [19]. Therefore, the introduction of materials within the body, such as microbubbles or droplets, may serve as cavitation nuclei depending on the rarefactional pressure levels of applied diagnostic or therapeutic US. Hence, the mechanical index (MI) is used as a metric to determine the susceptibility of IC with diagnostic US scanners.

The nucleation of ADV can occur in three regions: within the droplet core (i.e. PFC phase); adjacent to the surfactant shell (either inside or outside of the droplet); and external to the droplet within the bulk fluid phase. Previous work demonstrated that the ADV threshold at 1.44 MHz decreased when US contrast agent was present with the droplets [20]. In this case, it was surmised that the microbubbles acted as cavitation nuclei external to the droplet. Counter to this however, micrographs, taken using a high-speed camera, of single droplets undergoing ADV indicate that the nucleation location is within the imaged cross section of the droplet, when using transducers in the 3 to 10 MHz range with microsecond pulse lengths [21].

A previous study measured the *in vitro*, IC threshold of micron-sized PFC droplets as a function of droplet composition and US parameters [22]. This study investigates the relationship between ADV and IC, specifically the necessity of IC for ADV to occur, and adds insight into the location of ADV nucleation. The threshold pressures required to induce ADV and IC are simultaneously determined in an *in vitro* setup. The materials and methods, including ADV and IC threshold determination, utilized in this study are described in Section 2.2. Parameters that are known to influence both thresholds - bulk fluid properties such as gas saturation, temperature, viscosity, and surface tension; droplet parameters such

as degree of superheat, surfactant type, and size; and acoustic properties such as pulse repetition frequency and pulse width - are investigated with the intent of determining experimental conditions that yield ADV without IC and ADV with IC. These results are presented and discussed in Section 2.3, with a focus on connecting the experimental results with possible mechanisms involved in ADV. Section 2.4 describes conclusions concerning the ADV mechanism that are supported by the results in Section 2.3, as well as discussing similarities between the observed trends for the ADV and IC thresholds.

2.2 Materials and Methods

2.2.1 PFC Droplets

Albumin droplets were prepared according to a method established by Kripfgans *et al.* [7]. Briefly, 750 μL of 4 mg/mL bovine albumin (Sigma-Aldrich, St. Louis, MO, USA) in normal saline (0.9% w/v, Hospira Inc., Lake Forest, IL, USA) was added to a 2 mL glass vial (Shamrock Glass, Seaford, DE, USA). Liquid PFC - either perfluoro-n-pentane (C_5F_{12} , Alfa Aesar, Ward Hill, MA, USA), perfluoro-n-hexane (C_6F_{14} , SynQuest Labs Inc., Alachua, FL, USA), or perfluoro-n-octane (C_8F_{18} , Alfa Aesar) - was added gravimetrically to produce a final PFC volume fraction of 25%. Table 2.1 lists the different PFC core materials that were tested. The vial was sealed with a rubber stopper (Shamrock Glass) and metal cap (Shamrock Glass). The vial was then shaken for 45 seconds at 4550 cycles per minute using an amalgamator (VialMix, Lantheus Medical Imaging, Billerica, MA, USA).

Lipid droplets were made in a similar manner using 750 μL of a lipid blend rather than albumin. The blend consisted of 5 mg/mL 1,2-dipalmitoyl-*sn*-glycero-3-phosphocholine (DPPC, Avanti Polar Lipids, Alabaster, AL, USA) and 0.2 mg/mL 1,2-dipalmitoyl-*sn*-glycero-3-phosphate monosodium salt (DPPA, Avanti Polar Lipids) dissolved in propylene glycol (Acros Organics, Morris Plains, NJ, USA),

Table 2.1: Boiling points (T_b) of PFCs used to make emulsions and average droplet diameters, including standard deviations of the means, of the resulting emulsions. The emulsions were sized one day after their formulation so no significant Ostwald ripening has occurred. The average number density, including the standard deviation of the mean, is listed for the undiluted emulsions.

Name	Formula	CAS #	Abbreviation	T_b (°C)	Mean diameter (μm)	Mean number density ($\times 10^9$, number per mL)
Perfluoro-n-pentane	C_5F_{12}	678-26-2	PFP	29	2.09 ± 0.02	4.28 ± 0.05
Perfluoro-n-hexane	C_6F_{14}	355-42-0	PFH	56	2.20 ± 0.06	3.51 ± 0.20
Perfluoro-n-octane	C_8F_{18}	307-34-6	PFO	100	2.63 ± 0.04	4.20 ± 0.30

which was heated to 50°C . The resulting solution was then diluted with an equal volume of an 8:1 volumetric ratio of normal saline to glycerol (Sigma Aldrich) to produce the final lipid blend. PFC was then added gravimetrically and the vial sealed and shaken in the same manner as the albumin droplets.

The shaken vials were refrigerated (5°C) overnight prior to use. A droplet pre-dilution, used for sizing and flow tube experiments, was made by diluting 1 vial of droplets to 10 mL with normal saline that had been filtered with a syringe filter ($0.22 \mu\text{m}$, Millex GV, Millipore Co., Bedford, MA, USA). A Coulter counter (Multisizer 3, Beckman Coulter Inc., Fullerton, CA, USA) with a $50 \mu\text{m}$ aperture was used to determine the number and size of the resulting droplet solutions.

2.2.2 Experimental Setup

All experiments were conducted in a tank ($40 \times 60 \times 27 \text{ cm}$) containing degassed, deionized water heated to 37°C (Ex 7, ThermoNESLAB, Newington, NH, USA), unless otherwise noted. A calibrated 3.5 MHz single-element transducer (1.9 cm diameter, 3.81 cm focal length, A381S, Panametrics, Olympus NDT Inc., Waltham, MA, USA) was focused at the center of dialysis tubing (14.6 mm diameter, Spectra/Por, Spectrum Laboratories Inc., Laguna Hills, CA, USA), which was used as a flow tube. A droplet solution, containing approximately 9×10^4 droplets per milliliter, was prepared by adding $100 \mu\text{L}$ of the droplet pre-dilution to 500 mL of degassed, deionized water heated to the same temperature as the tank water, unless

otherwise noted. The same number density of droplets was used for all trials. By comparison, the droplet concentration used for previous lepus studies [11], assuming an average rabbit weight of 2.5 kg and a cardiac output of 250 mL per minute [23], was 6.4×10^5 droplets per mL. The droplet solution was pumped (Masterflex pump and speed controller, Cole-Parmer, Chicago, IL, USA) at $2 \text{ cm}\cdot\text{s}^{-1}$ (average linear speed in flow tube) against gravity in a recirculated manner from a 500 mL stirred flask. The single-element transducer was used to generate ADV while cross-sectional B-mode cineloops were simultaneously collected downstream using a 10 MHz linear array (L9, GE Healthcare, Milwaukee, WI, USA). Note that the imaging array is purposefully located downstream of the single-element transducer so that the imaging acoustics cannot impact the vaporization acoustics. A schematic of the setup is displayed in Fig. 2.1.

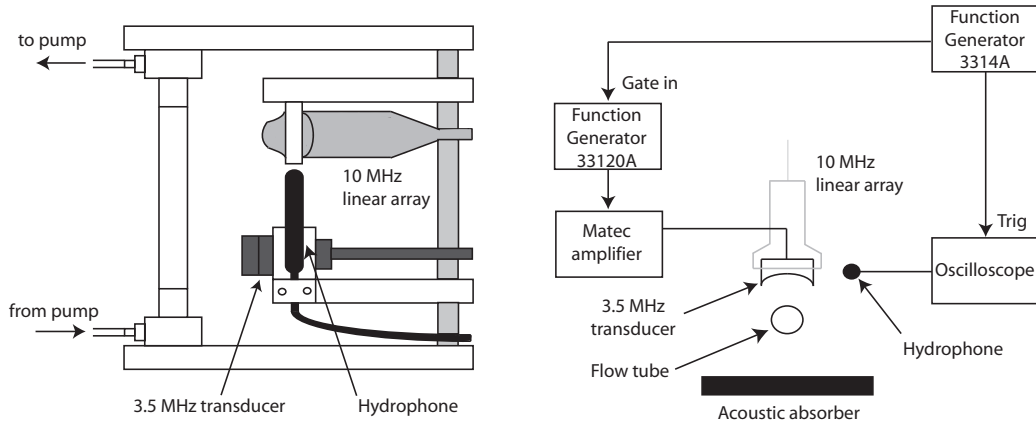


Figure 2.1: Side (left) and top (right) views of the *in vitro* setup used for measuring ADV and IC in flow. A 3.5 MHz single element transducer vaporized the flowing droplets while a 10 MHz linear array recorded cineloops; IC noise was simultaneously detected using the hydrophone.

Acoustic pulses sent to the single-element transducer were achieved using a master function generator (33120A, Agilent Technologies, Palo Alto, CA, USA) gated by a secondary function generator (3314A, Agilent Technologies). The gated output signal was sent to a power amplifier (60 dB, Model 350, Matec, Northborough, MA, USA). IC noise was passively detected using an omnidirectional

hydrophone (ITC-1089D, International Transducer Co., Santa Barbara, CA, USA) and radiofrequency (RF) segments ($n = 100$, 10 MHz sampling) were digitized using an oscilloscope (9314L, LeCroy, Chestnut Ridge, NY, USA), which was triggered with each transmitted acoustic pulse. A passive acoustic detector was used to detect IC since it has been demonstrated that an active detector can affect the cavitation process [24], especially considering the nature of this experiment where droplet vaporization is triggered acoustically. The gas content of both the tank water and the recirculated fluid was measured using a blood-gas analyzer (ABL5, Radiometer, Westlake, OH, USA). All ADV and IC measurements were taken while the fluid was being recirculated since it was confirmed, using the Coulter counter, that only a small fraction of the droplets were vaporized over the course of each run due to the relatively short on-time of the single-element transducer. The flow tube and pump tubing were thoroughly flushed with degassed, deionized water between runs to eliminate carryover of any residual droplets or bubbles. A new droplet solution was prepared for each run. Each run consisted of cycling through a range of acoustic pressures from the single-element transducer for the combination of parameters being interrogated for that particular run. By analyzing the range of pressures tested, it was possible to determine the ADV and IC thresholds (see next section).

2.2.3 ADV and IC Data Analysis

The recorded B-mode images were analyzed for an increase in echogenicity due to the presence of stable bubbles. The mean echo power (MEP) was computed, as seen in Eq. 2.1, using MATLAB (The MathWorks, Inc., Natick, MA, USA) from the decompressed amplitude data of the collected cineloops, where the compression algorithm used in the US system was reversed. Similar to the mean echo amplitude (MEA) [7], MEP is the sum of the squared amplitude (A) at pixel (i,j) for frame number (m) that has dimensions M by N .

$$MEP(m) = \frac{1}{MN} \sum_{i=1}^M \sum_{j=1}^N A^2(i, j) \quad (2.1)$$

As seen in Fig. 2.2, a circular region of interest, consisting of the entire interior of the flow tube cross section, was used for the MEP calculations. Each cine-loop (17 Hz frame rate, MI = 0.2) was 10 seconds in duration, with 3 seconds captured with the single-element transducer off. As seen in Fig. 2.2, each cine-loop consisted of four regions. A differential MEP value, Eq. 2.2, was used in this work so that any increases in baseline echogenicity due to the interference pattern from the single-element transducer were accounted for.

$$\Delta MEP = MEP_4 - MEP_2 \quad (2.2)$$

MEP_2 and MEP_4 are the mean MEP values of regions 2 and 4, respectively. MEP_2 includes the interference from the single-element transducer, but does not contain ADV-generated bubbles due to the spatial separation between the single-element transducer and the imaging array. It was confirmed, using polystyrene spheres (1-50 μm or 381 μm , Duke Scientific, Palo Alto, CA, USA) as IC nuclei, without droplets, that any bubbles produced by IC (detected by the hydrophone as described next) in the bulk fluid, but not associated with ADV, were not detected by the imaging array due to their collapse, fragmentation and/or dissolution. The bubble dissolution model [25] in a static fluid predicts that an air bubble would have to be at least 8 μm in diameter for the bubble to persist long enough to travel from its generation location (the focus of the single-element transducer) to the imaging plane of the linear array. Since only gas bubbles produced by ADV are stable or large enough, versus bubbles produced by the IC of the bulk fluid, MEP is a direct measure of bubbles produced by ADV.

The presence of IC in the RF segments was determined relative to a baseline

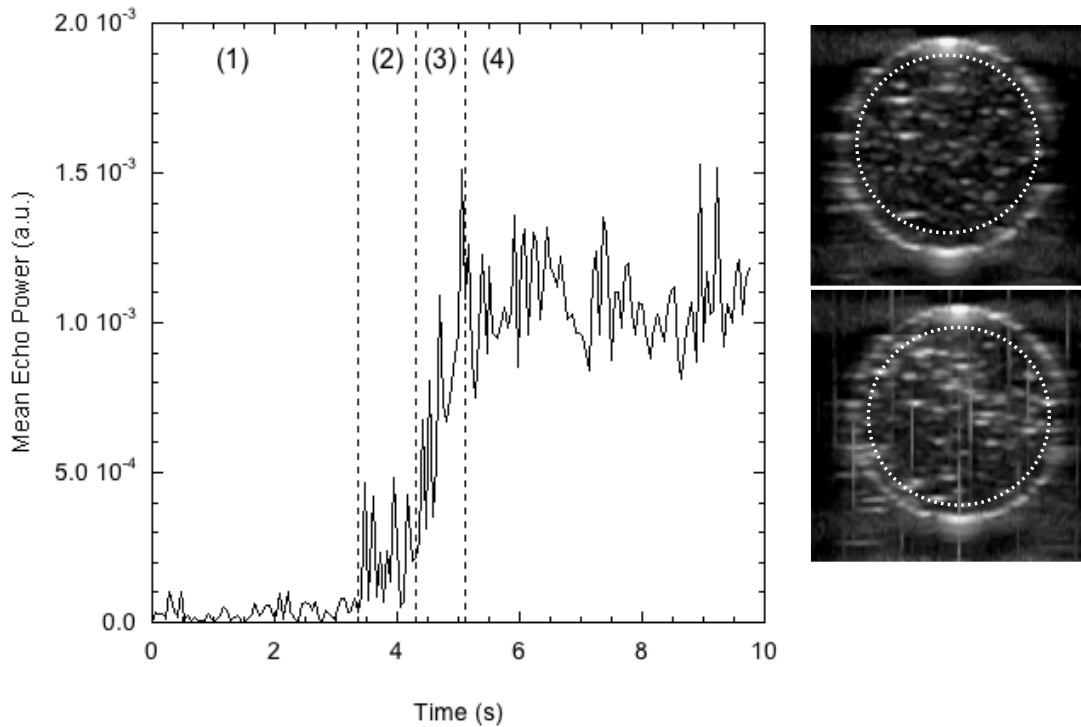


Figure 2.2: Left: MEP as a function of time for four different regions: US off (region 1); US on but no bubbles in the linear array field of view (FOV) (region 2); US on and the initial wave of bubbles appears in the linear array FOV, prior to achieving a steady state (region 3); US on with a steady state number of bubbles in the linear array FOV (region 4). Right: B-mode frames (compressed intensity scale) of a flow tube in region 1 (top) and region 4 (bottom). The exterior boundary of the region of interest used to calculate the MEP is denoted as a white, dashed circle.

of degassed water, where it was observed that no IC occurred. Figure 2.3 displays example RF and spectral data for a segment with and without IC. The integrated Fourier transform (IFT) in the range 5 to 60 kHz was used to differentiate segments with and without IC. The criterion for a segment containing IC, at a given acoustic pressure (P), is given in Eq. 2.3 where $IFT_{cav,P}$ is the IFT of a segment containing IC at acoustic pressure P , $IFT_{degas,P}$ is the IFT of the degassed water at acoustic pressure P , and σ is the standard deviation.

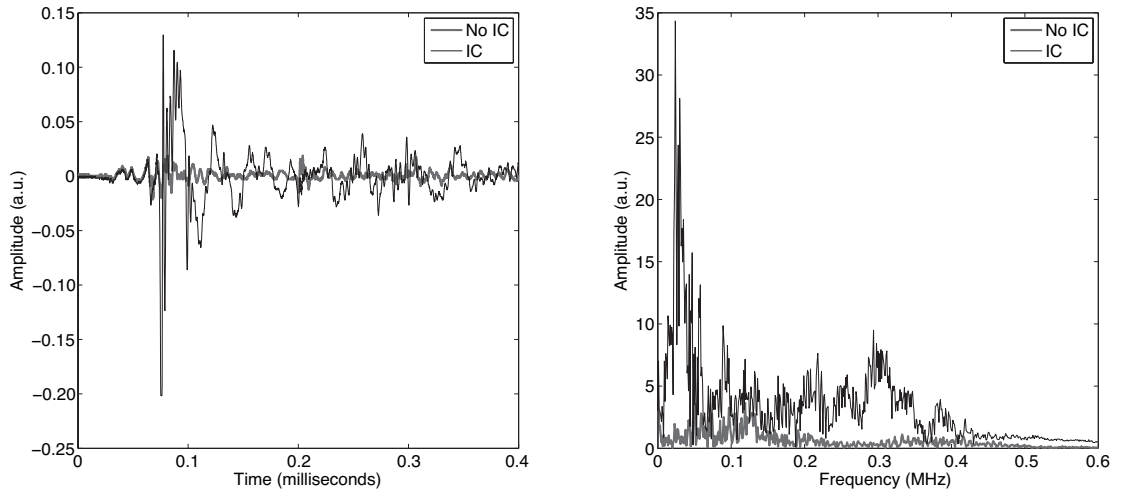


Figure 2.3: Left: RF data of a segment with and without IC. Right: Fourier transforms of RF data from left, showing the large spectral differences between a segment with and without IC. The following conditions were used: degassed water at 37°C with albumin-coated PFP droplets, 83 Hz PRF, 13 cycles, and 6.2 MPa.

$$IFT_{cav,P} \geq \text{mean}(IFT_{degas,P}) + 9 \cdot \sigma(IFT_{degas,P}) \quad (2.3)$$

Nine standard deviations were empirically chosen as a threshold to distinguish an IC event from the increase in acoustic backscatter due to the presence of droplets alone. As seen in Fig. 2.4, the calculated IC threshold is directly correlated with the number of standard deviations used to determine the threshold. However, from three to nine standard deviations the threshold increases only slightly. The 0.6 MPa increase in the IC threshold as the number of standard deviations is increased

from one to nine is smaller than the difference between the ADV and IC thresholds (see Section 2.3). Therefore, nine standard deviations minimizes the probability of falsely predicting IC at lower rarefactional pressures and reduces the variability of the calculated IC threshold while maintaining sensitivity to correctly detecting IC events. The RF data was processed using MATLAB. Each IC data point consists of the average of three runs with 100 RF lines collected for each run.

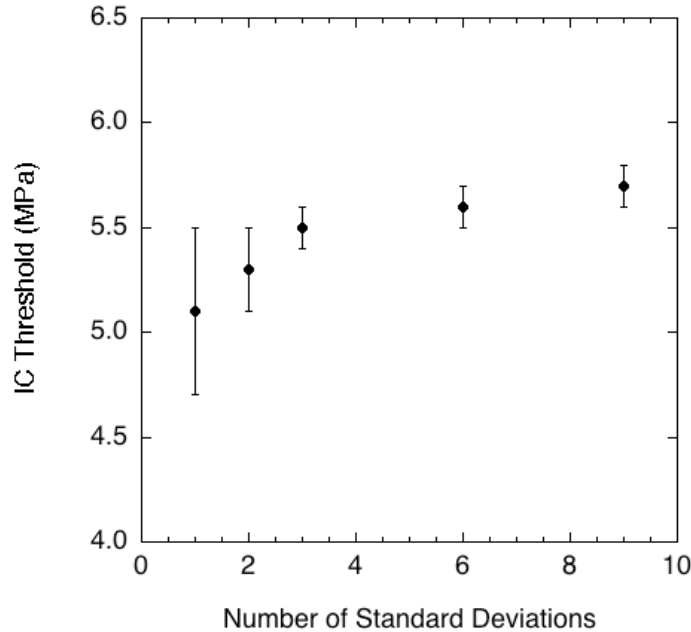


Figure 2.4: The effect of varying the number of standard deviations - $\sigma(IFT_{degas,P})$ - on the calculated peak rarefactional pressure IC threshold. Refer to Eq. 2.3 for the criterion used to determine the presence of IC in an RF segment. The average ($n = 3$) IC thresholds, plotted with the respective standard deviations, are from the following experimental conditions: degassed water at 37°C with albumin-coated PFP droplets, 83 Hz PRF, and 13 cycles.

2.2.4 ADV and IC Threshold Determination

Figure 2.5 displays an example of the normalized MEP and the percent of segments containing IC, which is the ratio of segments containing an IC event (defined according to the previous criterion) to the total number of collected segments, versus the peak rarefactional pressure for a given experimental condition. The raw MEP data was normalized, vertically shifted by 10^{-4} and scaled by 10^5 , to

facilitate display in Fig. 2.5. Two methods have been previously used to determine the ADV threshold. In the first method [7], the ADV threshold was the peak rarefactional pressure at the intersection of two line segments fit to the flat baseline portion and the upward sloping portion of the ADV data (peak rarefactional pressure versus MEA). In the second method [20], the slope between adjacent points in the ADV data was calculated. The threshold was defined as the pressure at which this slope exceeded a certain criterion. This work uses a refined version of the previously used slope method [20]. The data in each curve was fit to a sigmoid (Eq. 2.4), where m_1 is the maximum y -value, m_2 is the minimum y -value, m_3 is the x -value at the midpoint of y , and m_4 is the slope at the y -midpoint.

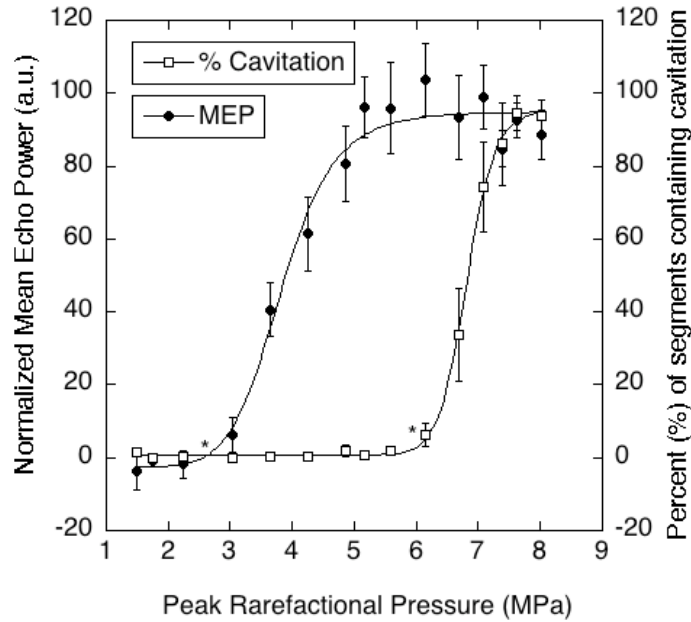


Figure 2.5: Mean ($n = 6$) normalized MEP and IC data plotted along with the respective sigmoidal curve fits and standard deviation at each data point. The raw MEP data was normalized - vertically shifted by 10^{-4} and scaled by 10^5 - to facilitate display on this plot. The threshold for each curve is denoted by an asterisk (*). The following conditions were used: degassed water at 37°C with albumin-coated PFP droplets, 83 Hz PRF, and 13 cycles.

$$y = m_1 + \frac{m_2 - m_1}{1 + \left(\frac{x}{m_3}\right)^{m_4}} \quad (2.4)$$

The ADV and IC thresholds were defined as the pressures where the slope of the sigmoidal curve fit exceeded a predefined value (10^{-4} for raw MEP and 1 for IC). The predefined values were determined by observing the values of the derivative at the pressure threshold as determined by the two line intersection approach for a small subset of data. The predefined value was then applied to all of the data sets. The sigmoid derivative method was used in general because it is not as susceptible to variance in the experimental data. The locations of the derivative thresholds for both the ADV and IC curves are denoted in Fig. 2.5 by asterisks.

2.3 Results and Discussion

2.3.1 Bulk Fluid Parameters

Table 2.2 displays the ADV and IC thresholds for albumin-coated perfluoro-n-pentane (PFP) droplets in different bulk fluids used. The thresholds in heparinized whole blood, water, and water-glycerol mixtures were measured to determine the impact of gas saturation, viscosity, and surface tension. Heparin (Elkins-Sinn Inc., Cherry Hill, NJ, USA) was added to whole, canine blood (8 units per mL blood) to prevent coagulation; the blood was used within 2 hours of withdrawal. The ADV threshold is lower than the IC threshold for the presented cases ($p < 0.001$). In the case of gas saturation, both the ADV ($p = 0.7$) and the IC ($p = 0.4$) thresholds were not statistically different for the degassed and gas saturated conditions. Additionally, the presence of droplets caused the IC threshold to decrease for the degassed water condition while the IC threshold was not statistically different ($p = 0.1$) in the gas saturated water condition. Increasing the gas saturation of a highly filtered bulk fluid, containing polystyrene spheres as nuclei, is known to decrease the IC threshold for heterogeneous nucleation [26]. The rate at which a bubble dissolves increases as the dissolved gas concentration of the bulk fluid decreases; the dissolved gas concentration is also known to affect the nucleation threshold [26]. This lack

of gas saturation dependence on the IC threshold may be explained with three relevant scenarios. First, the wettability of the albumin surface, adjacent to the bulk fluid, may be so high that there are few hydrophobic crevices with gas nuclei present. Second, there are still enough gas nuclei on the droplet exterior, even in the degassed fluid, to be above the critical concentration of nuclei necessary for IC. Third, IC occurs only when gas bubbles are present, presumably created via ADV. Therefore, since the ADV threshold did not display a dependence on gas saturation, then neither would the IC threshold. The ADV findings are consistent with results found by Kripfgans, who noted no difference in the ADV threshold in degassed or gas saturated fluids [27]. This result goes towards rejecting the hypothesis that heterogeneous nucleation causes the IC measured in this experimental setup.

Table 2.2: The effect of bulk fluid gas saturation, surface tension, and viscosity on the mean ($n = 5$) ADV and IC thresholds. All fluids were heated to 37°C and contained albumin-coated, PFP droplets at a concentration of 9×10^4 droplets per mL. The IC threshold of gas-saturated water without droplets, tested under the same conditions, was 5.6 ± 0.2 MPa while no IC was observed for degassed water without droplets.

Fluid	Gas Saturation (mmHg O ₂)	Density (g/mL)	Surface Tension (mN/m)	Viscosity (mPa·s)	Rarefactional ADV Threshold (MPa)	Rarefactional IC Threshold (MPa)
Water	60	0.995	72	0.7	2.7 ± 0.2	5.7 ± 0.4
Water	170	0.995	72	0.7	2.8 ± 0.1	6.0 ± 0.3
Whole Blood	141	1.059	48	5.0	3.6 ± 0.3	7.1 ± 0.1
Glycerol (60 wt%)	60	1.146	66.9	5.2	3.3 ± 0.1	> 8.0
Glycerol (80 wt%)	60	1.199	65.7	24.7	3.8 ± 0.2	> 8.0

In the tested cases, an increase in both the ADV and IC thresholds was observed in whole, heparanized canine blood as well as aqueous solutions of glycerol. The relationship between the IC threshold and fluid properties such as surface tension and viscosity has been derived by Holland and Apfel [28]. Assuming the presence of preexisting bubbles, the IC threshold should scale directly with the bulk fluid viscosity [28]. Our data is qualitatively consistent with this as the IC threshold increased with increasing bulk fluid viscosity. Concerning surface tension, an experimental study by Holland and Apfel - which measured the IC cavitation

threshold of polystyrene spheres in water or an ethylene glycol solution - noted a lower IC threshold in the ethylene glycol solution, which was attributed to the reduction in surface tension [29]. For submicron-sized nuclei, the effects of decreasing surface tension dominate, even in the case of increasing viscosity [28]. Given that the viscosity trend and not the surface tension trend was observed, it is likely that the IC nuclei for this experiment were not submicron in size, suggesting that the bubbles generated by ADV were the IC nuclei.

The ADV results in whole blood are consistent with previous findings [7]. No IC was observed in the glycerol solutions with PFP droplets for the tested pressures. Church proposes a higher IC threshold in blood due to the extra damping associated with the higher blood viscosity [30]. It is hypothesized that bulk fluids of higher viscosity retard the expansion of the ADV nucleus, possibly even causing a recondensation of the vaporized nucleus at lower acoustic pressures. Therefore larger rarefactional pressures are required to overcome this effect.

2.3.2 Droplet Parameters

Apfel patented the use of superheated immiscible droplets in medical applications and experimentally showed that the vaporization threshold of such droplets can be controlled using chemical ad-mixtures [6]. Droplets composed of a highly superheated dispersed phase, relative to normal body temperature, could be vaporized with less energy than droplets with a lower degree of superheat. The degree of superheat is defined as the difference between the bulk fluid (or body) temperature and the bulk boiling point of the dispersed phase. An example of the ad-mixture approach was published by Kawabata *et al.*, in which the ADV threshold of a PFC emulsion was adjusted by varying the ratio of PFP to 2H,3H-perfluoropentane [12]; the latter component has a boiling point of 53.5°C. Table 2.1 lists the different PFC core materials that were tested in our experiments as a function of degree of superheat. The bulk fluid temperature was adjusted and it was assumed, due to the small size of

the droplets, that the droplets equilibrated to the bulk fluid temperature before they were circulated to the focus of the vaporization transducer. Due to the increased pressure within the droplets, described by the Laplace equation, the boiling point of the dispersed phase increases, relative to the bulk PFC boiling point, as the diameter of the droplet decreases [31; 32]. The increase in droplet diameter from PFP to PFH to PFO is attributed to the increase in viscosity across the homologous PFC series, since increasing the viscosity of an emulsion phase causes an increase in particle size [33]. Unless otherwise stated, the droplets used in the experiments had a mean diameter as listed in Table 2.1 .

The behaviors of the ADV and IC thresholds as a function of superheat are displayed in Fig. 2.6. All tested cases reveal an ADV threshold that is lower than the IC threshold ($p < 0.01$ for both PFP and PFH droplets). For both thresholds, an inversely proportional trend exists for negative degrees of superheat. In the case of PFH droplets, the 95% confidence interval (CI) of the slope through the IC data, for negative degrees of superheat is [-0.07, -0.02] with the squared correlation coefficient (R^2) equal to 0.99, thus indicating a non-zero slope. For positive degrees of superheat, the ADV threshold remains relatively constant (95% CI of the slope of the PFP data is [-0.03, 0.01]) as well as the IC threshold (95% CI of the slope of the PFP data is [-0.07, 0.01]). No ADV or IC was observed for PFP, PFH, or PFO droplets at 19°C, 25°C, and 63°C below their respective bulk boiling points. An IC threshold was observed for PFP and PFH droplets at 11°C and 19°C, respectively, below the bulk boiling points, though no corresponding ADV was recorded. It is likely that both ADV and IC occurred in these cases, but the resulting bubbles of PFP or PFH gas either condensed or dissolved into the surrounding bulk fluid before reaching the linear array. Therefore using the setup seen in Fig. 2.1, there are three regions of activity for droplets with negative degrees of superheat: no ADV or IC detected, IC without detected ADV, and both ADV and IC detected. However, if

the experimental setup allowed for the imaging of bubbles generated at the focus of the vaporization transducer, there are likely only two regions of activity - no ADV or IC and both ADV and IC. The functional dependence of IC on the degree of superheat, at least below the bulk PFC boiling point (i.e. negative degrees of superheat), suggests that the event leading to IC is internal to the droplet. If the ADV or IC nucleus were external to the droplet, then the probability of an IC event external to the droplet should be relatively constant regardless of whether the PFC is or is not superheated.

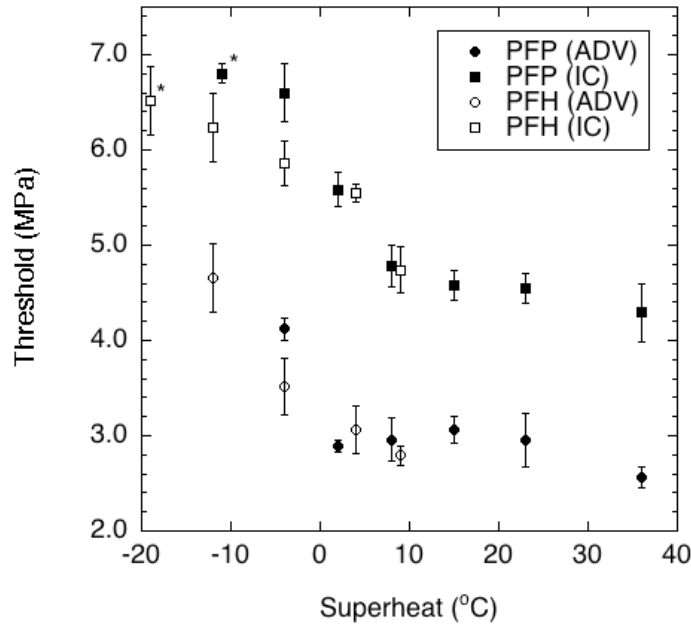


Figure 2.6: Mean ($n = 5$) ADV and IC thresholds, plotted with standard deviations, for PFP and PFH droplets as a function of degree of superheat. The points denoted with asterisks (*) are cases where IC was measured 11°C or 19°C below the boiling point of PFP or PFH, respectively - though no corresponding increase in MEP was recorded. The following conditions were used: degassed water with albumin-coated droplets, 83 Hz PRF, and 13 cycles.

Figure 2.7 (left) displays the relationship between the ADV and IC thresholds and the mean droplet diameter. Different droplet diameters were obtained by either centrifuging the droplets or by allowing the droplets to grow in diameter due to Ostwald ripening [5], as seen in Fig. 2.7 (right). The ADV threshold is inversely

proportional to the mean droplet diameter below $2.5 \mu\text{m}$ (95% CI of the slope is $[-1.99, -0.73]$, $R^2 = 0.86$); the ADV threshold then appears to plateau for droplets larger than $2.5 \mu\text{m}$. This is qualitatively consistent with the diameter above which albumin-coated PFP droplets become superheated at 37°C (i.e. $> 3.8 \mu\text{m}$) [32; 34]. The IC threshold is statistically constant for the size range tested (95% CI of the slope is $[-0.45, 0.13]$), occurring at a higher rarefactional pressure than the ADV threshold ($p < 0.001$). It is important to note that the droplet distributions are not monodispersed in size, and thus the effect of a polydisperse distribution must be considered, such as the preferential vaporization of larger droplets for each distribution. A similar trend, as observed in Fig. 2.7, was obtained by plotting the ADV threshold versus $d_{10\%}$ or $d_{25\%}$, defined respectively as the droplet diameter at which 10% or 25% of the droplets, by number, are larger than that diameter. Extrapolating based on the inverse relationship below $2.5 \mu\text{m}$, it becomes apparent that submicron-sized droplets can be phase-transitioned below the corresponding IC threshold. Particle size is known to affect the IC threshold, with smaller diameter polystyrene spheres yielding higher IC thresholds than larger diameter polystyrene spheres [24]. The statistically similar IC threshold for the size range of droplets tested indicates that despite an almost sixteen fold increase in the droplet surface area, the IC threshold does not decrease as the average droplet diameter increases. This suggests that the IC nucleation process involved in ADV is dissimilar to the nucleation process of IC of polystyrene spheres. It is speculated that IC nuclei are generated from the presence of gas pockets on the surface of the spheres, due to the hydrophobicity and surface roughness on the sphere. Considering the favorable wettability properties of albumin and lipid shells in the bulk fluid, as well as the high fluidity of the PFC in the dispersed phase, it may be likely that the presence of gas pockets, compared to polystyrene spheres, is minimal.

Based on an approximate five-fold expansion of a droplet as it is vaporized into

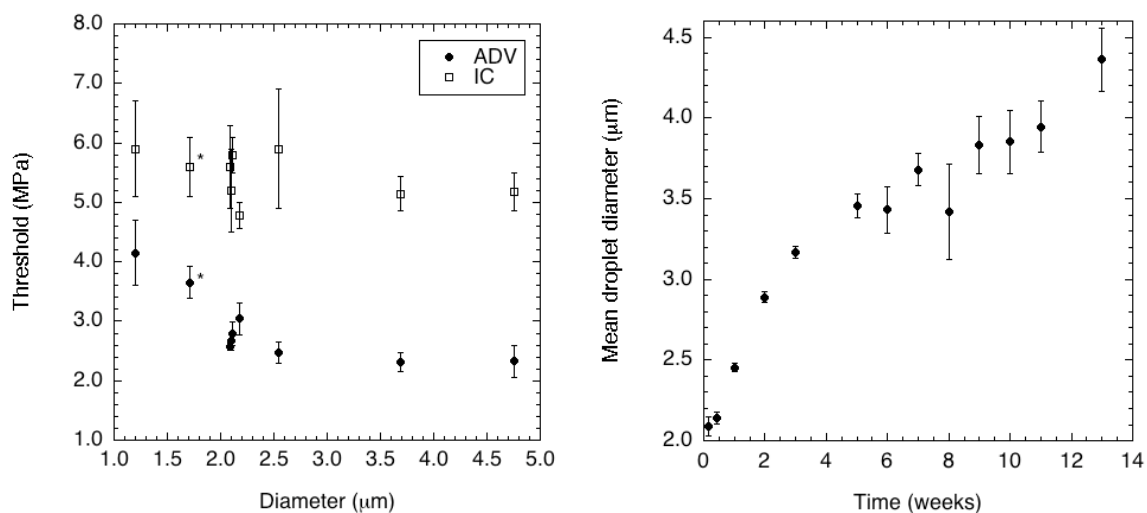


Figure 2.7: Left: Mean ($n = 3$) ADV thresholds and IC thresholds, plotted with standard deviations, for albumin-coated PFP droplets of various mean diameters. The points denoted with an asterisk (*) are lipid-coated droplets, whereas the other points are albumin-coated droplets. The following conditions were used: degassed water at 37°C, 83 Hz PRF, and 13 cycles. Right: Increase in mean droplet diameter over time (i.e. since day of manufacturing) for albumin-coated PFP droplets. All droplets used in this study were manufactured on the same day and stored at 5°C throughout the study. Each data point, plotted with the standard deviation, is the average of three vials.

a gas bubble [7], a 1 μm and 10 μm droplet would yield a 5 μm and 50 μm bubble, respectively. Using an analytical model [28], the minimum acoustic rarefactional pressures required to produce IC in the aforementioned bubbles sizes, using a 3.5 MHz insonation frequency, are 3.77 MPa and 39.2 MPa, respectively. This is based on a collapse temperature of 5000 K and the surface tension, viscosity, and density of water as input parameters to the model; additionally, the heat capacity ratio of PFP at 37°C was determined to be 1.044 using the Universal Functional Activity Coefficient (UNIFAC) method in Aspen Plus software (Aspen Technology Inc., Cambridge, MA, USA). For a micron-sized or larger bubble, the viscous and inertial effects of the surrounding fluid cause the IC threshold to increase as the diameter of the bubble (IC nucleus) increases. This range of computed values supports the hypothesis that gas bubbles generated by ADV can undergo IC due the application of US from the single-element transducer.

Figure 2.7 also displays the effect of the shell material - albumin versus lipid - that is seemingly negligible relative to the effect of the mean diameter. For gaseous contrast agents, lipid shells, which are on average 1 to 2 nm thick, are more stable and inhibit diffusion due to their greater flexibility than albumin shells, which are on average 10 to 15 nm thick and more rigid [35]. If this is the case, then the smaller diffusion coefficients of liquid PFCs relative to gaseous PFCs coupled with the mechanistic differences between ADV and contrast agent destruction may render the effects of the shell negligible except for Ostwald ripening. This further indicates that the nucleation mechanism does not occur at the shell of the droplet.

2.3.3 Acoustic Parameters

The effects of the pulse repetition frequency (PRF) on the ADV and IC thresholds are shown in Fig. 2.8. In all cases, the ADV threshold is lower than the IC threshold ($p < 0.001$). Additionally, an inverse trend is observed for both thresholds below 25 Hz while the thresholds are statistically constant above 25 Hz (95% CI of the

slopes of ADV and IC data are $[-6.3 \times 10^{-5}, 3.0 \times 10^{-4}]$ and $[-6.7 \times 10^{-4}, 4.8 \times 10^{-4}]$, respectively). The ADV and IC data above and below 25 Hz form two distinct populations with respective p -values of < 0.03 and < 0.02 . The decrease in both thresholds, clearly seen from 10 to 100 Hz PRF, relates to the number of times a fluid volume passing the single element transducer is exposed to an acoustic pulse. The time needed for a new fluid volume to traverse the -6 dB beam width, based on the average flow speed within the tube, is 40 ms (or 25 Hz). Therefore, at PRF values less than 25 Hz each fluid volume is exposed to only a single pulse whereas above 25 Hz PRF each fluid volume is exposed to multiple pulses. The slowest and fastest particle velocities within the tube were estimated by calculating the rate at which the MEP increased and decreased from vaporized droplets for a specific US on-time (i.e. a bolus of ADV generated bubbles). The velocities were calculated from the known distance between the single-element transducer and the time delay between the single-element transducer on-time and the passage of bubbles in the linear array FOV; the single-element transducer on-time was also subtracted from the delay in the decreasing MEP. The time delays were calculated based on an MEP threshold, which was at least three-times the average MEP of the initial or final baselines (i.e. no bubbles present). Therefore, the behavior of the MEP was similar to Fig. 2.2, except that the MEP later decreased to the baseline value since the single-element transducer was turned off while the linear array was still recording. The slowest and fastest velocities were $1.2 \text{ cm}\cdot\text{s}^{-1}$ and $4.3 \text{ cm}\cdot\text{s}^{-1}$, corresponding to transit times of 67 and 19 ms, or fluid volume refresh rates of 15 and 53 Hz, respectively. Therefore, referring back to Fig. 2.8 and considering the range of velocities in the flow tube, it becomes evident that when a fluid volume is exposed to multiple exposures of US, both the ADV and IC thresholds decrease relative to when a fluid volume is exposed to only a single pulse.

The effect of pulse width on the ADV and IC thresholds is displayed in Fig.

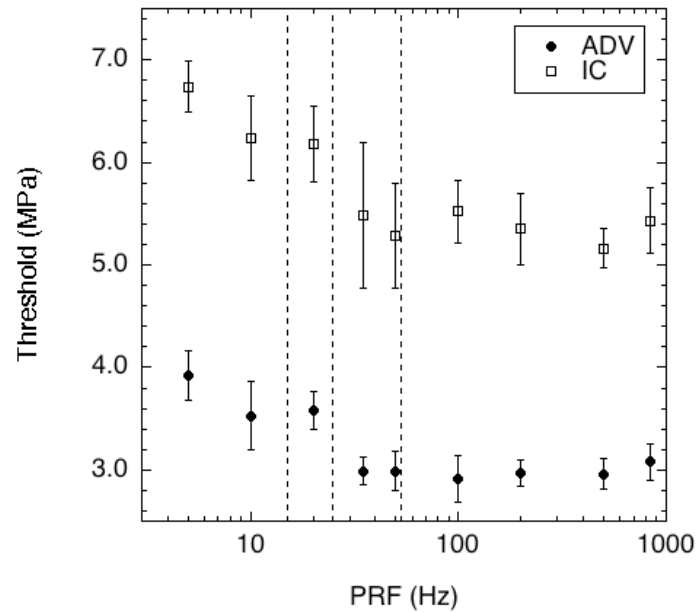


Figure 2.8: Mean ($n = 5$) ADV and IC threshold, plotted with standard deviations, for various PRFs. The following conditions were used: degassed water at 37°C and 13 cycles. By comparison, the rate at which a new volume of fluid crossed the -6 dB beam width of the single-element transducer, based on the average flow velocity, was 25 Hz (middle dotted line). Therefore, each fluid volume was exposed to only a single acoustic pulse from the single element transducer for PRFs less than 25 Hz. The left and right dotted lines display the slowest and fastest rates, respectively, at which a fluid volume passes the single element US beam width, based on the experimental data.

2.9. Two different PRFs - 10 Hz and 83 Hz - were chosen as cases where each flow volume was exposed to a single exposure versus multiple exposures, respectively. In both cases, for a given PRF, the ADV threshold was statistically constant (95% CI of the slopes for 10 Hz and 83 Hz are [-0.003, 0.004] and [-0.006, 0.013], respectively) over the range of pulse widths tested, which is consistent with results by Lo *et al.* where the ADV threshold was relatively constant for microsecond pulse lengths [20]. Additionally, the IC threshold decreased as the pulse width increased, which could imply that longer pulse widths increase the probability of interacting with a bubble that can undergo IC, perhaps as a bubble begins to dissolve or fragment.

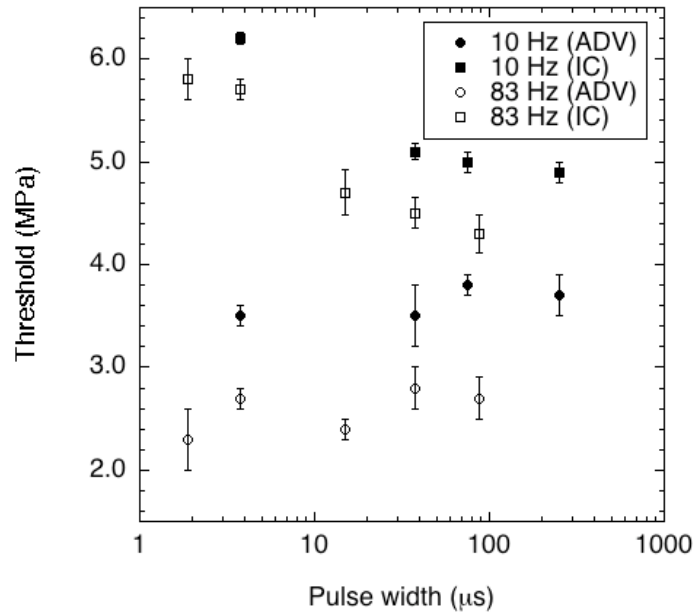


Figure 2.9: Mean ($n = 3$) ADV thresholds and IC threshold (right), plotted with standard deviations, for various pulse widths at two different PRFs (10 Hz and 83 Hz). The following conditions were used: degassed water at 37°C and albumin-coated PFP droplets.

2.4 Conclusions

The elucidation of the physical mechanisms involved in ADV can allow for the optimization of ADV in therapeutic applications such as embolotherapy and drug delivery. Since acoustic cavitation is one possible mechanism for ADV, it is

important to understand the role of IC due to its bioeffects. As discussed previously, the minimization or maximization of IC, depending on the application, may be integral to the success of therapeutic ADV.

Table 2.3 is a summary of the presented results from Figs. 2.6 through 2.9. Based on these results, it is possible to relate the observed trends of the ADV and IC thresholds to physical mechanism of ADV. The possibilities include that IC helps initiate ADV, ADV helps initiate IC (possibly by providing a bubble), or the two events are totally uncorrelated. The correlation between ADV and IC varies for the tested parameters. For the case of PRF, ADV and IC are highly correlated with an R^2 of 0.94, which for nine data points yields less than a 0.1% probability, the percentage probability [36] ($Prob_N$), that the data points are actually uncorrelated. For droplet superheat, the R^2 values are 0.74 and 0.76 for PFP and PFH droplets, respectively; based on the number of data points, the $Prob_N$ values are less than 5.6% and 20%, respectively. Alternatively, the ADV and IC thresholds are more uncorrelated in the cases of droplet diameter ($R^2 = 0.12$) and pulse width ($R^2 = 0.39$ for 10 Hz and $R^2 = 0.21$ for 83 Hz) where the $Prob_N$ values are less than 43%, 40%, and 50%, respectively. Given that ADV and IC are correlated for some of the tested parameters, the next most important fact is that the ADV threshold is always less than the IC threshold. Thus, an IC event is not necessary to cause vaporization, though it has been shown that IC nuclei, specifically US contrast agent, external to the droplet can lower the ADV threshold, which is beneficial in certain situations [20]. Instead it appears that ADV occurs and (possibly) provides a bubble that can then go through IC. The distinct nature of ADV and IC is also supported by examining the frequency dependence of ADV and IC. It was previously shown that the ADV threshold decreased as frequency increased [8], which is opposite of the theoretical behavior of the IC threshold [37] and the experimental results from Giesecke and Hynynen [22] for micron-sized PFC droplets. This may imply that the

role of IC in ADV may change for lower frequencies since as the frequency decreases and the IC threshold in the host medium approaches the ADV threshold, IC could then be the dominant mechanism for triggering ADV.

Table 2.3: Summary of the effects of the various bulk fluid, droplet, and acoustic properties on the ADV and IC thresholds. Refer to Table 2.2 and Figs. 2.6 through 2.9 for each parameter and its corresponding ADV/IC data.

Properties	Parameter	ADV Threshold	IC Threshold
Bulk Fluid	Gas saturation	No effect	No effect
	Viscosity	Direct	Direct
Droplet	PFC superheat	Inverse (below boiling point)	Inverse (below boiling point)
		No effect (above boiling point)	No effect (above boiling point)
	Diameter	Inverse (1 - 2.5 μm)	No effect
		No effect (2.5 - 5 μm)	No effect
Shell	No effect	No effect	
Acoustic	PRF	No effect (multiple US exposures)	No effect (multiple US exposures)
	Pulse width	No effect	Inverse

Knowing that ADV and IC are related, the next point of interest is to determine where the nucleation for ADV and IC occur. Since the IC threshold remained constant when the gas saturation of the bulk fluid was changed, as well as when the droplet diameter increased, it is likely that the nucleus for IC is not external to the droplet and may be the ADV bubble itself. This is supported by the IC threshold correlation with viscosity and not surface tension, which indicated that the IC nuclei were likely greater than one micron. However, high-speed photography would be needed to definitively verify this. Additionally, both thresholds are dependent on the degree of superheat of the dispersed phase, thereby suggesting that the nucleus of ADV or IC is within the droplet. This is further supported by the fact that the droplet shell material did not affect the ADV threshold. Interestingly, the viscosity of the bulk fluid - which is known to affect the IC threshold - also influenced the ADV threshold. It is possible that a viscous fluid retards the initial expansion of the gas bubble generated by ADV, even causing recondensation of the gas nucleus at lower rarefactional pressures due to increasing pressure within the collapsing gas nucleus. Overall, the IC threshold occurred at a higher rarefactional pressure

than the ADV threshold. Therefore, it is possible to operate with a given set of experimental parameters and achieve either ADV with IC or ADV without IC. The results suggest that the ADV nucleus is internal to the droplet and within the PFC phase while the IC nucleus may be the bubble generated by ADV.

Additional studies will be needed to further understand the initiation mechanism for ADV. This work can assist future *in vivo* studies by the selection of a droplet formulation and acoustic parameters that can be vaporized with or without IC, depending on the intended therapeutic application.

2.5 Acknowledgments

This work was supported in part by NIH grant 5R01EB000281.

REFERENCES

- [1] G. M. Lanza and S. A. Wickline, “Targeted ultrasonic contrast agents for molecular imaging and therapy,” *Progress in Cardiovascular Diseases*, vol. 44, no. 1, pp. 13–31, 2001.
- [2] P. A. Dayton, S. Zhao, S. H. Bloch, P. Schumann, K. Penrose, T. O. Matsunaga, R. Zutshi, A. Doinikov, and K. W. Ferrara, “Application of ultrasound to selectively localize nanodroplets for targeted imaging and therapy,” *Molecular Imaging*, vol. 5, pp. 160–174, July 2006.
- [3] J. Y. Fang, C. F. Hung, M. H. Liao, and C. C. Chien, “A study of the formulation design of acoustically active lipospheres as carriers for drug delivery,” *European Journal of Pharmaceutics and Biopharmaceutics*, vol. 67, no. 1, pp. 67–75, 2007.
- [4] N. Rapoport, Z. Gao, and A. Kennedy, “Multifunctional nanoparticles for combining ultrasonic tumor imaging and targeted chemotherapy,” *Journal of the National Cancer Institute*, vol. 99, no. 14, pp. 1095–1106, 2007.
- [5] J. G. Riess, “Oxygen carriers (“blood substitutes”) - raison d’etre, chemistry, and some physiology,” *Chemical Reviews*, vol. 101, no. 9, pp. 2797–2919, 2001.
- [6] R. E. Apfel, “Activatable infusible dispersions containing drops of a superheated liquid for methods of therapy and diagnosis,” Patent 5,840,276, Apfel Enterprises, Inc., November 1998.
- [7] O. D. Kripfgans, J. B. Fowlkes, D. L. Miller, O. P. Eldevik, and P. L. Carson, “Acoustic droplet vaporization for therapeutic and diagnostic applications,” *Ultrasound in Medicine and Biology*, vol. 26, no. 7, pp. 1177–1189, 2000.
- [8] O. D. Kripfgans, J. B. Fowlkes, M. Woydt, O. P. Eldevik, and P. L. Carson, “*In vivo* droplet vaporization for occlusion therapy and phase aberration correction,” *IEEE Transactions on Ultrasonics, Ferroelectrics, and Frequency Control*, vol. 49, no. 2, pp. 726–738, 2002.
- [9] K. J. Haworth, J. B. Fowlkes, P. L. Carson, and O. D. Kripfgans, “Towards aberration correction of transcranial ultrasound using acoustic droplet vaporization,” *Ultrasound in Medicine and Biology*, vol. 34, pp. 435–445, March 2008.

- [10] J. C. Hogg, “Neutrophil kinetics and lung injury,” *Physiological Reviews*, vol. 67, pp. 1249–1295, October 1987.
- [11] O. D. Kripfgans, C. M. Orifici, P. L. Carson, K. A. Ives, O. P. Eldevik, and J. B. Fowlkes, “Acoustic droplet vaporization for temporal and spatial control of tissue occlusion: a kidney study,” *IEEE Transactions on Ultrasonics, Ferroelectrics, and Frequency Control*, vol. 52, pp. 1101–1110, July 2005.
- [12] K.-I. Kawabata, N. Sugita, H. Yoshikawa, T. Azuma, and S.-I. Umemura, “Nanoparticles with multiple perfluorocarbons for controllable ultrasonically induced phase shifting,” *Japanese Journal of Applied Physics*, vol. 44, no. 6B, pp. 4548–4552, 2005.
- [13] E. Neppiras, “Acoustic cavitation,” *Physics Reports*, vol. 61, no. 3, pp. 159–251, 1980.
- [14] C. Brennen, *Cavitation and Bubble Dynamics*. New York, NY: Oxford University Press, 1995.
- [15] T. Leighton, *The Acoustic Bubble*. San Diego, CA: Academic Press Inc., 1994.
- [16] D. Dalecki, “Mechanical bioeffects of ultrasound,” *Annual Review of Biomedical Engineering*, vol. 6, no. 1, pp. 229–248, 2004.
- [17] C. C. Coussios and R. A. Roy, “Applications of acoustics and cavitation to noninvasive therapy and drug delivery,” *Annual Review of Fluid Mechanics*, vol. 40, pp. 395–420, 2008.
- [18] E. L. Carstensen, S. Gracewski, and D. Dalecki, “The search for cavitation *in vivo*,” *Ultrasound in Medicine and Biology*, vol. 26, no. 9, pp. 1377–1385, 2000.
- [19] C. C. Church, “Spontaneous homogeneous nucleation, inertial cavitation and the safety of diagnostic ultrasound,” *Ultrasound in Medicine and Biology*, vol. 28, no. 10, pp. 1349–1364, 2002.
- [20] A. H. Lo, O. D. Kripfgans, P. L. Carson, E. D. Rothman, and J. B. Fowlkes, “Acoustic droplet vaporization: effects of pulse duration and contrast agent,” *IEEE Transactions on Ultrasonics, Ferroelectrics, and Frequency Control*, vol. 54, pp. 933–946, May 2007.
- [21] O. D. Kripfgans, M. L. Fabiilli, P. L. Carson, and J. B. Fowlkes, “On the acoustic vaporization of micrometer-sized droplets,” *Journal of the Acoustical Society of America*, vol. 116, no. 1, pp. 272–281, 2004.
- [22] T. Giesecke and K. Hynynen, “Ultrasound-mediated cavitation thresholds of liquid perfluorocarbon droplets *in vitro*,” *Ultrasound in Medicine and Biology*, vol. 29, no. 9, pp. 1359–1365, 2003.
- [23] Y. Ruckebusch, L.-P. Phaneuf, and R. Dunlop, *Physiology of Small and Large Animals*. Philadelphia, PA: B.C. Decker Inc., 1991.

- [24] S. I. Madanshetty, R. A. Roy, and R. E. Apfel, “Acoustic microcavitation: its active and passive acoustic detection,” *Journal of the Acoustical Society of America*, vol. 90, no. 3, pp. 1515–1526, 1991.
- [25] P. Epstein and M. Plesset, “On the stability of gas bubbles in liquid-gas solutions,” *Journal of Chemical Physics*, vol. 18, pp. 1505–1509, November 1950.
- [26] R. A. Roy, S. I. Madanshetty, and R. E. Apfel, “An acoustic backscattering technique for the detection of transient cavitation produced by microsecond pulses of ultrasound,” *Journal of the Acoustical Society of America*, vol. 87, pp. 2451–2458, June 1990.
- [27] O. D. Kripfgans, *Acoustic droplet vaporization for diagnostic and therapeutic applications*. PhD thesis, University of Michigan, Ann Arbor, MI, 2002.
- [28] C. K. Holland and R. E. Apfel, “An improved theory for the prediction of microcavitation thresholds,” *IEEE Transactions on Ultrasonics, Ferroelectrics, and Frequency Control*, vol. 36, pp. 204–208, March 1989.
- [29] C. K. Holland and R. E. Apfel, “Thresholds for transient cavitation produced by pulsed ultrasound in a controlled nuclei environment,” *Journal of the Acoustical Society of America*, vol. 88, pp. 2059–2069, November 1990.
- [30] C. C. Church, “Frequency, pulse length, and the mechanical index,” *Acoustics Research Letters Online*, vol. 6, pp. 162–168, June 2005.
- [31] D. R. Evans, D. F. Parsons, and V. S. Craig, “Physical properties of phase-change emulsions,” *Langmuir*, vol. 22, no. 23, pp. 9538–9545, 2006.
- [32] N. Y. Rapoport, A. M. Kennedy, J. E. Shea, C. L. Scaife, and K.-H. Nam, “Controlled and targeted tumor chemotherapy by ultrasound-activated nanoemulsions/microbubbles,” *Journal of Controlled Release*, vol. 138, no. 2, pp. 268–276, 2009.
- [33] M. Jumaa and B. W. Möller, “The effect of oil components and homogenization conditions on the physicochemical properties and stability of parenteral fat emulsions,” *International Journal of Pharmaceutics*, vol. 163, no. 1, pp. 81–89, 1998.
- [34] M. A. Kandadai, P. Mohan, G. Lin, A. Butterfield, M. Skliar, and J. J. Magda, “Comparison of surfactants used to prepare aqueous perfluoropentane emulsions for pharmaceutical applications,” *Langmuir*, vol. 26, no. 7, pp. 4655–4660, 2010.
- [35] J. E. Chomas, P. Dayton, J. Allen, K. Morgan, and K. W. Ferrara, “Mechanisms of contrast agent destruction,” *IEEE Transactions on Ultrasonics, Ferroelectrics, and Frequency Control*, vol. 48, no. 1, pp. 232–248, 2001.
- [36] E. M. Pugh and G. H. Winslow, *The analysis of physical measurements*. Reading, MA: Addison-Wesley, 1966.

- [37] R. E. Apfel and C. K. Holland, “Gauging the likelihood of cavitation from short-pulse, low-duty cycle diagnostic ultrasound,” *Ultrasound in Medicine and Biology*, vol. 17, no. 2, pp. 179–185, 1991.

CHAPTER III

Delivery of Chlorambucil using an Acoustically-Triggered, Perfluoropentane Emulsion

3.1 Introduction

Perfluorocarbon (PFC) colloids, either microbubbles or emulsions, are being studied in diagnostic and therapeutic applications of ultrasound (US). The use of these colloids as delivery systems, either for therapeutic agents or genetic material, is motivated by their spatially and temporally-selective activation via US. Recent reviews [1–3] highlight examples of drug and gene delivery using microbubbles. The incorporation of the drug or gene is typically accomplished using one of the following methods: attachment (covalent or non-covalent) to the shell either directly or using a secondary carrier, such as a liposome or nanoparticle [4; 5]; intercalation within the shell [6; 7]; or incorporation within a fluid inside the shell. The last technique is employed in acoustically active lipospheres (AALs) [8; 9], and is thus amenable to the dissolution of lipophilic drugs, including chemotherapy agents such as paclitaxel [10; 11]; alternatively, hydrophilic or lipophilic agents can be incorporated into US activated echogenic liposomes [12]. The ability to localize the release of a chemotherapeutic agent via US could be used to increase the local drug concentration at the intended, target site while minimizing the overall systemic toxicity. This could expand the therapeutic window of many chemotherapeutics that possess a narrow distinction between efficacy and unacceptable toxicity [13].

Though not as echogenic as microbubble-based delivery systems, unless phase-transitioned or accumulated due to targeting, PFC liquid emulsions are also being studied as delivery systems due to their increased circulation half-life relative to microbubbles [14]. Additionally, compared to microbubbles, stable PFC emulsions can be formulated with mean diameters of about 200 nm [15]. These nanoparticles can extravasate in the microvasculature of tumors due to the presence of large inter-endothelial gaps [16]. Formulation approaches, similar to those used for microbubble delivery systems, have been used for PFC emulsions [17–20] due to the hydrophobicity and lipophobicity of the dispersed, PFC phase [21]. These PFC emulsions can be activated (i.e. phase transitioned from a liquid to a gas) either thermally upon systemic injection [22], or via US, a mechanism termed acoustic droplet vaporization (ADV) [23–25]. ADV is a threshold phenomenon where the phase-transition can only take place if the acoustic amplitudes are greater than a particular threshold value. In the case of ADV, the resulting gas bubbles have been used *in vivo* to selectively reduce cerebral [26] and renal [27] perfusion.

This study focuses on the characterization and *in vitro* performance of an ADV-triggered emulsion, termed a dual-phase emulsion, that contains both chlorambucil (CHL) and PFC. CHL is a lipophilic nitrogen mustard derivative that, similar to other alkylating agents, is predominately non-cell cycle specific. CHL has been used clinically to treat chronic lymphatic leukemia and lymphoma as well as advanced ovarian and breast cancers [28]. The use of CHL is limited, despite its good oral bioavailability (Leukeran, GlaxoSmithKline, London, United Kingdom), by its toxic side effects that include myelosuppression and neurological toxicity [29]. Therefore, the ability to localize the effects of CHL - by encapsulation and subsequent release using US - could be used to minimize systemic toxicity while increasing the local concentration of CHL at the target site. Additionally, incorporation of CHL into an emulsion has been shown to improve the pharmacokinetic profile of the drug and

increase its therapeutic activity relative to a CHL solution [30]. The presented PFC emulsion is micron-sized - unlike the submicron-sized, PFC droplets investigated by other groups [15; 17–20; 22]. The ADV-triggered drug release from this emulsion could potentially be coupled with ADV-induced occlusion [26; 27].

This study is composed of three main sections. First, the micron-sized, PFC emulsion is prepared and characterized, with a focus on emulsion morphology and its effect on the ADV threshold. Second, US-activated drug release from the emulsion is studied, in terms of growth inhibition, in chambers containing Chinese hamster ovary (CHO) cells. Third, the relationship between droplet size, ADV efficiency (i.e. the fraction of droplets that vaporize per US exposure), and drug release is analyzed.

3.2 Materials and Methods

3.2.1 Emulsion preparation

All chemicals were obtained from Sigma-Aldrich (St. Louis, MO, USA) unless otherwise noted. Albumin droplets were prepared by modifying a previously established protocol [24]. Briefly, 750 μL of 4 mg/mL bovine albumin in normal saline (0.9% w/v, Hospira Inc., Lake Forest, IL, USA) was added to a 2 mL glass vial (Shamrock Glass, Seaford, DE, USA). Chlorambucil (CHL) was dissolved in soybean oil at a concentration of 25 mg/mL. The soybean oil and perfluoro-n-pentane (PFP, 29°C normal boiling point, Alfa Aesar, Ward Hill, MA, USA) were added gravimetrically to produce a final volume fraction of 12.5% for each component. The vial was sealed with a rubber stopper (Shamrock Glass) and metal cap (Shamrock Glass). The vial was then shaken for 45 seconds at 4550 cycles per minute using an amalgamator (VialMix, Lantheus Medical Imaging, Billerica, MA, USA).

The shaken vials were refrigerated (5°C) overnight prior to use. The droplets were diluted in normal saline that had been filtered with a syringe filter (0.22 μm , Millex GV, Millipore, Billerica, MA, USA) and sized using a Coulter counter

(Multisizer 3, Beckman Coulter Inc., Fullerton, CA, USA) with a 50 μm aperture. For *in vitro* experiments with cells, all materials used in the droplet formulation procedure were autoclaved and all solutions were filtered using a 0.22 μm filter to yield sterile vials of emulsion.

3.2.2 Optical characterization of the emulsions

To determine the location of the oil (i.e. drug laden phase) within each droplet, a fluorescent dye - Vybrant[®] DiI (Invitrogen, Eugene, OR, USA) - was used as a surrogate for CHL. The utilization of a lipophilic dye to mimic an oil-soluble compound (such as a therapeutic agent) and to confirm where such an oil-soluble compound would reside in a microbubble or droplet has been used extensively in microscopy or drug release studies [8; 10; 11; 31; 32]. The resulting emulsions were diluted in normal saline and samples were aliquoted onto a hemacytometer (Brightline, Hausser Scientific, Horsham, PA, USA). Visible and fluorescent micrographs of the droplets were taken with a microscope (Leica DMRB, Bannockburn, IL, USA) and camera (Spot FLEX, Diagnostic Instruments Inc., Sterling Heights, MI, USA) using Spot Advanced Software (Diagnostic Instruments Inc.).

The acquired images were analyzed in MATLAB (The Mathworks Inc., Natick, MA, USA). The pixel resolution within each image was calibrated using the hemacytometer grid spacing. Since the emulsions contained two immiscible, dispersed phases, the inner and outer diameters for each droplet were manually sized. Magnification limitations restricted this manual sizing to droplets with an outer diameter greater than or equal to 1.5 μm .

3.2.3 ADV threshold measurements

The ADV threshold was determined using identical methodologies as previously described [33]. Briefly, diluted emulsions were exposed to acoustic pulses from

a calibrated, 3.5 MHz single-element transducer (1.9 cm diameter, 3.81 cm focal length, A381S, Panametrics, Olympus NDT Inc., Waltham, Ma) while in a flow tube setup. The increase in echogenicity, recorded via B-mode US, was used to detect the presence of bubbles generated by ADV and hence the ADV threshold.

3.2.4 Evaluation of CHL loading in emulsion

The CHL concentration in the drug-loaded emulsion was determined via high performance liquid chromatography (HPLC) using a Hitachi 7000 series HPLC system (Pleasanton, CA, USA). EZChrom EliteTM software (Agilent Technologies, Santa Clara, CA, USA) was used to control the system as well as acquire and process data. The mobile phase, filtered through a 0.22 μm filter (Durapore GS, Millipore), consisted of methanol (CHROMASOLV Plus for HPLC) and 0.1% (w/v) ammonium acetate (65:35 (v/v)) and was pumped at 1 mL/min through a Luna[®] column (C5, 150 x 4.6 mm, 5 μm , Phenomenex, Torrance, CA, USA). Samples were manually injected using a 20 μL injector loop. The column was kept at ambient temperature and samples were analyzed at a wavelength of 254 nm. The CHL peak eluted at approximately 4.1 minutes.

CHL standards were prepared, via serial dilution, by dissolving CHL in a solution of methanol and 0.1% (w/v) ammonium acetate (80:20 (v/v)). The HPLC method was validated for linearity in the range of 1 to 500 $\mu\text{g}/\text{mL}$ ($R^2 > 0.999$) using the CHL peak area. Triplicate injections of each standard yielded peak area variabilities of less than 3% relative standard deviation. The ability to extract CHL from the soybean oil was validated by adding CHL solubilized in soybean oil to 2 mL glass vials containing 1 mL of extraction solvent - methanol and 0.1% (w/v) ammonium acetate (80:20 (v/v)). The vial was capped, sealed, and then shaken for 45 seconds at 4550 cycles per minute using an amalgamator in order to facilitate the extraction of CHL. The standard was then centrifuged at 3000 rpm for 10 minutes in order to separate the oil from the solvent. The solvent phase was then injected onto the

HPLC. It was confirmed that complete extraction of the CHL from the oil was achieved in this sample processing and that any solubilized soybean oil did not chromatographically interfere with the CHL peak.

Emulsion samples were processed similarly to the CHL-laden soybean oil samples by adding an aliquot of emulsion to methanol. The emulsion was broken by shaking the sample, which was evident by the presence of precipitated albumin. The samples were centrifuged and the solvent phase was injected onto the HPLC. It was validated that this sample processing yielded complete extraction of CHL from the emulsion. Also, it was confirmed that the presence of any solubilized albumin within the solvent did not chromatographically interfere with the CHL peak.

3.2.5 Cytotoxicity of CHL in solution

Chinese hamster ovary (CHO) cells (American Type Culture Collection, Manassas, VA, USA) were cultured in RPMI 1640 growth media (Invitrogen) supplemented with 10% (v/v) defined fetal bovine serum (Hyclone, Logan, UT, USA), 100 U/mL penicillin, and 100 $\mu\text{g}/\text{mL}$ streptomycin (Invitrogen). The cells were grown in a humidified 5% carbon dioxide environment at 37°C. The cells were plated at approximately 2.0×10^4 cells/mL, determined via Coulter counter, in 6-well microtiter plates (Fisher Scientific, Pittsburgh, PA, USA) 24 hours prior to treatment. A CHL solution was prepared by dissolving CHL in dimethyl sulfoxide (DMSO, Sigma-Aldrich). The cells were then incubated with varying concentrations of CHL solution for either 15 or 60 minutes. The concentration of DMSO within each well did not exceed 1% (v/v) in any experimental group, which consisted of 6 wells per CHL concentration as well as a control group (without DMSO or CHL) and a group treated with DMSO alone. Following the incubation period, the medium from each well was removed and the cells were washed in triplicate with warmed (37°C) Dulbecco's phosphate buffered saline (DPBS, with calcium chloride and magnesium chloride, Invitrogen). Fresh medium was added to each well and the cells

were grown for an additional 48 hours post treatment. After 48 hours, the control cells had reached approximately 80-90% confluence, which was visibly estimated using an inverted microscope (Leica DMIL). The cells were then harvested using trypsin-EDTA (Invitrogen), centrifuged at 1200 rpm for 3 minutes, resuspended in new medium, and counted using a Coulter counter with a 100 μm aperture. Particles larger than 10 μm were counted as intact cells and used for subsequent calculations [34–36].

The percent growth inhibition (GI) for each experimental group was determined as seen in Eq. 3.1, where $N_{control,t_o}$ is the initial number of cells seeded in the control group, N_{exp,t_o} is the initial number of cells seeded in the experimental group, $N_{control,t_f}$ is the final number of cells in the control group, and N_{exp,t_f} is the final number of cells in the experimental group.

$$\%GI = 100 - 100 \left(\frac{N_{exp,t_f} - N_{exp,t_o}}{N_{control,t_f} - N_{control,t_o}} \right) \quad (3.1)$$

The GI data, as a function of CHL concentration in DMSO, was fit using a sigmoidal curve as seen in Eq. 3.2 where m_1 is the maximum y -value, m_2 is the minimum y -value, m_3 is the x -value at the midpoint of y , and m_4 is the slope at the y -midpoint.

$$y = m_1 + \frac{m_2 - m_1}{1 + \left(\frac{x}{m_3} \right)^{m_4}} \quad (3.2)$$

3.2.6 Ultrasound triggering of CHL-loaded emulsion

OptiCell™ (Thermo Fisher Scientific, Rochester, NY, USA) chambers were coated with 20 $\mu\text{g}/\text{cm}^2$ collagen (type I, BD Biosciences, Bedford, MA, USA) 24 hours prior to plating approximately 4.0×10^4 cells/mL CHO cells within the chambers. The cells, seeded 24 hours prior to treatment, were grown using the same conditions as previously described for the 6-well plate experiments. Figure 3.1 displays the experimental setup and exposure conditions. For experimental

groups treated with droplets, the emulsion was diluted with DPBS and introduced into the OptiCell™, yielding a concentration of 7.0×10^7 droplets/mL within the chamber. The chamber was gently and repeatedly inverted to homogenously mix the droplets, then inverted to allow the droplets to settle onto the bottom window; the chamber was then placed into the OptiCell™ holder which was located within a tank ($40 \times 60 \times 27$ cm) that contained degassed, deionized water heated to 37°C (Ex 7, ThermoNESLAB, Newington, NH, USA). The surface of the tank water, located 5 cm above the OptiCell™, was covered with air-filled plastic balls (Cole-Parmer Inc., Vernon Hills, IL, USA) to minimize regassing and heat loss as well as to reduce the planar reflection of the US at the air/water surface. A linear array (10L probe, Logiq 9, GE Healthcare, Milwaukee, WI, USA) operating at the following conditions - 6.3 MHz, contrast mode, single focus at 2.5 cm, 1.57 MPa peak rarefactional focal pressure, 0.8 μ s pulse duration per scan line, 12 kHz scan line pulse repetition frequency, 10 Hz frame rate - was positioned below the chamber such that the 2.5 cm focus was at the bottom window of the chamber. The array was rastered in a minimally-overlapping manner, via a computer-controlled positioning system, at 2 mm/s across the chamber surface in order to vaporize the emulsion. Only two rasters of the linear array were required to insonify the entire chamber (approximately 75 seconds to scan the entire chamber). Following the exposure, the chamber was removed from the tank, inverted so that the cells were once again on the bottom window, and incubated for 60 minutes. During the incubation, any droplets that did not vaporize remained in contact with the cells; bubbles, and hence PFP gas, generated due to ADV were not in contact with the cells due to their buoyancy and size. The chamber was then washed using similar methods as used for the 6-well plate experiments and the cells were grown for another 48 hours post washing. The cells were counted as previously described and the GI was calculated for all experimental groups listed in Table 3.1. Due to the fluid movement into and

out of the OptiCell™ during washing, a relatively large shear force was exerted on the cells adjacent to the OptiCell™ injection port, resulting in their deplating. The GI for each chamber was normalized by the deplated area to account for this loss. All control groups received the same handling during the exposure and washing processes. The same CHL concentration was used for groups receiving CHL in DMSO or emulsified CHL. Analysis of variance (ANOVA) was used to establish the significance between the different experimental groups. The Tukey-Kramer method was applied to differentiate significant differences between the groups.

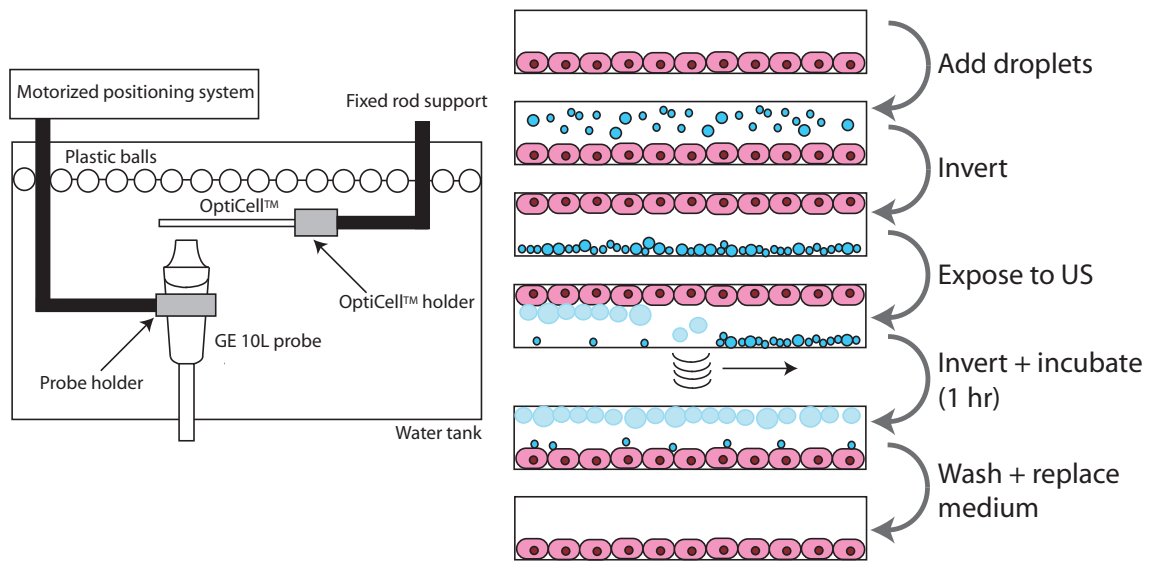


Figure 3.1: Left: Experimental setup used to perform ADV experiments with OptiCells™. Right: Exposure conditions utilized during experiments. The emulsion was added to the chamber containing adherent CHO cells and subsequently exposed to US to cause ADV of the introduced droplets.

Table 3.1: Groups used in the OptiCellTM experiments. For each group, the positive (+) and negative (−) symbols indicate the presence or absence, respectively, of each parameter. In the case of group 5 or 8, the CHL is present within the dispersed phase of the emulsion.

Group	Droplets	CHL	US
1	−	−	−
2	+	−	−
3	−	+	−
4	−	−	+
5	+	+	−
6	+	−	+
7	−	+	+
8	+	+	+

3.2.7 ADV efficiency

The ADV efficiency in the OptiCellTM, using the experimental setup and acoustic parameters from the previous section, was determined using chambers without cells. The emulsion was introduced into the chamber, exposed to US, and the droplets remaining post-exposure were counted with the Coulter counter. The droplet sample was briefly over-pressurized in a syringe and then diluted prior to counting, thereby decreasing the likelihood that bubbles were still present in solution. The ADV efficiency was defined as the ratio of the droplet concentration remaining in the chamber post US exposure to the initial droplet concentration (i.e. before US exposure). The experiment was repeated using 1, 2, and 5 passes of the US array across the chamber surface.

3.3 Results

3.3.1 Emulsion characterization

Figure 3.2 displays the visible and fluorescent images of the droplets, where two distinct phases are clearly seen within the droplets. The dye is contained within the oil phase due to the lipophilicity of the dye and the lipophobicity, and also hydrophobicity, of the PFP phase [21]. The oil phase surrounds the PFP core due

to the relative hydrophobicities of the two phases; fluorocarbons are significantly more hydrophobic than hydrocarbons [21]. A similarly structured emulsion, with a fluorocarbon surrounded by oil, was observed when silicone was emulsified with a perfluoropolyether and water [32].

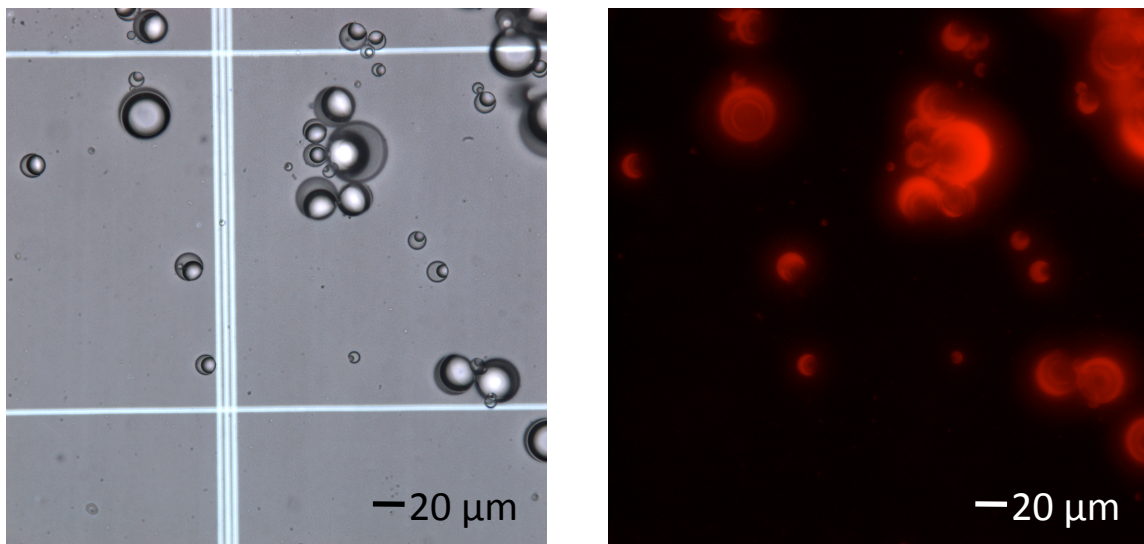


Figure 3.2: A visible image (left) and its corresponding fluorescent image (right) of the dual-phase emulsion containing PFP and soybean oil stained with a fluorescent dye. The spacing between the two horizontal lines on the hemacytometer is $200 \mu\text{m}$. A $20 \mu\text{m}$ scale is included in each image. Although large droplets appear in this figure, droplets larger than $10 \mu\text{m}$ in diameter account for only 4.9% (by number) of total droplets. Refer to Fig. 3.4 for a size distribution, obtained via Coulter counter, for the emulsion.

Based on the micrographs, Fig. 3.3 displays the ratio of the inner droplet diameter (PFP) to the outer droplet diameter (PFP plus soybean oil) for the emulsion. Microscopy magnification limitations prevented the optical sizing of droplets with outer diameters smaller than $1.5 \mu\text{m}$. Even though these smaller droplets could not be sized, it is evident that as the outer droplet diameter increases, the ratio of the inner to outer diameter also increases. Therefore, larger droplets tend to have a larger volume percentage of PFP relative to smaller droplets and a tighter distribution of the ratio. It also appears that there is a cutoff for each droplet diameter that limits how small the ratio may be for a given size. The ratio

distribution has a slight positive skew with a mean ratio of 0.45. The actual outer diameter size distribution, as obtained by the Coulter counter, is displayed in Fig. 3.4.

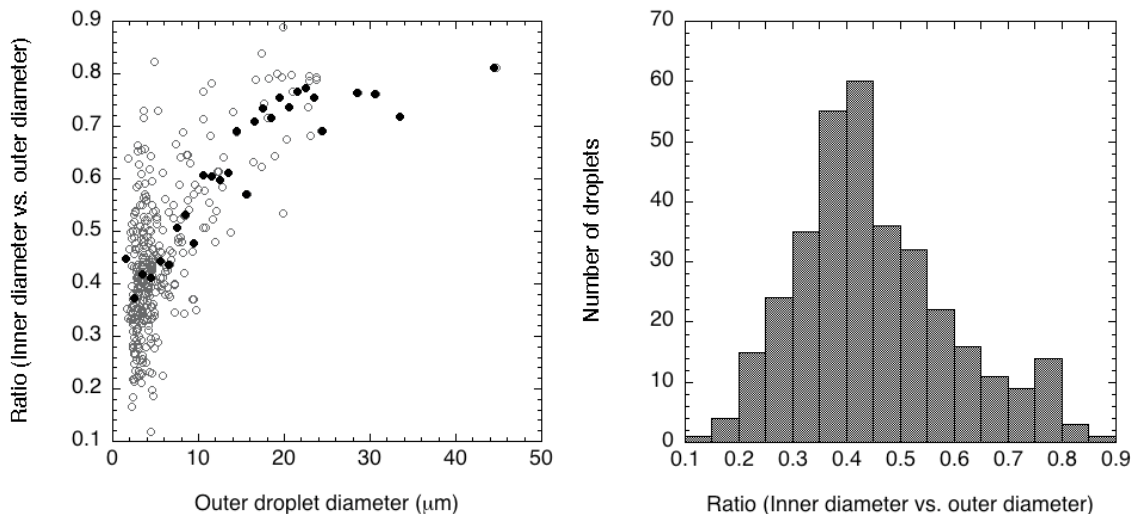


Figure 3.3: Left: For $n = 338$ droplets, the ratio of the inner to outer droplet diameter is plotted as a function of the outer droplet diameter. The raw data is plotted using open, gray circles and the averaged, binned ($1 \mu\text{m}$) data is presented as closed, black circles. Right: A histogram of the raw data.

Characterizing the ratio of the inner and outer droplet diameters may enable a clearer interpretation of the ADV threshold for the dual-phase emulsion, which is seen in Fig. 3.5. Previous findings using PFP droplets [33] demonstrated that the ADV threshold was inversely proportional to the mean droplet diameter below $2.5 \mu\text{m}$ and relatively constant for mean droplet diameters larger than $2.5 \mu\text{m}$; the shell material, either albumin or lipid, had a negligible effect on the ADV threshold. The ADV thresholds for the dual-phase droplets as a function of their outer droplet diameter (solid squares) is plotted along with the ADV threshold for single-phase droplets (x's) from previous work [33]. Using the results from Fig. 3.3, the mean inner diameter of the dual-phase droplets can be estimated based on the mean outer diameter so that the plotted diameters are the PFP core diameters (open squares).

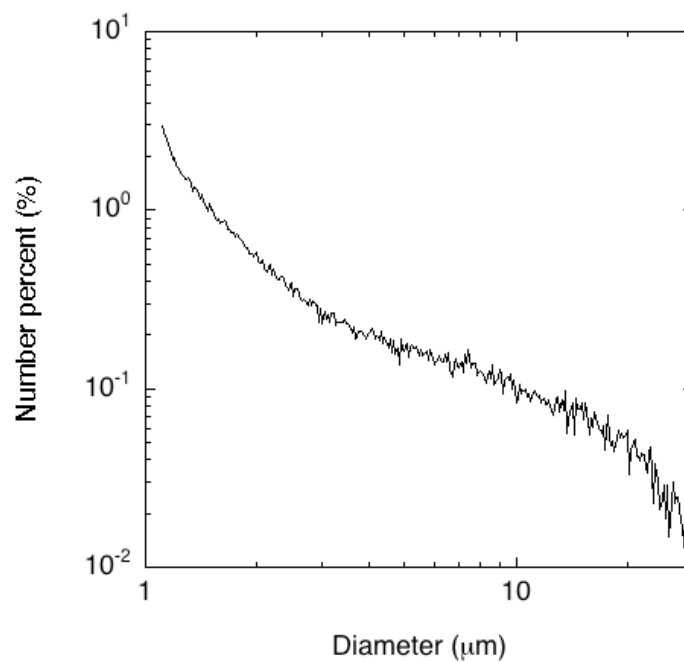


Figure 3.4: The emulsion size distribution, obtained using a Coulter counter, plotted as the number percent of total droplets. The 50 μm aperture enables the sizing of particles whose diameters are between 1 and 30 μm . The mean droplet diameter is $3.06 \pm 0.21 \mu\text{m}$ with 4.9% (by number) of the droplets larger than 10 μm in diameter. The CHL loading in the droplets is $3.12 \pm 0.01 \text{ mg/mL}$ emulsion.

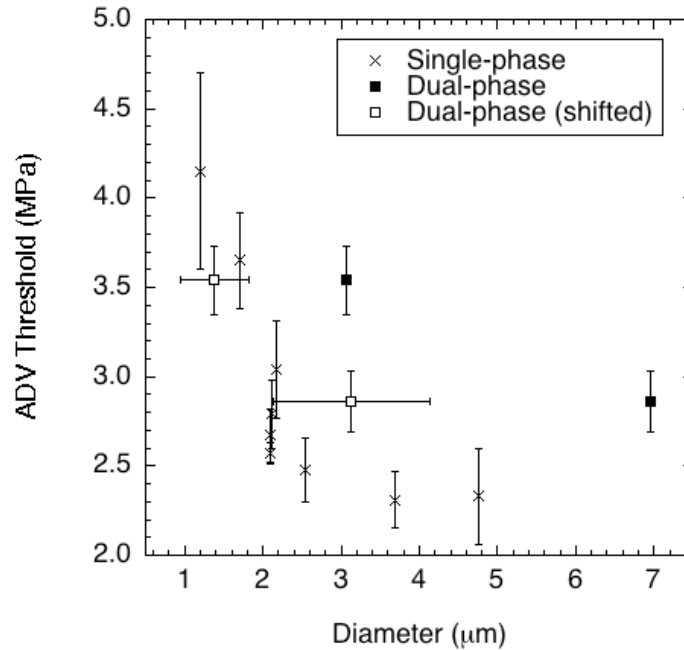


Figure 3.5: A comparison of the mean ($n = 3$) ADV thresholds, plotted with standard deviations, for single-phase and dual-phase droplets as a function of average droplet diameter. The single-phase ADV thresholds are taken from a previous study [33]. The dual-phase droplets with a mean diameter of $6.96 \mu\text{m}$ were obtained by centrifuging the emulsion. The data labeled ‘dual-phase (shifted)’ has been corrected for the estimated mean PFP core diameter, using Fig. 3.3. The horizontal error bars were obtained based on the standard deviation in Fig. 3.3 (right). The following experimental conditions were used: degassed water at 37°C , 3.5 MHz single element transducer, 83 Hz pulse repetition frequency, and 13 cycles.

3.3.2 CHL cytotoxicity on CHO cells

Figure 3.6 displays the cytotoxicity of CHL initially dissolved in DMSO on CHO cells for 15 and 60-minute exposures. The group treated with DMSO alone yielded a GI that was not statistically different ($p > 0.01$) than the control group (without DMSO or CHL). Based on the sigmoidal curve fits ($R^2 > 0.99$ in both cases), the CHL concentration required to produce 50% GI was 167 μM and 57 μM , respectively, for 15 and 60-minute exposures. By comparison, the IC_{99} - the concentration required to kill 99% of cultured cells - was 20 μM and 60 μM for 1-hour exposures of CHL with murine P388 tumor cells at a pH of 7.2 and 7.8, respectively [37]. Similarly, CHO and human SKOV3 adenocarcinoma cells incubated with CHL for 48 hours yielded IC_{50} values, similarly defined as IC_{99} , of 40 μM [38] and 8.5 μM [30], respectively. As is evident, cancer cells are more susceptible to CHL, which displays a log-linear dose response effect, than normal (ex. CHO) cells since the former are more likely to be in cell cycle at any given time [39]. Additionally, cancer cells are slower than normal cells in repairing cellular damage induced by exposure to cytotoxic agents [13].

Figure 3.6 also displays the linear correlation ($R^2 > 0.94$) between the mean CHO cell diameter 48 hours post-incubation and the GI for the CHL in DMSO data. The increase in mean cell diameter can be used as an indicator of CHL exposure. Cell volume, and hence diameter, is known to increase in response to exposure to a variety of chemotherapeutic agents, including CHL [40; 41]. Though not fully understood, the increase in cell volume is likely due to the continued protein synthesis by the cell despite the disruption in DNA synthesis and function. If the GI is due to CHL and additional factors, as will be discussed below, the change in mean cell diameter should only be used as a qualitative indicator of whether CHL was or was not a contributor to GI.

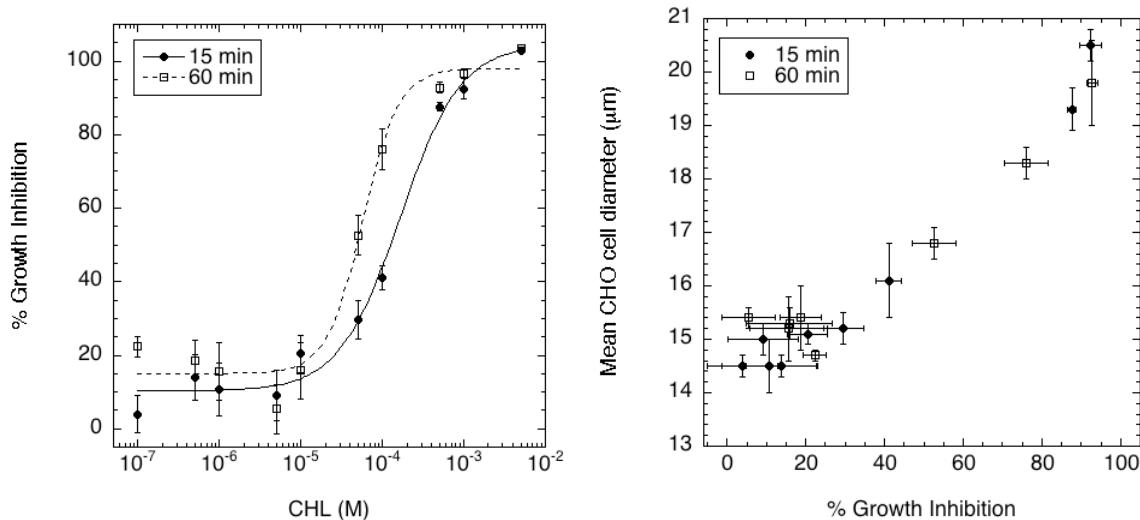


Figure 3.6: Left: Cytotoxicity of CHL initially dissolved in DMSO on CHO cells for 15 and 60-minute exposures. Right: The mean CHO cell diameter as a function of the GI. For both the left and right plots, each data point is the average of six wells, from three independent experiments. Additionally, error bars are standard deviations of the means.

3.3.3 Ultrasound triggering of the CHL-loaded emulsion

Figure 3.7 displays the GI for the eight experimental groups 48 hours post treatment and Table 3.2 lists the results of Tukey’s test for the groups. As per the definition of GI (Eq. 3.1), the control group (group 1) has a mean GI of zero. The application of US (group 4) yielded a GI that was not statistically different from the control group.

The blank emulsion alone (group 2) and the combination of US with the blank emulsion (group 6) yielded $18.6 \pm 3.4\%$ GI and $22.6 \pm 2.4\%$ GI, respectively. Inverting group 2 during the 60-minute incubation period (i.e. droplets were not in direct contact with the cells - see Fig. 3.1) resulted in a $17.0 \pm 7.6\%$ GI, indicating that merely the presence of sham droplets within the chamber caused GI. It was found that the GI experienced by group 2 was a result of increased detachment of the CHO cells during the washing of the chamber when droplets were introduced. Cell detachment in the OptiCellTM can be an issue due to the deformable nature of the

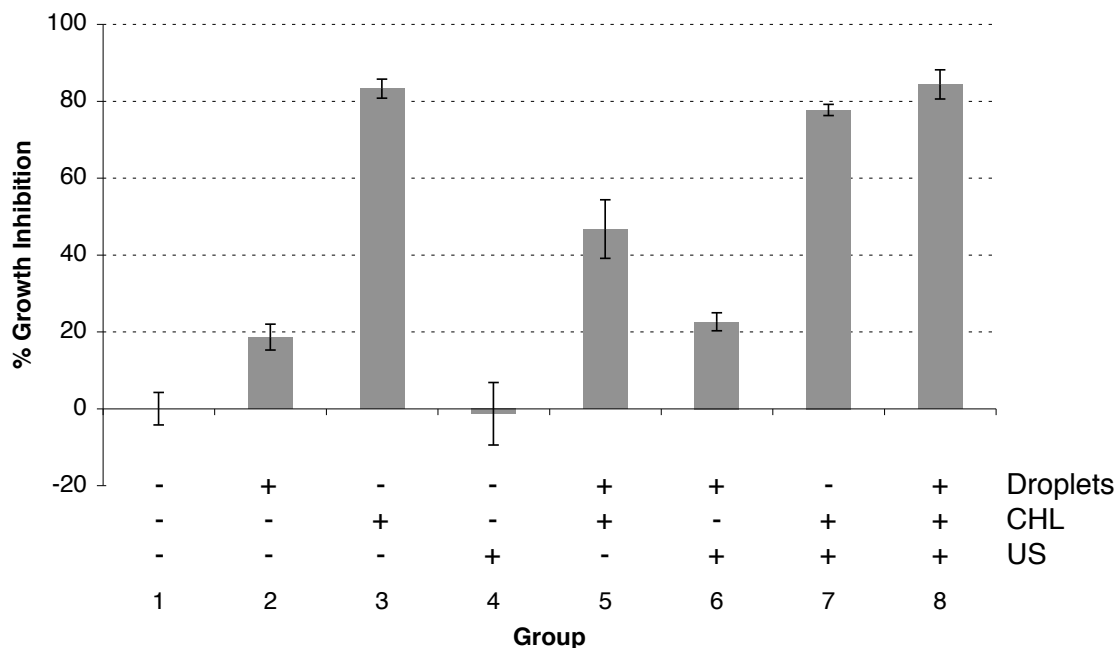


Figure 3.7: Mean ($n = 5$) percent GI and standard deviation for each of the eight experimental groups. The presence (+) or absence (-) of each parameter - droplets, CHL, and US - is indicated above each group number. The same exposure procedure, acoustic parameters, droplet concentration, and CHL concentration ($100 \mu\text{M}$ whether in DMSO or emulsified) was used for all groups.

Table 3.2: Results of Tukey's test on percent GI (upper right triangle) and mean diameter (lower left triangle) data. An 'x' indicates groups that are not statistically different at a 0.01 or 0.05 level. Statistically significant differences at a 0.01 or 0.05 level are indicated by '0.01' and '0.05', respectively.

Group	1	2	3	4	5	6	7	8
1		0.01	0.01	x	0.01	0.01	0.01	0.01
2	x		0.01	0.01	0.01	x	0.01	0.01
3	0.01	0.01		0.01	0.01	0.01	x	x
4	x	x	0.01		0.01	0.01	0.01	0.01
5	0.01	0.01	0.01	0.01		0.01	0.01	0.01
6	x	x	0.01	x	0.01		0.01	0.01
7	0.01	0.01	0.05	0.01	0.05	0.01		x
8	0.01	0.01	0.01	0.01	x	0.01	x	

chamber growth surfaces, unlike the rigid nature of conventional microtiter plates. Therefore, OptiCells™ can be coated with fibronectin or collagen, as was done in this manuscript, to minimize cell detachment. Despite coating the chambers with collagen, cell detachment was still appreciable during the vigorous washing step. The washing step was critical in ensuring that the cells were not incubated with drug-carrying emulsion after the 1-hour treatment. This detachment was confirmed, via microscopy and using the Coulter counter, by adding the blank emulsion to the chamber and then immediately washing the chamber. The droplets became attached to the cells following their introduction into the chamber, possibly due to an electrostatic interaction. During the washing of the chamber, the adherence of the droplets to the cells coupled with the vigorous movement of droplets during the procedure caused this GI. Different emulsion shells or different cell types could influence the amount of droplet attachment, and therefore the amount of cells that are depleted. All of these effects lie outside of the intended demonstration of drug release by ADV and were considered as correction factors in the final examination of drug release described below. Additionally, it is not known whether these depleted cells would have been viable had they not been depleted.

Groups 2 and 6 were not statistically different ($p > 0.05$), indicating the ADV process (group 6) did not cause any additional GI when compared to the droplets alone (group 2). The GI experienced by group 6 may include two potentially offsetting phenomena: 1) the reduction in the number of droplets due to ADV, and thus the decrease in cell detachment due to a decrease in droplet shearing; 2) GI induced by the ADV process itself. This second phenomena is clearly obtained when the chamber is not inverted prior to US exposure (see Fig. 3.1). When the droplets are resting on the cells and they are vaporized, there is a $74.9 \pm 8.5\%$ GI. However again, the viability of these detached cells is unknown since they are removed from the OptiCell™ during the washing.

The groups treated with CHL in DMSO (group 3) and CHL in DMSO with US (group 7) yielded GI values of $83.3 \pm 2.5\%$ and $77.7 \pm 1.5\%$, respectively, which is similar to the results obtained at the same concentration in Fig. 3.6. Additionally, groups 3 and 7 are not statistically different ($p > 0.05$), which is expected assuming a lack of appropriately-sized cavitation nuclei within the medium lacking droplets. The groups treated with emulsified CHL (group 5) and emulsified CHL with US (group 8) experienced $46.7 \pm 7.6\%$ and $84.3 \pm 3.8\%$ GI, respectively. Groups 5 and 8 are statistically different (see Table 3.2) indicating that the application of US did cause an increase in CHL release from the emulsion. Since group 5 is statistically different from both groups 3 and 7, and group 8 is not statistically different from groups 3 and 7, it can be surmised that the retention of CHL within the emulsion reduces its cytotoxicity until US is applied. Upon insonation, the cytotoxicity of emulsified CHL is equivalent to non-emulsified CHL (i.e. CHL in DMSO, group 3). It should be noted that a portion of the GI for groups 5 and 8 was due not only to CHL release (via leakage or US), but also the droplet-cell adhesion described above for groups 2 and 6. To determine the percent GI caused by CHL release, the effects of the droplets and ADV must be estimated. One option is to subtract the approximate 20% GI experienced by groups 2 and 6 from groups 5 and 8 in Fig. 3.7. Alternatively, groups 5 and 8 could be scaled by a fraction of 20% GI, considering that some of the cells exposed to CHL will also be removed during the washing of the chamber.

Figure 3.8 displays the mean cell diameter for the eight experimental groups. As indicated in Fig. 3.6, the average cell diameter can be used to assess whether CHL exposure contributed to GI. The level of CHL exposure can only be estimated from Fig. 3.1 if no other factors contributed to the GI. Groups that were not exposed to CHL - 1, 2, 4, and 6 - possessed mean diameters that were not statistically different (Table 3.2), when comparing any of the two groups. Groups 3 and 8 are statistically

different, suggesting that the GI observed in group 8 is not solely due to the presence of CHL but from other factors such as droplets or ADV. Additionally, groups 3 and 7 are statistically different, though only at a 0.05 level. Group 5 displayed a smaller average cell diameter than group 8, but the groups are not statistically different ($p > 0.05$), implying that the dominant cause of GI in group 8 is caused by CHL exposure. Overall, the GI obtained via cell counts is a more robust metric, when compared to using the mean cell diameter, though the latter metric can be used to gain insight into the mechanism driving the GI experienced by each group.

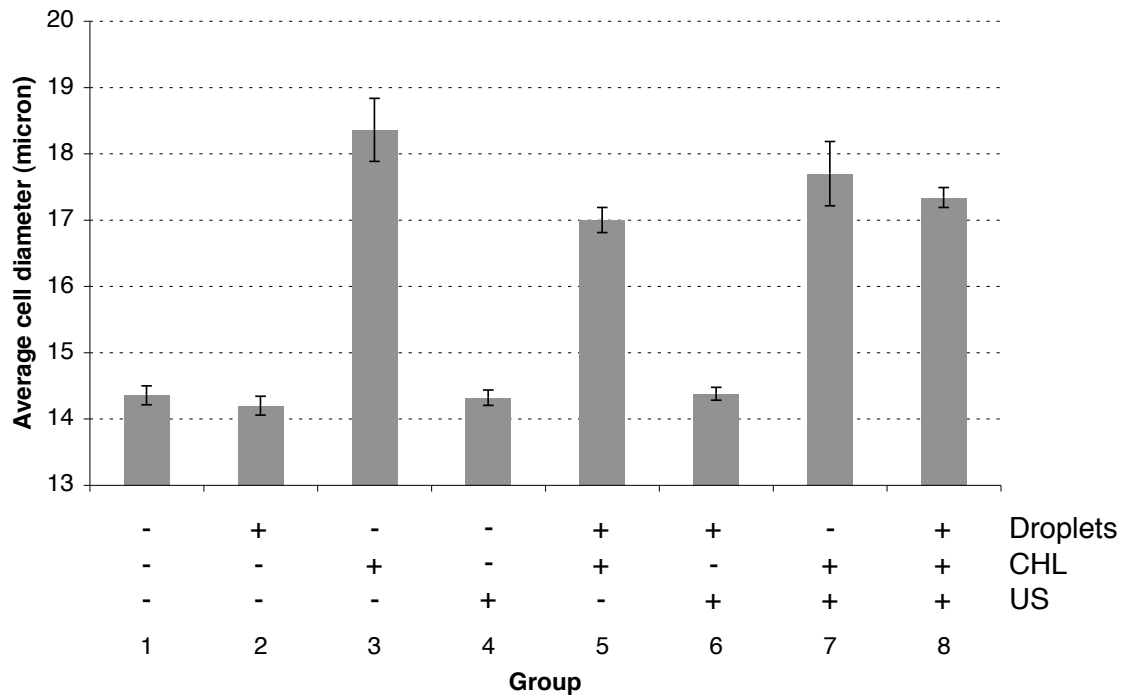


Figure 3.8: Mean ($n = 5$) cell diameter and standard deviation for each of the eight experimental groups. The presence (+) or absence (-) of each parameter - droplets, CHL, and US - is indicated above each group number. The same exposure procedure, acoustic parameters, droplet concentration, and CHL concentration ($100 \mu\text{M}$ whether in DMSO or emulsified) was used for all groups.

3.3.4 ADV efficiency

Figure 3.9 displays the ADV efficiency - the fraction of droplets that vaporize - as a function of droplet diameter. The ADV efficiency was measured with a

Coulter counter using the same setup described in Fig. 3.1. A sigmoidal relationship exists between the fraction of droplets vaporized and the droplet diameter, with the ADV efficiency relatively constant above $12\ \mu\text{m}$. The direct correlation between droplet diameter and ADV efficiency, at least between 2 and $12\ \mu\text{m}$, is qualitatively consistent with a probability of ADV stemming from the droplet distribution (i.e. larger droplets have larger PFP cores (Fig. 3.3) that are more likely to possess nuclei that could facilitate ADV).

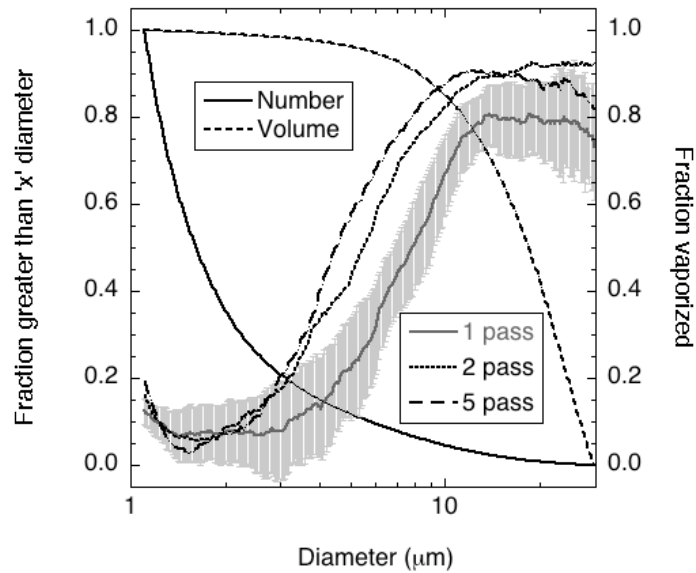


Figure 3.9: The number and volume weighted distributions for the dual-phase droplets are plotted along with the mean ($n = 3$) fraction of droplets vaporized, as a function of droplet size, for different number of exposure passes by the US array. The standard deviation is plotted for the single pass case, with similarly sized standard deviations obtained for the 2 and 5 pass cases. The small decrease in efficiency between 1 and $2\ \mu\text{m}$ is due to the subtraction errors between the treated (with US) and untreated (without US) cases.

Repeated passes of the US array across the chamber cause further ADV of remaining droplets, though the incremental difference in efficiency is larger going from 0 to 1 passes (where it was shown that no recordable droplet vaporization occurred by merely adding the droplets in the chamber and subsequently withdrawing them) than from 1 to 2 passes. This supports the possibility that for each pass of the US array, a constant fraction of the remaining droplets undergo ADV.

3.4 Discussion

This study focuses on the development of a micron-sized, drug delivery vehicle - containing a superheated PFC phase - which releases the drug payload upon ADV of the PFC. Other groups formulating drug-carrying PFC emulsions have focused on submicron sized droplets [17–20; 22]. The use of micron-sized droplets that are transpulmonary enables the coupling of ADV-induced drug delivery and localized occlusion. Localized occlusion results from relatively large microbubbles blocking perfusion at the capillary level. This selective generation of transient, vascular occlusion has been previously demonstrated *in vivo* [26; 27]. ADV-induced occlusion can complement ADV-induced drug delivery in two ways. First, the ischemic conditions created could increase the residence time of therapeutic material at the intended site, resulting in greater diffusion into the target tissue. A simple example of this phenomenon is obtained by comparing the 50% GI concentration for CHO cells when incubated with CHL for either 15 minutes (167 μM) or 60 minutes (57 μM). Second, the ischemic conditions can generate hypoxia that could be used to activate bioreductive prodrugs [42] that may be encapsulated within the emulsion. Thus, the proof-of-concept studies presented here serve as a foundation in developing future therapies that incorporate ADV.

The emulsion discussed in this work was prepared using a single emulsification step with only an aqueous-soluble surfactant, similar to other drug-carrying PFC emulsions [17; 18] and contrast agents [7; 10; 11]. In contrast, double emulsions are typically prepared in two stages with two types of surfactants, where the innermost droplets are first emulsified followed by their subsequent emulsification in a secondary fluid [43]. The presence of natural emulsifiers within soybean oil, including phospholipids [44] may help stabilize the PFP core.

The effect on the ADV threshold of encapsulating the PFP core within a layer of oil is currently unknown, though from Fig. 3.5 it does not appear to be as significant

for smaller droplets as larger droplets. In the case of AALs, the presence of an oil layer causes the pulse length required for contrast agent destruction to increase at least five-fold relative to contrast agent without an oil shell [9]. The thickness of the oil-lipid layer in AALs is 500 to 1000 nm and 300 to 700 nm for AALs containing triacetin and soybean oil, respectively [9]. By comparison, the mean oil-albumin layer thickness for the dual-phase droplets described in this study, measured using optical microscopy, is 1390 ± 720 nm. It is possible that the oil layer could inhibit or dampen the expansion of any gas nuclei generated within the PFP core during the ADV process, possibly even causing a recondensation of the PFP at lower rarefactional pressures. This is similar to results where the ADV threshold of PFP droplets increased as the viscosity of the bulk fluid containing the droplets increased [33].

Concerning the GI observed for group 2, PFC emulsions are known to cause cellular growth inhibition, but only in phagocytic cell lines [45; 46]. While this GI was well explained by droplet-cell adhesion and subsequent detachment from the OptiCellTM during washing, it was also hypothesized that the GI experienced by group 2 might be attributable to the fact that PFC emulsions can modulate the oxygen content of media due to their high gas dissolving capabilities [21; 47]. Based on the amount of PFP injected into each chamber and the solubility of oxygen in PFP - 80% (v/v) [48] - the maximum change in the oxygen concentration within the chamber, assuming that the PFP did not initially contain any oxygen, is 10% by weight. Hypoxic conditions can decrease the growth rate of CHO cells, but only when the cells are exposed to an oxygen concentration less than 3.5%, relative to the atmospheric oxygen concentration, for prolonged periods (i.e. > 10 hrs) [49]. By comparison, after injecting the emulsion into the OptiCellTM, the measured change in dissolved oxygen concentration was negligible (i.e. less than 1%) over one hour. This is likely due to the gas permeable nature of the OptiCellTM windows and that

the PFP was partially saturated with oxygen prior to injection due to atmospheric contact.

The cellular bioeffects of ADV are currently unknown, though some insights can be obtained from the presented studies. The cell detachment due to the ADV process may be a result of droplet displacement prior to vaporization, where velocities up to 20 m/s have been recorded [50]. Additionally, the rapid consumption of the liquid PFP and expansion of the resulting bubble during the ADV process [51], combined with bioeffects stemming from cavitation [52], could cause cell detachment. It is unknown whether ADV could cause cell detachment *in vivo* or if the vaporization process could cause increased cell or vascular permeability, similar to results observed with microbubble cavitation [1; 2].

Since the intended mechanism of drug release from the dual-phase emulsion is US, the ADV efficiency is directly related to the amount of oil, and hence CHL, that could be potentially available for cellular exposure. As seen in Fig. 3.5, an inverse trend exists between the ADV threshold and the droplet diameter. Though this trend is confounded by the use of polydisperse droplets, it is hypothesized that droplets with a lower ADV threshold will also display a higher ADV efficiency for a given acoustic exposure. Additionally, it is possible that the ADV efficiency trend observed in Fig. 3.9 can be attributed to the distribution of rarefactional pressures within the focal volume of the US array as well as the duration in which droplets of a given diameter are exposed to rarefactional pressures greater than their respective ADV thresholds. Assuming an infinite US exposure duration at a given acoustic pressure, while neglecting the dissolution of the droplets, the ADV efficiency should either be zero (for small droplets whose diameters render high ADV thresholds) or one. The step function dependence of the ADV efficiency, with respect to droplet diameter, is supported by computing the slopes of the ADV efficiency data between 2 to 12 μm . The slopes - which increase as the number of exposure passes increases

- are 0.07, 0.09, and 0.10 μm^{-1} for 1, 2, and 5 passes, respectively.

The inverse relationship between ADV threshold and droplet diameter is similar to the relationship between the thermal vaporization temperature of PFP droplets and droplet diameter. Using the Laplace pressure and Antoine equations, the diameter above which PFP droplets will undergo thermal vaporization at 37°C is 6.4 μm and 4.0 μm for surface tensions of 50 mN/m and 30 mN/m, respectively [20]; shell effects beyond surface tension reduction are ignored in these estimates. Therefore, the distinct ADV thresholds and defined ADV efficiencies of the emulsions, coupled with the observation that PFP emulsions are thermally stable up to 60°C [24], indicate these emulsions are relatively free of nuclei that enable the emulsion to stably exist in a superheated state.

Table 3.3 lists the fraction of total droplets vaporized in terms of both number and volume weighted distributions. The droplets in the 1 to 6 μm range are transpulmonary, and thus amenable to intravenous administration, whereas the droplets in the 6 to 30 μm range are amenable to intra-arterial administration. The number and volume-weighted fractions (without volume correction) were estimated by using the respective distributions and ADV efficiency in Fig. 3.9. The volume corrected fractions were estimated by correlating the ratio of the inner to outer diameter to the outer droplet diameter (Fig. 3.3). This correction was then applied to determine the volume of oil, and thus CHL, released upon ADV. The correction has a more significant impact on the larger droplets that, as seen in Fig. 3.3, have a larger PFP core. Thus, for a single pass of the US array - which was used in the cell experiments - approximately 50% of the oil is released upon ADV. Assuming an equal distribution of CHL within the oil, the actual concentration of CHL released via ADV in the chamber is 50 μM , which causes a 51% GI (based on Fig. 3.6). In Fig. 3.7, group 8 displayed an 84.3% GI, which when the GI caused by the emulsion alone (groups 2 and 6) is subtracted, the percent GI from released CHL is

approximately 64.3%. This is qualitatively consistent with the percent GI predicted by the ADV efficiency.

Table 3.3: The fraction of total droplets vaporized, expressed in terms of number and volume fraction. The data without volume correction is the fraction of droplets vaporized, based on Fig. 3.9. The volume corrected data uses the relationship between the inner and outer droplet diameters (Fig. 3.3) to estimate the fraction of oil released.

Diameter Range	Counts	Volume corrected	Number of Passes		
			1	2	5
1 - 6 μm	Number	No	0.08	0.11	0.10
	Volume	No	0.01	0.02	0.02
	Volume	Yes	0.01	0.02	0.02
6 - 30 μm	Number	No	0.06	0.08	0.08
	Volume	No	0.72	0.85	0.83
	Volume	Yes	0.49	0.58	0.57

3.5 Conclusions

In summary, a stable, superheated, micron-sized emulsion has been developed that carries a lipophilic, therapeutic agent. The emulsion is triggered via US to produce gas bubbles and enhance the release of the encapsulated agent, as demonstrated with cultured cells. Current efforts are focused on increasing the drug loading of the dual-phase emulsions, minimizing the effect of non-US related drug release, and controlling the size distribution of the emulsions.

3.6 Acknowledgments

The authors would like to thank Dr. Douglas Miller and Dr. Chunyan Dou (Department of Radiology, University of Michigan, Ann Arbor, MI) for assistance with the cell studies as well as Dr. Xia Shao and Dr. Lihsueh Lee (Department of Nuclear Medicine, University of Michigan, Ann Arbor, MI) for use of their HPLC system. This work was supported in part by NIH grant 5R01EB000281.

REFERENCES

- [1] S. Hernot and A. L. Klibanov, "Microbubbles in ultrasound-triggered drug and gene delivery," *Advanced Drug Delivery Reviews*, vol. 60, no. 10, pp. 1153–1166, 2008.
- [2] E. C. Pua and P. Zhong, "Ultrasound-mediated drug delivery," *IEEE Engineering in Medicine and Biology Magazine*, vol. 28, no. 1, pp. 64–75, 2009.
- [3] S. Tinkov, R. Bekeredjian, G. Winter, and C. Coester, "Microbubbles as ultrasound triggered drug carriers," *Journal of Pharmaceutical Sciences*, vol. 98, no. 6, pp. 1935–1961, 2009.
- [4] A. Kheirrolomoom, P. A. Dayton, A. F. Lum, E. Little, E. E. Paoli, H. Zheng, and K. W. Ferrara, "Acoustically-active microbubbles conjugated to liposomes: characterization of a proposed drug delivery vehicle," *Journal of Controlled Release*, vol. 118, no. 3, pp. 275–284, 2007.
- [5] I. Lentacker, B. G. D. Geest, R. E. Vandenroucke, L. Peeters, J. Demeester, S. C. D. Smedt, and N. N. Sanders, "Ultrasound-responsive polymer-coated microbubbles that bind and protect DNA," *Langmuir*, vol. 22, no. 17, pp. 7273–7278, 2006.
- [6] M. A. Borden, C. F. Caskey, E. Little, R. J. Gillies, and K. W. Ferrara, "DNA and polylysine adsorption and multilayer construction onto cationic lipid-coated microbubbles," *Langmuir*, vol. 23, no. 18, pp. 9401–9408, 2007.
- [7] J. Eisenbrey, P. Huang, J. Hsu, and M. Wheatley, "Ultrasound triggered cell death *in vitro* with doxorubicin loaded poly lactic-acid contrast agents," *Ultrasonics*, vol. 49, no. 8, pp. 628–633, 2009.
- [8] K. Kooiman, M. R. Bohmer, M. Emmer, H. J. Vos, C. Chlon, W. T. Shi, C. S. Hall, S. H. de Winter, K. Schroen, M. Versluis, N. de Jong, and A. van Wamel, "Oil-filled polymeric microcapsules for ultrasound-mediated delivery of lipophilic drugs," *Journal of Controlled Release*, vol. 133, no. 2, pp. 109–118, 2009.
- [9] D. J. May, J. S. Allen, and K. W. Ferrara, "Dynamics and fragmentation of thick-shelled microbubbles," *IEEE Transactions on Ultrasonics, Ferroelectrics, and Frequency Control*, vol. 49, no. 10, pp. 1400–1410, 2002.

- [10] M. S. Tartis, J. McCallan, A. F. Lum, R. LaBell, S. M. Stieger, T. O. Matsunaga, and K. W. Ferrara, "Therapeutic effects of paclitaxel-containing ultrasound contrast agents," *Ultrasound in Medicine and Biology*, vol. 32, no. 11, pp. 1771–1780, 2006.
- [11] E. Unger, T. McCreery, R. Sweitzer, V. Caldwell, and Y. Wu, "Acoustically active lipospheres containing paclitaxel - a new therapeutic contrast agent," *Investigative Radiology*, vol. 33, no. 12, pp. 886–892, 1998.
- [12] J. A. Kopechek, T. M. Abruzzo, B. Wang, S. M. Chrzanowski, D. A. Smith, P. H. Kee, S. Huang, J. H. Collier, D. D. McPherson, and C. K. Holland, "Ultrasound-mediated release of hydrophilic and lipophilic agents from echogenic liposomes," *Journal of Ultrasound in Medicine*, vol. 27, no. 11, pp. 1597–1606, 2008.
- [13] T. Priestman, *Cancer chemotherapy in clinical practice*. London, UK: Springer-Verlag, 2008.
- [14] G. M. Lanza and S. A. Wickline, "Targeted ultrasonic contrast agents for molecular imaging and therapy," *Progress in Cardiovascular Diseases*, vol. 44, no. 1, pp. 13–31, 2001.
- [15] E. C. Unger, T. Porter, W. Culp, R. LaBell, T. Matsunaga, and R. Zutshi, "Therapeutic applications of lipid-coated microbubbles," *Advanced Drug Delivery Reviews*, vol. 56, no. 9, pp. 1291–1314, 2004.
- [16] V. Shenoy, I. Vijay, and R. Murthy, "Tumour targeting: biological factors and formulation advances in injectable lipid nanoparticles," *Journal of Pharmacy and Pharmacology*, vol. 57, no. 4, pp. 411–421, 2005.
- [17] J. Y. Fang, C. F. Hung, M. H. Liao, and C. C. Chien, "A study of the formulation design of acoustically active lipospheres as carriers for drug delivery," *European Journal of Pharmaceutics and Biopharmaceutics*, vol. 67, no. 1, pp. 67–75, 2007.
- [18] J. Y. Fang, C. F. Hung, S. C. Hua, and T. L. Hwang, "Acoustically active perfluorocarbon nanoemulsions as drug delivery carriers for camptothecin: drug release and cytotoxicity against cancer cells," *Ultrasonics*, vol. 49, no. 1, pp. 39–46, 2009.
- [19] T. L. Hwang, Y. J. Lin, C. H. Chi, T. H. Huang, and J. Y. Fang, "Development and evaluation of perfluorocarbon nanobubbles for apomorphine delivery," *Journal of Pharmaceutical Sciences*, vol. 98, no. 10, pp. 3735–3747, 2009.
- [20] N. Y. Rapoport, A. M. Kennedy, J. E. Shea, C. L. Scaife, and K.-H. Nam, "Controlled and targeted tumor chemotherapy by ultrasound-activated nanoemulsions/microbubbles," *Journal of Controlled Release*, vol. 138, no. 2, pp. 268–276, 2009.

- [21] J. G. Riess, “Oxygen carriers (“blood substitutes”) - raison d’etre, chemistry, and some physiology,” *Chemical Reviews*, vol. 101, no. 9, pp. 2797–2919, 2001.
- [22] N. Rapoport, Z. Gao, and A. Kennedy, “Multifunctional nanoparticles for combining ultrasonic tumor imaging and targeted chemotherapy,” *Journal of the National Cancer Institute*, vol. 99, no. 14, pp. 1095–1106, 2007.
- [23] R. E. Apfel, “Activatable infusible dispersions containing drops of a superheated liquid for methods of therapy and diagnosis,” Patent 5,840,276, Apfel Enterprises, Inc., November 1998.
- [24] O. D. Kripfgans, J. B. Fowlkes, D. L. Miller, O. P. Eldevik, and P. L. Carson, “Acoustic droplet vaporization for therapeutic and diagnostic applications,” *Ultrasound in Medicine and Biology*, vol. 26, no. 7, pp. 1177–1189, 2000.
- [25] K.-I. Kawabata, N. Sugita, H. Yoshikawa, T. Azuma, and S.-I. Umemura, “Nanoparticles with multiple perfluorocarbons for controllable ultrasonically induced phase shifting,” *Japanese Journal of Applied Physics*, vol. 44, no. 6B, pp. 4548–4552, 2005.
- [26] O. D. Kripfgans, J. B. Fowlkes, M. Woydt, O. P. Eldevik, and P. L. Carson, “*In vivo* droplet vaporization for occlusion therapy and phase aberration correction,” *IEEE Transactions on Ultrasonics, Ferroelectrics, and Frequency Control*, vol. 49, no. 2, pp. 726–738, 2002.
- [27] O. D. Kripfgans, C. M. Orifici, P. L. Carson, K. A. Ives, O. P. Eldevik, and J. B. Fowlkes, “Acoustic droplet vaporization for temporal and spatial control of tissue occlusion: a kidney study,” *IEEE Transactions on Ultrasonics, Ferroelectrics, and Frequency Control*, vol. 52, pp. 1101–1110, July 2005.
- [28] P. Price and K. Sikora, eds., *Treatment of Cancer*. New York, NY: Oxford University Press, 4th ed., 2002.
- [29] M. C. Perry, ed., *The Chemotherapy Source Book*. Philadelphia, PA: Lippincott Williams and Wilkins, 4th ed., 2008.
- [30] S. Ganta, H. Devalapally, B. C. Baguley, S. Garg, and M. Amiji, “Microfluidic preparation of chlorambucil nanoemulsion formulations and evaluation of cytotoxicity and pro-apoptotic activity in tumor cells,” *Journal of Biomedical Nanotechnology*, vol. 4, no. 2, pp. 165–173, 2008.
- [31] S. Ganta, J. W. Paxton, B. C. Baguley, and S. Garg, “Pharmacokinetics and pharmacodynamics of chlorambucil delivered in parenteral emulsion,” *International Journal of Pharmaceutics*, vol. 360, pp. 115–121, 2008.
- [32] D. H. Lee, Y. M. Goh, J. S. Kim, H. K. Kim, H. H. Kang, K. D. Suh, and J. W. Kim, “Effective formation of silicone-in-fluorocarbon-in-water double emulsions: Studies on droplet morphology and stability,” *Journal of Dispersion Science and Technology*, vol. 23, no. 4, pp. 491–497, 2002.

- [33] M. L. Fabiilli, K. J. Haworth, N. H. Fakhri, O. D. Kripfgans, P. L. Carson, and J. B. Fowlkes, "The role of inertial cavitation in acoustic droplet vaporization," *IEEE Transactions on Ultrasonics, Ferroelectrics, and Frequency Control*, vol. 56, no. 5, pp. 1006–1017, 2009.
- [34] R. I. Freshney, *Culture of animal cells - a manual of basic technique*. Hoboken, NJ, USA: John Wiley & Sons, Inc., 5th ed., 2005.
- [35] E. A. Hussain-Hakimjee, X. Peng, R. R. Mehta, and R. G. Mehta, "Growth inhibition of carcinogen-transformed MCF-12F breast epithelial cells and hormone-sensitive BT-474 breast cancer cells by 1 α -hydroxyvitamin D₅," *Carcinogenesis*, vol. 27, no. 3, pp. 551–559, 2006.
- [36] N. M. Lopes, E. G. Adams, T. W. Pitts, and B. K. Bhuyan, "Cell kill kinetics and cell cycle effects of taxol on human and hamster ovarian cell lines," *Cancer Chemotherapy and Pharmacology*, vol. 32, no. 3, pp. 235–242, 1993.
- [37] G. T. Brophy and N. Sladek, "Influence of pH on the cytotoxic activity of chlorambucil," *Biochemical Pharmacology*, vol. 32, no. 1, pp. 79–84, 1983.
- [38] Y. Yamazaki, S. Kunimoto, and D. Ikeda, "Rakicidin A: a hypoxia-selective cytotoxin," *Biological and Pharmaceutical Bulletin*, vol. 30, no. 2, pp. 261–265, 2007.
- [39] W. Bruce, B. Meeker, and F. Valeriote, "Comparison of sensitivity of normal hematopoietic and transplanted lymphoma colony-forming cells to chemotherapeutic agents administered in vivo," *Journal of the National Cancer Institute*, vol. 37, no. 2, pp. 233–245, 1966.
- [40] S. Detke, J. L. Stein, and G. S. Stein, "Influence of chlorambucil, a bifunctional alkylating agent, on DNA replication and histone gene expression in HeLa S₃ cells," *Cancer Research*, vol. 40, no. 4, pp. 967–974, 1980.
- [41] D. W. Ross, "The nature of unbalanced cell growth caused by cytotoxic agents," *Virchow Archiv B - Cell Pathology*, vol. 37, no. 2, pp. 225–235, 1981.
- [42] S. McKeown, R. Cowen, and K. Williams, "Bioreductive drugs: from concept to clinic," *Clinical Oncology*, vol. 19, no. 1, pp. 427–442, 2007.
- [43] C. Goubault, K. Pays, D. Olea, P. Gorria, J. Bibette, V. Schmitt, and F. Leal-Calderon, "Shear rupturing of complex fluids: application to the preparation of quasi-monodisperse water-in-oil-in-water double emulsions," *Langmuir*, vol. 17, pp. 5184–5188, August 2001.
- [44] D. T. Wasan, M. E. Ginn, and D. O. Shah, eds., *Surfactants in chemical/process engineering*, vol. 28. New York: Marcel Dekker, Inc., 1988.
- [45] R. Bucala, M. Kawakami, and A. Cerami, "Cytotoxicity of a perfluorocarbon blood substitute to macrophages *in vitro*," *Science*, vol. 220, no. 4600, pp. 965–967, 1983.

- [46] V. Centis, C. J. Doillon, and P. Vermette, “Perfluorocarbon emulsions cytotoxic effects on human fibroblasts and effect of aging on particle size distribution,” *Artificial Organs*, vol. 31, no. 8, pp. 649–653, 2007.
- [47] K. C. Lowe, M. R. Davey, and J. B. Power, “Perfluorochemicals: their applications and benefits to cell culture,” *Trends in Biotechnology*, vol. 16, no. 6, pp. 272–277, 1998.
- [48] J. L. Johnson, M. C. Dolezal, A. Kerschen, T. O. Matsunaga, and E. C. Unger, “*In vitro* comparison of dodecafluoropentane (DDFP), perfluorodecalin (PFD), and perfluorooctylbromide (PFOB) in the facilitation of oxygen exchange,” *Artificial cells, blood substitutes, and biotechnology*, vol. 37, no. 4, pp. 156–162, 2009.
- [49] A. A. Lin and W. M. Miller, “CHO cell responses to low oxygen: regulation of oxygen consumption and sensitization to oxidative stress,” *Biotechnology and Bioengineering*, vol. 40, no. 4, pp. 505–516, 1992.
- [50] O. D. Kripfgans, M. L. Fabiilli, P. L. Carson, and J. B. Fowlkes, “On the acoustic vaporization of micrometer-sized droplets,” *Journal of the Acoustical Society of America*, vol. 116, no. 1, pp. 272–281, 2004.
- [51] K. J. Haworth and O. D. Kripfgans, “Initial growth and coalescence of acoustically vaporized perfluorocarbon microdroplets,” *IEEE International Ultrasonics Symposium Proceedings*, pp. 623–626, 2008.
- [52] D. Dalecki, “Mechanical bioeffects of ultrasound,” *Annual Review of Biomedical Engineering*, vol. 6, no. 1, pp. 229–248, 2004.

CHAPTER IV

Delivery of Water-Soluble Drugs using Acoustically-Triggered, Perfluorocarbon Double Emulsions

4.1 Introduction

Particles that release a therapeutic payload upon interaction with an internal stimulus, such as pH or hypoxia, or the application of an externally-applied stimulus, such as heat or ultrasound (US), are being studied in an effort to localize drug delivery to target areas [1–5]. The control of localized delivery is especially important for drugs that possess narrow therapeutic windows, thereby minimizing systemic side-effects. US-triggered drug delivery is unique since US affords diagnostic and therapeutic capabilities, spatial and temporal control of delivery, and the ability to focus onto deeply located tissues. The interaction of US with payload-containing particles can generate acoustic cavitation, heating, radiation forces, and sonoporation. The last effect, the transient increase in cell membrane permeability, can greatly enhance the uptake of drugs, genes, and peptides contained within US-activated particles [6–9]. These particle-US interactions can also produce therapeutic effects to be utilized in diverse applications such as thrombolysis [10] or in the reversible disruption of the blood-brain barrier [11].

Colloidal particles utilized in US-mediated drug release are typically shell-stabilized microbubbles or droplets containing, respectively, perfluorocarbon (PFC)

gases or liquids. The former colloids evolved from clinically-utilized US contrast agents, which are micron-sized gas bubbles that increase the echogenicity in perfused tissue upon intravenous administration. Due to their size, the microbubbles are transpulmonary and resonant at frequencies utilized in clinical imaging systems [12]. Therapeutic agents are typically incorporated into the microbubbles using one of the following methods: attachment to or intercalation within the shell; complexation of secondary carriers to the microbubble shell; or incorporation within a fluid inside the shell [13; 14].

As highlighted in a recent review [15], PFC emulsions have also been studied as US contrast agents and drug delivery systems due to their increased stability, longer circulation times, and ability to extravasate if formulated as nanoparticles. Due to the hydrophobicity and lipophobicity of the dispersed PFC phase [16], therapeutic agents are typically loaded into the emulsion using similar techniques as those mentioned for microbubble delivery systems. One commonly utilized method is the use of an oil-phase, containing the therapeutic agent, co-emulsified with the PFC phase during formulation [17–20]. PFC emulsions, with or without a therapeutic payload, can be vaporized into gas bubbles using US, a mechanism termed acoustic droplet vaporization (ADV) [21–25]. ADV is a phenomenon whereby vaporization occurs only if the emulsion is exposed to acoustic amplitudes greater than a threshold value. PFCs used in emulsions suitable for ADV applications typically possess bulk boiling points that are lower than normal body temperature (37°C), such as perfluoropentane (29°C boiling point). Upon injection *in vivo*, the emulsions do not spontaneously vaporize due to the increased internal (i.e. Laplace) pressure, and hence boiling point elevation, of the PFC when formulated as droplets [25]. Low boiling point PFCs, such as perfluoropentane, also enable the use of lower acoustic amplitudes to generate ADV [17] and the production of stable gas bubbles *in vivo* [26–28]. The ADV of PFC emulsions containing a lipophilic, therapeutic

payload can be used to facilitate the delivery and release of the therapeutic agent, as demonstrated with *in vitro* [17–20] and *in vivo* [25] studies.

The ADV of micron-sized PFC emulsions, administered intravenously or intraarterially, has also been used to generate localized, vascular occlusion *in vivo* [26–28]. The temporal duration of an ADV-generated occlusion is transient, especially for gas emboli generated from intravenously administered emulsions [28]. Therefore, the ability to extend this duration may be therapeutically beneficial for surgical applications that require longer occlusion times such as radiofrequency ablation [29] and high intensity focused US thermal therapy [30]. ADV-generated occlusion could also be potentially used to treat hemorrhaging associated with vascular damage or other internal bleeding, which are currently treated using transcatheter embolization [31; 32]. One option is the simultaneous formation of a chemically-generated embolus and gas embolus within the feeder artery of the target tissue, thereby prolonging the duration of ADV-generated embolization. Chemical embolic agents - such as N-butyl cyanoacrylate, ethylene vinyl alcohol copolymer, and Eudragit E-100 (used in the treatment of arteriovenous malformations [33–35]) or thrombin (used in the treatment of pseudoaneurysms [36; 37]) - are typically administered via the use of a catheter. Therefore, the encapsulation of a chemical embolic agent within a PFC emulsion could provide a minimally-invasive means of producing a localized, sustained embolization via ADV with millimeter precision and without the use of ionizing fluoroscopy.

The aim of this study was to develop a PFC emulsion containing a water-soluble, chemical embolic agent - thereby expanding the range of therapeutic agents delivered via ADV beyond oil-soluble compounds. The micron-sized, PFC emulsions were formulated as double emulsions with the following structure: water-in-PFC-in-water ($W_1/PFC/W_2$). These double emulsions can serve as a prototype carrier for other water-soluble therapeutic agents. In the first section, PFC double emulsions

containing fluorescein - a hydrophilic fluorophore - are prepared and studied to demonstrate the proof-of-concept that fluorescein encapsulation within a PFC double emulsion delays its release until US exposure. The ability of ADV to release the encapsulated fluorescein is also evaluated. In the second section, the encapsulation of a chemical embolic agent, thrombin (factor IIa) - a serine protease in the coagulation cascade that converts fibrinogen into fibrin - is explored using different emulsification techniques. The effects of the various techniques are studied in terms of the resulting emulsion, with a focus on thrombin stability and retention. ADV of the thrombin-loaded emulsion is achieved using ultrasound parameters suitable for *in vivo* applications.

4.2 Materials and Methods

4.2.1 Fluorosurfactant synthesis

The copolymer used to stabilize the primary emulsion (W_1 /PFC) was synthesized using a two-step process, as seen in Fig. 4.1 and outlined in Holtze *et al.* [38]. First, Krytox 157 FSL (DuPont, Wilmington, DE, USA) - a perfluoroether with carboxylic acid functionality - was converted to an acid chloride using methods previously described [39; 40]. Briefly, under a nitrogen purge, Krytox 157 FSL was added to a round bottom flask containing HFE-7100 (3M, St. Paul, MN, USA), a mixture of methyl nonafluoroisobutyl ether and methyl nonafluorobutyl ether. Thionyl chloride (Sigma Aldrich, St. Louis, MO, USA) was then added in a 10:1 molar excess relative to the Krytox 157 FSL. The flask was refluxed with a condenser and stirred for 24 hours at 50°C while under a nitrogen purge. The resulting mixture was concentrated using a rotary evaporator. Second, the acid chloride was reacted with polyoxyethylene (PEG) diamine (Sigma Aldrich) to form a copolymer, analogous to previously described methods [39; 40]. The solvent was a 5:3 volumetric ratio of HFE-7100 and benzotrifluoride (Alfa Aesar, Ward Hill,

MA, USA). Similar experimental conditions were used as in the first reaction step. The resulting copolymer, termed Krytox-PEG copolymer, was concentrated using a rotary evaporator and its structure was confirmed using ^1H , ^{13}C , and ^{19}F NMR spectroscopy.

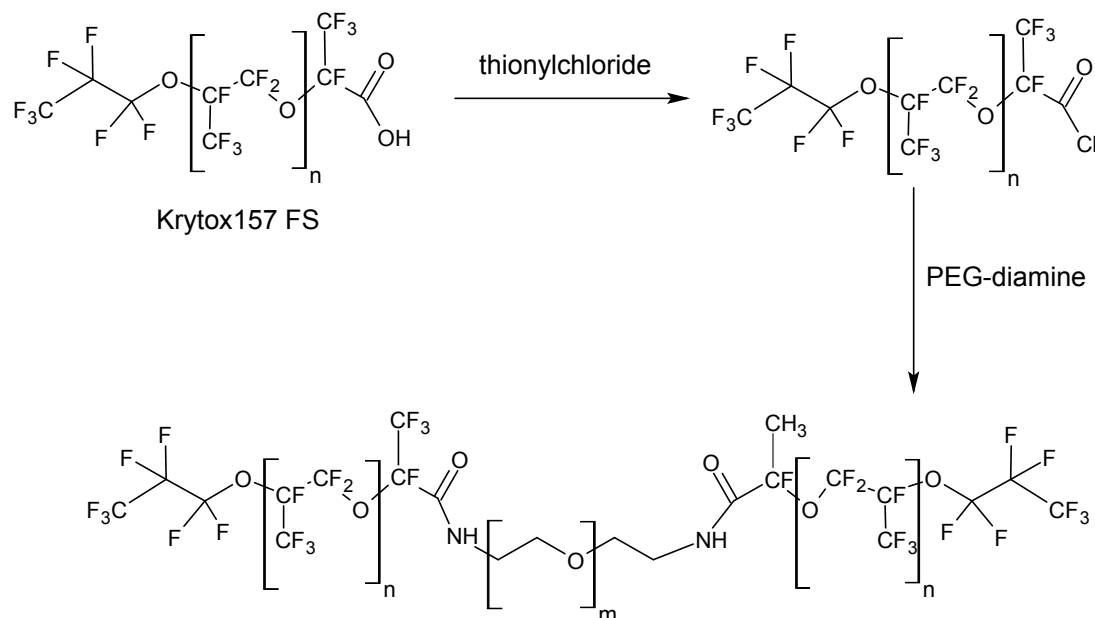


Figure 4.1: The Krytox 157 FSL is first converted into an acid chloride and then reacted with PEG-diamine to form a copolymer via amide linkages.

4.2.2 Fluorescein emulsion preparation

The primary emulsion was formed by first dissolving, in a 1.5 mL centrifuge tube (Thermo Fisher Scientific, Waltham, MA, USA), Krytox-PEG copolymer (6 mg/mL PFC) in 400 μL of either perfluoro-n-pentane (PFP, Alfa Aesar) or perfluoro-n-hexane (PFH, Alfa Aesar). Next, 200 μL of a 100 mg/mL solution of fluorescein sodium salt (Sigma Aldrich) in normal saline (0.9% w/v, Hospira Inc., Lake Forest, IL, USA) was added to the PFC phase. The mixture was emulsified, while in an ice bath, via sonication using a microtip (model 450, 20 kHz, 3.2 mm diameter, Branson, Danbury, CT, USA) operating at 125 W/cm^2 for 30 seconds in continuous mode. In

a 2 mL glass vial (Shamrock Glass, Seaford, DE, USA), 250 μL of primary emulsion was then added to 750 μL of a 10 mg/mL solution of Pluronic F-68 (Poloxamer 188, Sigma Aldrich) dissolved in normal saline. The vial was sealed with a rubber stopper and metal cap and subsequently shaken for 45 seconds at 4550 cycles per minute using an amalgamator (VialMix, Lantheus Medical Imaging, Billerica, MA, USA). The resulting double emulsion was used immediately after processing, though it was confirmed that the emulsion was stable, in terms of encapsulation efficiency and droplet size distribution, for at least 24 hours if stored at 5°C . Table 4.1 summarizes the fluorescein emulsions and associated processing parameters.

Table 4.1: Summary of fluorescein and thrombin emulsions used for studies. In all cases, the primary emulsion was formed using sonication.

Formulation	Compound	PFC	Processing ^a
F1	fluorescein	PFP	shaking
F2	fluorescein	PFH	shaking
T1	thrombin	PFP	sonication
T2	thrombin	PFP	shaking
T3	thrombin	PFP	stirring
T4	thrombin	PFP	stirring + glass beads
T5	thrombin ^b	PFP	stirring + glass beads

^aDuring second emulsification step

^bXanthan gum dissolved in the W₁ phase

4.2.3 Thrombin emulsion preparation

Thrombin (Thrombin-JMI, bovine-origin, King Pharmaceuticals, Bristol, TN, USA) was dissolved in normal saline at a concentration of 5000 international units (IU) per mL. In a microcentrifuge tube, 300 μL of thrombin solution was combined with 650 μL of PFP, which already contained dissolved Krytox-PEG copolymer (6 mg/mL PFC). The mixture was then sonicated, as previously described for the fluorescein emulsions, to form the primary emulsion. The primary emulsion (475 μL) was combined with a 10 mg/mL solution of Pluronic F-68 in saline (1200 μL) and emulsified to form the double emulsion. Three processing techniques

were explored for the second emulsification step: sonication, shaking, or magnetic stirring. For emulsification via sonication, the primary emulsion was added to a microcentrifuge tube along with the Pluronic F-68 solution and then sonicated as previously described. For emulsification via shaking, the primary emulsion and Pluronic F-68 solution were added to a 2 mL glass vial and processed similarly to the second emulsification step of the fluorescein emulsions. For emulsification via magnetic stirring, the primary emulsion was added to the Pluronic F-68 solution, contained in a 2 mL glass vial, while being stirred at 1100 rpm for 15 minutes. The vial was placed in an ice bath during the stirring process. Borosilicate glass balls (2 mm diameter, Chemglass Inc., Vineland, NJ, USA) were added in two formulations (T4 and T5) to reduce the droplet size during the stirring step. Xanthan gum (Sigma Aldrich) was dissolved in the thrombin solution (10 mg/mL) in one formulation (T5) in order to increase the viscosity of the encapsulated aqueous phase; this was done in an effort to decrease the mobility of the thrombin in the W_1 phase and hence the diffusion rate of thrombin from the emulsion [41]. All experiments were conducted with emulsions that had been processed immediately prior to use, though it was confirmed that the emulsions were stable, in terms of encapsulation efficiencies and droplet size distributions, for at least 24 hours if stored at 5°C. Table 4.1 summarizes the various thrombin formulations that were investigated.

4.2.4 Physical characterization of emulsions

The structures of the double emulsions containing fluorescein were determined using visible and fluorescent microscopy. Visible micrographs of the thrombin emulsions were also taken. The emulsions were diluted in normal saline and images were taken using a microscope (Leica DMRB, Bannockburn, IL, USA) and camera (Spot FLEX, Diagnostic Instruments Inc., Sterling Heights, MI, USA), controlled by Spot Advanced software (Diagnostic Instruments Inc.). The emulsions were sized using a Coulter counter (Multisizer 3, Beckman Coulter Inc., Fullerton, CA, USA).

Prior to sizing, the emulsions were diluted in normal saline that had been filtered through a 0.22 μm filter (GSWP, Millipore, Billerica, MA, USA). All formulations were sized using a 50 μm aperture, which can count particles between 1.0-30 μm . The T3 formulation was also sized with a 140 μm aperture, which can count particles between 2.8-84 μm , due to the presence of larger droplets.

4.2.5 Encapsulation efficiency of fluorescein emulsions

The fluorescein emulsions were washed in triplicate to remove unencapsulated fluorescein. Due to the densities of PFP (1.6 g/mL) and PFH (1.7 g/mL), the washing was accomplished by centrifuging the droplets at 1200 rpm for 3 minutes. Repeated centrifugation did not cause significant droplet breaking, which was confirmed by measuring the fluorescein concentration in the supernatant between the second and third washings. The concentration of encapsulated fluorescein was determined by adding an aliquot of the washed emulsion to methanol (CHROMASOLV Plus for HPLC, Sigma Aldrich), thereby breaking the emulsion. The fluorescein concentration was determined via fluorescence spectroscopy (LS-50B, PerkinElmer, Waltham, MA, USA) with excitation and emission wavelengths of 485 nm and 525 nm, respectively. The encapsulation efficiency was calculated as the ratio of encapsulated fluorescein to the initial amount of fluorescein loaded into the emulsion (i.e. prior to washing).

4.2.6 *In vitro* fluorescein release

Fluorescein release from the PFP and PFH emulsions was measured using a Franz diffusion cell (PermeGear, Inc., Hellertown, PA, USA). A cellulose membrane (6-8 kDa molecular weight cutoff, Spectrum Laboratories, Inc., Rancho Dominguez, CA, USA), soaked in normal saline 30 minutes prior to use, was mounted between the donor and receptor compartments. By comparison, the molecular weight of the ionized form of fluorescein is 328.3 Da. The donor media consisted of 2 mL of fluorescein emulsion, washed in triplicate to remove unencapsulated fluorescein.

The receptor media consisted of 7.5 mL of normal saline. Near sink conditions were maintained in the receptor compartment throughout the experiment, with the fluorescein concentration in the receptor compartment never exceeding 0.01% of saturation. . The diffusion area between both compartments was 1.77 cm². The stirring rate and temperature in the receptor compartment were kept at 600 rpm and 37°C, respectively. Note that for F1, the temperature inside the receptor is above the boiling point of PFP whereas for F2 the receptor is below the boiling point of PFH. In order to prevent settling of the emulsion onto the membrane, due to the densities of PFP and PFH, an overhead stirrer operating at 600 rpm was used in the donor compartment. At 15-minute intervals, aliquots of the receptor medium were withdrawn and immediately replaced with an equal volume of fresh, normal saline. The amount of fluorescein released was determined via fluorescence spectroscopy as previously described.

To determine the effect of ADV on fluorescein release, the PFP and PFH emulsions were placed in 15 mL centrifuge tubes (Thermo Fisher Scientific) and immersed in a water bath heated to 37°C and 64°C, respectively. In each case, the emulsion was warmed to 8°C of superheat since the normal boiling points of PFP and PFH are 29°C and 56°C, respectively. The emulsions were continuously sonicated for 2 minutes using the microtip operating at 20 kHz and 312 W/cm² in order to generate ADV. Low frequency, continuous wave US, which is difficult to focus *in vivo*, was used to generate ADV - compared to previous studies which used higher frequency (1-10 MHz), pulsed US [17; 23; 26; 27; 42; 43] - to maximize the cavitation-assisted vaporization of the emulsion during these proof-of-concept studies. The resulting mixture (post-sonication) was then added to the donor compartment of the diffusion cell and the fluorescein release was determined as previously described. The fluorescein release rates from the emulsion studies were compared to mass fluxes obtained when an equal concentration of fluorescein solution

was loaded into the donor compartment. The volume fraction of droplets vaporized after ADV was determined by counting the droplets remaining in the tube post US exposure versus a control case (i.e. without US) with a Coulter counter [17]. The droplet sample was briefly over-pressurized in a gas-tight syringe in order to destroy existing microbubbles and decrease the likelihood of counting these as droplets.

4.2.7 Encapsulation efficiency and stability of thrombin emulsions

The encapsulation efficiency of the thrombin double emulsions, immediately following the second emulsification step, was determined by separating the droplets from the continuous, aqueous phase via repeated centrifugation using similar methods as for the fluorescein emulsions. Minimal droplet breakage, assessed as previously described for the fluorescein emulsions, occurred during the washing steps. The non-encapsulated thrombin concentration was estimated using the Pierce 660 nm protein assay (Thermo Fisher Scientific) and the encapsulation efficiency was determined as previously described. The stability of the thrombin encapsulation in the emulsions was determined by heating the emulsion to 37°C while stirring at 1100 rpm. At 15-minute intervals, aliquots were removed, centrifuged to separate the droplets from the continuous phase, and the non-encapsulated thrombin concentration was estimated as previously stated.

4.2.8 *In vitro* thrombin release

Thrombin release from the emulsions, in blood, was assessed using a modified activated clotting time (ACT) assay. Fresh, whole canine blood was acquired and immediately mixed with citrate-phosphate-dextrose (CPD) solution (Sigma Aldrich), an anticoagulant, in a volumetric ratio of 10:1.4, respectively. CPD, used in the storage of whole blood, prevents coagulation via the chelation of calcium ions with citrate [44]. The blood was stored at 4°C and used within 7 days of acquisition.

All protocols involved in the blood acquisition were approved by the University of Michigan Committee on the Use and Care of Animals (UCUCA).

The effect of thrombin concentration on the ACT was determined as follows. First, 0.4 mL of blood containing CPD was added to a plastic, ACT test tube (International Technidyne Corporation, Edison, NJ, USA), which contained approximately 30 mg glass beads (119.6 μm mean diameter) and a magnet. Then, an aliquot of thrombin solution was added to the tube. The volume of thrombin added never exceeded 50 μL . Finally, the tube was capped, gently mixed, and placed into the Hemochron 400 (International Technidyne Corporation). The instrument mechanically detected the formation of a fibrin clot via the rotation of the magnet within the tube. Upon clotting, the magnet lifted within the tube; the time for this to occur was the ACT. Due to the possibility of thrombin denaturation or loss of activity during the emulsion processing, thrombin solutions were subjected to identical processing conditions, as seen in Table 4.1. These solutions were tested for thrombin activity using the ACT assay. Additionally, due to the antithrombotic properties of Pluronic F-68 [45; 46], each emulsion component - Pluronic F-68, PFP, and Krytox-PEG copolymer - and the blank emulsion (i.e. without thrombin) were combined with a known concentration of thrombin to determine its effect on the ACT. The ACT was measured with each thrombin emulsion as well.

To determine the effect of ADV on thrombin release, each emulsion was injected into an OptiCellTM (Thermo Fisher Scientific) chamber and exposed to US using a previously utilized experimental setup [17]. The chamber was placed into an OptiCellTM holder that was located within a tank (40 \times 60 \times 27 cm) containing degassed, deionized water heated to 37°C. The surface of the tank water was covered with air-filled plastic balls (Cole-Parmer Inc., Vernon Hills, IL, USA) to minimize regassing and heat loss as well as scattering the reflected US at the air/water surface. A calibrated 3.5 MHz single-element transducer (1.9 cm diameter, 3.81 cm focal

length, A381S, Panametrics, Olympus NDT Inc., Waltham, MA) was positioned below the chamber and focused on the bottom window of the chamber. Acoustic pulses generated by the transducer - 3.7 μ s pulse duration, 10 ms pulse repetition period (PRP), 4.7 MPa peak rarefactional pressure, 11.3 MPa peak compressional pressure - were achieved using a function generator (33120A, Agilent Technologies, Palo Alto, CA, USA) and power amplifier (55 dB, model A-300, E & I, Rochester, NY, USA). The transducer was rastered via a computer-controlled positioning system, at 4 mm/s across the chamber surface in order to vaporize the emulsion. Due to the volume of emulsion introduced into the OptiCellTM(1 mL), only a fraction of the chamber surface was covered by the emulsion and subsequently insonified. The raster spacing was 0.5 mm; by comparison, the -6 dB lateral beam width of the transducer was 0.88 mm. The total exposure time was 5 minutes. Following the US exposure, the mixture was removed from the OptiCellTM and the ACT was measured as described previously. The volume fraction of droplets vaporized was determined by counting the droplets remaining in the OptiCellTM post US exposure versus a control case (i.e. without US) with the Coulter counter, as described previously for the fluorescein emulsions.

4.2.9 Statistical analysis

Each experimental value is expressed as mean \pm standard deviation and the result of at least three independent measurements. Statistically significant differences between experimental groups was determined using a Student's *t*-test. A significance level of 0.01 was used for all comparisons.

4.3 Results

4.3.1 Physiochemical characterization of fluorescein emulsions

Representative micrographs of the fluorescein emulsions are displayed in Fig. 4.2. The aqueous droplets containing fluorescein (W_1), stabilized by the Krytox-PEG copolymer, are surrounded by PFC. The fluorescein droplets comprise a large volume fraction and are homogenously distributed within the PFC globule. Similar structures were observed for the thrombin emulsions. As seen in Table 4.2, the mean diameter of fluorescein emulsions containing PFP and PFH - F1 and F2, respectively - were not statistically different. Additionally, the encapsulation efficiencies for F1 and F2 were not statistically different either.

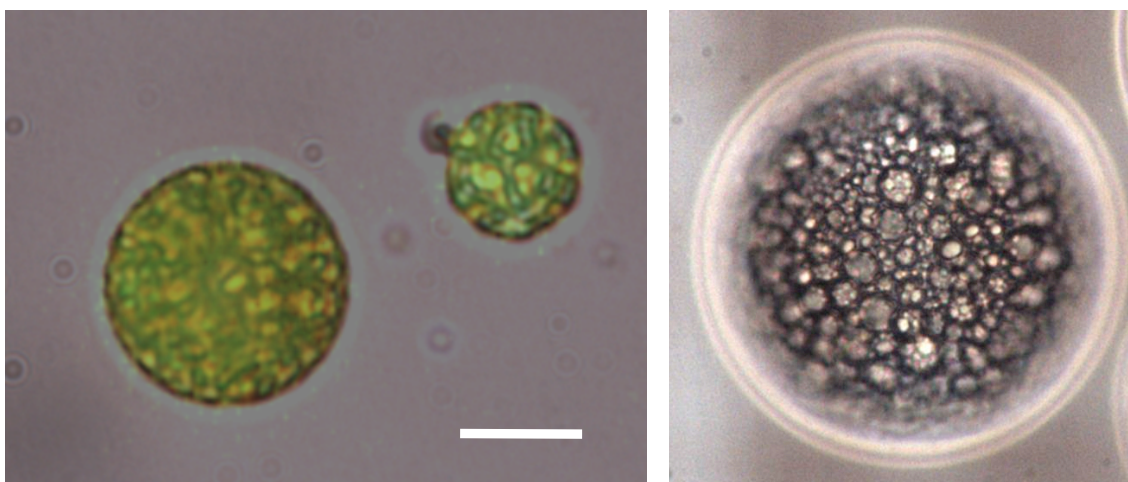


Figure 4.2: Micrographs of a W_1 /PFC/ W_2 emulsion containing fluorescein in the W_1 phase. The left image is an overlay of both visible and fluorescent micrographs. The scale bar is $8 \mu\text{m}$. The structure of the W_1 /PFC/ W_2 emulsion - water droplets containing fluorescein within a globule of PFC - can be clearly seen in the right image, which displays a $100 \mu\text{m}$ diameter globule.

4.3.2 *In vitro* release of fluorescein

The retention of fluorescein within the emulsions, as evaluated using a Franz diffusion cell, is shown in Fig. 4.3. The values in Fig. 4.3 were corrected for

Table 4.2: Characterization of fluorescein and thrombin emulsions. Thrombin precipitation, during the second emulsification step, and subsequent inactivation of thrombin during ADV was suspected in T2.

Formulation	Mean diameter (μm)	Percent of droplets $>6 \mu\text{m}$		Percent (%) encapsulation	Volume percent vaporized ^a	Percent (%) change in ACT upon ADV ^b
		Number	Volume			
F1	2.5 ± 0.1	4.3 ± 1.3	53.1 ± 9.4	5.4 ± 1.0	100	NA
F2	2.4 ± 0.2	2.6 ± 1.8	32.3 ± 15.4	3.8 ± 1.1	100	NA
T1	1.6 ± 0.1	0.04 ± 0.02	6.7 ± 3.0	76.3 ± 3.4	10.2 ± 4.2	-7.4 ± 1.6
T2 ^c	2.6 ± 0.2	6.5 ± 1.4	83.2 ± 1.0	63.7 ± 22.9	25.6 ± 7.1	63.0 ± 12.2
T3	27.4 ± 5.9	89.2 ± 1.1	99.9 ± 0.1	97.5 ± 0.6	100	-78.0 ± 13.5
T4	3.5 ± 0.1	15.5 ± 0.8	89.4 ± 4.5	98.8 ± 1.1	28.7 ± 10.2	-23.3 ± 5.9
T5	3.9 ± 0.1	17.6 ± 0.5	88.9 ± 3.1	97.2 ± 0.5	34.3 ± 15.9	-19.0 ± 4.9

^aCases where complete vaporization was observed, and thus the number of droplets remaining in solution after ADV is below the noise threshold of the Coulter counter, are denoted by '100'.

^bExcept for T1, all changes in the ACT were statistically significant.

^cParameters affected by thrombin precipitation include percent encapsulation and percent change in ACT upon ADV.

the aliquots of solution and hence fluorescein mass removed during sampling. An aqueous solution of fluorescein, equal in concentration to each emulsion, was used as a control. It was confirmed, by mixing blank emulsion (i.e. without fluorescein) and fluorescein solution, that the presence of droplets within the donor compartment did not statistically change the fluorescein diffusion across the membrane for the fluorescein in solution. Therefore, the encapsulation of fluorescein within the emulsion delayed its release, as is evident in Fig. 4.3, relative to the fluorescein solution.

The fluorescein flux was calculated based on a linear regression of the data between 15 and 60 minutes, which yielded squared correlation coefficients (R^2) greater than 0.95 in all cases. The fluxes for F1 and F2 were $0.19 \pm 0.02 \mu\text{g}/\text{cm}^2/\text{min}$ and $0.07 \pm 0.01 \mu\text{g}/\text{cm}^2/\text{min}$, respectively. Note that the concentration of encapsulated fluorescein in F1 is higher than F2, 0.6 mg/mL versus 0.3 mg/mL. By comparison, when F1 and F2 are exposed to US and fluorescein is released via ADV, the fluxes increase to $1.12 \pm 0.24 \mu\text{g}/\text{cm}^2/\text{min}$ and $0.60 \pm 0.04 \mu\text{g}/\text{cm}^2/\text{min}$, respectively. This corresponds to a 5.7 ± 1.4 and 8.2 ± 1.3 fold increase in flux for F1 and F2, respectively. These fluxes are not statistically different than the fluxes obtained for fluorescein solutions of equal concentration. This is expected

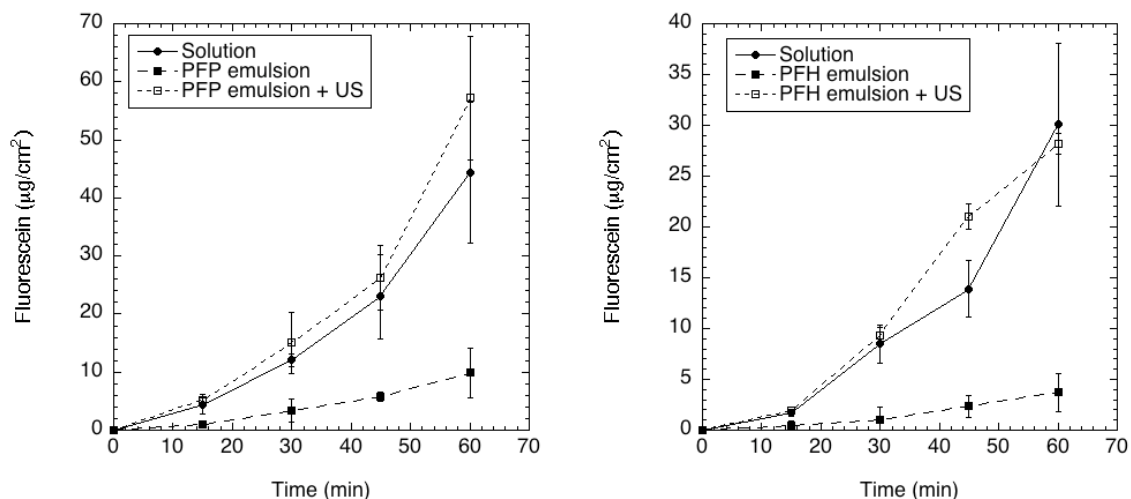


Figure 4.3: *In vitro* release profiles of PFP (left) and PFH (right) double emulsions containing fluorescein at 37°C. In each case, the release profiles obtained from the emulsion, with and without ADV, are compared to a solution of fluorescein of equal concentration. The fluorescein concentration for the PFP and PFH emulsions are 0.6 mg/mL and 0.3 mg/mL, respectively.

considering that all of the droplets had been vaporized as a result of ADV, as seen in Table 4.2.

4.3.3 Physiochemical characterization of thrombin emulsions

Table 4.2 lists the mean diameters for the five different thrombin emulsions (T1-T5). The percent of droplets greater than 6 μm diameter, in terms of both number and volume, are included to indicate how suitable the emulsions are for intravenous administration. The percent of thrombin encapsulation is also included in Table 4.2. T1, processed via sonication during the second emulsification step, yielded the smallest mean diameter (1.6 μm). The shaken formulation, T2, yielded a mean diameter (2.6 μm) that was not statistically different than the similarly processed fluorescein emulsions (F1 and F2). Alternatively, T3 - processed via stirring - yielded the largest mean diameter (27.4 μm). The addition of glass beads, in an effort to increase the shear force generated during stirring, caused the mean diameters of T4 and T5 to decrease to 3.5 μm and 3.9 μm , respectively.

The thrombin emulsions were initially loaded with a thrombin concentration of 417 IU/mL. The largest encapsulation efficiencies were obtained for the emulsions that were stirred in the second emulsification step (T3-T5). The second emulsification step is critical when forming double emulsions since excess shear or mixing can cause the W_1 phase of the primary emulsion (i.e. W_1 /PFC) to coalesce with the external aqueous phase (i.e. W_2) [47]. Therefore, emulsification techniques that generate lower shear forces, such as stirring, are amenable in the second emulsification step [48]. Pair-wise comparisons between T3, T4, and T5 indicate no statistically significant differences in the encapsulation efficiencies. Thus, in the case of T4, the addition of glass beads decreased the droplet size without compromising thrombin encapsulation. Additionally, increasing the viscosity of the W_1 phase more than 1000x fold [49], as in T5, did not affect the encapsulation efficiency. As will be discussed in the next section, the encapsulation efficiency of T2 is skewed by the denaturation of thrombin during the second emulsification step. Upon warming the thrombin emulsions to 37°C and stirring simultaneously, no statistically significant changes were observed in the encapsulation efficiency over a 1-hour period for any of the thrombin emulsions.

4.3.4 Formulation parameters affecting thrombin activity

Figure 4.4 displays the measured ACT for different thrombin levels. The data was fit ($R^2 > 0.94$) using a sigmoidal curve used in previous works [17; 42]. There were no statistically significant differences with the ACT data between 2.4 IU/mL and 24 IU/mL. Due to the susceptibility of proteins to aggregate, denature, or lose activity during encapsulation processes [50], the thrombin activity was measured - in terms of ACT - for thrombin solutions that had been subjected to sonication, shaking, or stirring. No statistically significant differences were observed in ACT, compared to the data in Fig. 4.4, when the thrombin solution was sonicated, shaken, or stirred. For the sonicated and stirred cases, the thrombin solution was placed in an ice

bath during the processing and no significant temperature increase was measured throughout the processing. For the shaken case, the thrombin solution was chilled to 0°C prior to shaking; the temperature of the thrombin solution inside the sealed vial, measured using a needle-type thermocouple inserted through the rubber stopper, was 30°C after shaking. By comparison, human thrombin begins to denature above 45°C [51]. Processing the thrombin solution twice, as seen in Table 4.1 for T1-T5, yielded no statistically significant differences, relative to Fig. 4.4, except in the case of T2 (i.e. sonication followed by shaking), where an approximate 300% increase in ACT was observed. This increase in ACT was attributed to thrombin precipitation, as confirmed visually and also with the colorimetric protein assay. Interestingly, switching the processing order (i.e. shaking followed by sonication) did not cause a statistically significant difference in the ACT.

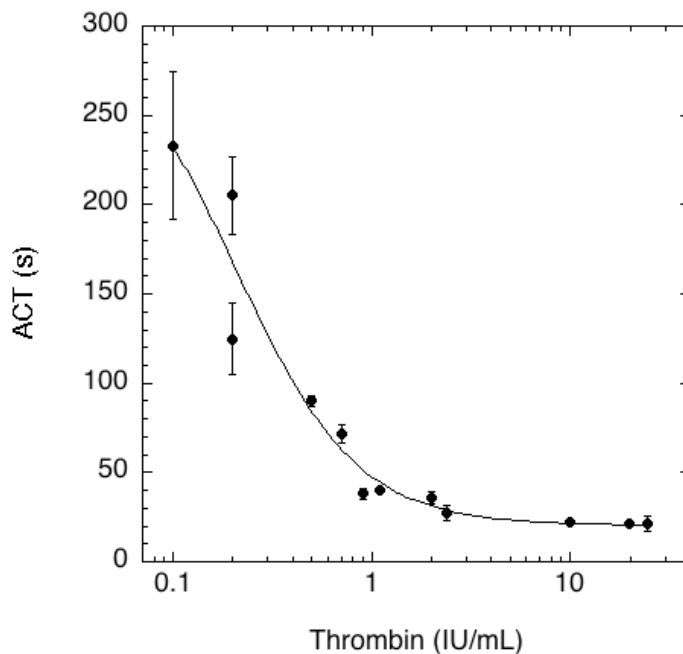


Figure 4.4: Reference curve displaying the activated clotting time (ACT) for canine blood, stored with citrate-phosphate-dextrose (CPD) solution, as a function of thrombin concentration.

Each emulsion component - Krytox-PEG copolymer, PFP, and Pluronic F-68 - along with the blank emulsion was combined with a known concentration of

thrombin (in solution) to determine its effect on the ACT. The addition of PFP, up to 1000x greater in concentration relative to the emulsions, did not cause a statistically significant difference in the ACT. Pluronic F-68, a polymer with known antithrombotic properties [45; 46] even in the presence of weak coagulation agonists, did not produce a statistically significant difference in the ACT when added at concentrations up to 100 mg/mL, which is 10x greater than the concentration used for the emulsions. This is likely due to the use of thrombin, which is a strong coagulation agonist, to form clots. As seen in Fig. 4.5, blank emulsions produced with increasing levels of Krytox-PEG copolymer did produce a statistically significant increase in the ACT. The introduction of low concentrations of copolymer (i.e. ≤ 0.018 mg/mL blood) did not significantly change the ACT, but a very large change (i.e. $> 1100\%$ increase) was observed at higher Krytox-PEG copolymer concentrations (i.e. ≥ 0.05 mg/mL blood). No statistically significant differences were observed in mean droplet diameter or droplet number density (i.e. number of droplets per mL emulsion) across the range of tested Krytox-PEG copolymer concentrations. Therefore, the thrombin emulsions used for subsequent experiments, including for the data generated in Table 4.2, were formulated using low concentrations of Krytox-PEG copolymer.

4.3.5 *In vitro* release of thrombin

The validation of ADV-triggered release of thrombin from double emulsions was determined using the ACT assay. As an indicator of thrombin retention within the emulsion, the goal was to maximize and minimize the ACT without and with ADV, respectively. Conceptually, the former goal translates into an infinite ACT for the case where thrombin is highly retained in the emulsion due to the presence of CPD in the blood. The latter goal, as seen in Fig. 4.4, corresponds to an ACT of approximately 22 seconds. Figure 4.6 displays the ACT obtained for each thrombin emulsion listed in Table 4.2 with and without ADV. For 4 out of 5 formulations, T1 and T3-T5, a decrease in ACT was observed when the emulsion was exposed

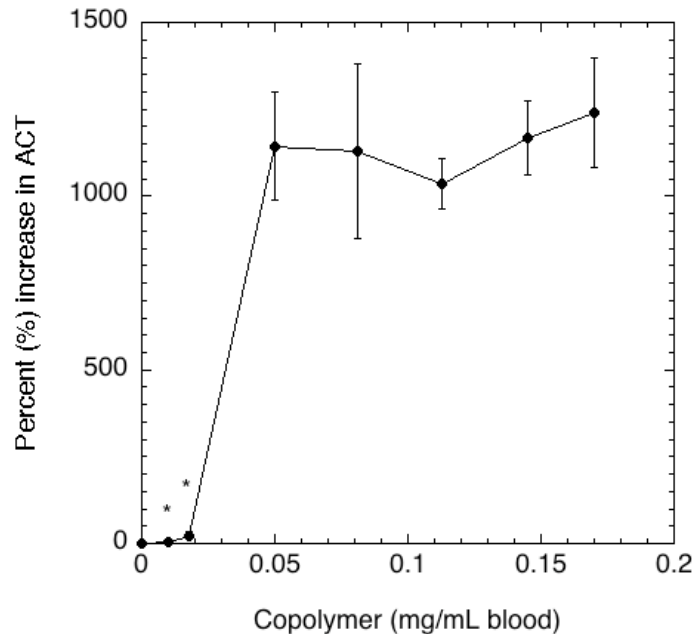


Figure 4.5: Anticoagulative effect of the Krytox-PEG copolymer used in the thrombin emulsions. A blank emulsion, containing copolymer was mixed with thrombin solution. An aliquot of the resulting mixture, containing 1 IU thrombin, was added to blood containing CPD. Points marked with an asterisk (*) indicate copolymer levels that are not statistically different than control case (i.e. without copolymer).

to US, compared to the case without US; 3 out of 5 formulations (T3-T5) exhibited decreases that were statistically significant. Upon US exposure, T2 displayed an increase in ACT compared to the case without US. The largest and smallest ACT, prior to US exposure, were exhibited by T3 and T4, respectively. T3 displayed the smallest ACT and largest absolute percent change in ACT after ADV. A higher ACT (without ADV case) was observed for T5 (with xanthan gum) relative to T4 (without xanthan gum), though the percent change in ACT upon ADV was not statistically different for T4 and T5. Additionally, as indicated in Table 4.2, the droplets in T2 were completely vaporized after ADV. Table 4.3 shows the thrombin concentration in blood, with and without ADV, calculated using the sigmoidal fit in Fig. 4.4 and the ACT values in Fig. 4.6. The values in Table 4.3 are smaller than the theoretical thrombin concentration (46.3 IU/mL), assuming the complete release of thrombin from the emulsion and no inactivation.

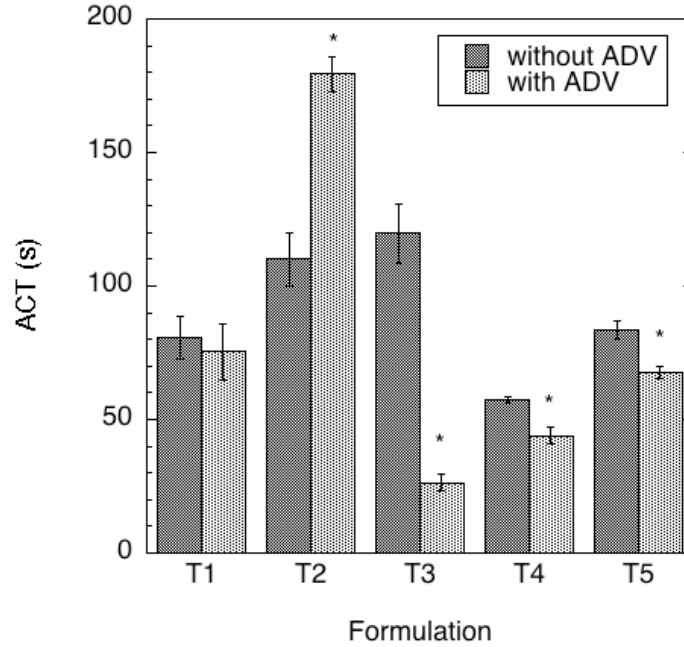


Figure 4.6: The effect of ADV (3.5 MHz, 3.7 μ s pulse duration, 10 ms PRP, 4.7 MPa peak rarefactional pressure, 11.3 MPa peak compressional pressure, 5 minute exposure) on the ACT for five different thrombin formulations. Cases where the ACT was statistically different after ADV are denoted by an asterisk (*).

Table 4.3: The thrombin concentration in blood, estimated from the regression in Fig. 4.4 and the data from Fig. 4.6. The thrombin concentration, assuming the complete release of thrombin from the emulsion and no inactivation, should have been 46.3 IU/mL.

Formulation	Thrombin (IU/mL blood)	
	without ADV	with ADV
T1	0.5 \pm 0.05	0.6 \pm 0.09
T2	0.4 \pm 0.03	0.2 \pm 0.01
T3	0.3 \pm 0.03	3.1 \pm 0.4
T4	0.8 \pm 0.01	1.1 \pm 0.7
T5	0.5 \pm 0.02	0.6 \pm 0.02

4.4 Discussion

This study focuses on the development of PFC double emulsions that carry a water-soluble payload and release the payload upon ADV. In general, the coupling of drug release with ADV has three potential therapeutic advantages, beyond the advantages previously described for US-triggered drug delivery; these synergisms are unique to therapies involving ADV and build upon previous studies involving ADV-induced vascular occlusion [26–28]. First, the simultaneous release of a chemical embolic agent, such as thrombin, upon ADV can be used to sustain an ADV-generated microbubble embolization. Second, the ischemia generated by vascular occlusion could increase the residence time of a therapeutic agent within the occluded tissue region, potentially increasing the amount of agent that diffuses into the tissue. Third, prolonged ischemia can generate hypoxia, which could be used to activate water-soluble, bioreductive prodrugs, such as NLCQ-1 [52], encapsulated within the emulsion.

Due to the extremely hydrophobic and lipophobic qualities of PFCs [16], the choice of surfactants suitable for stabilizing reverse PFC emulsions (i.e. W/PFC) are quite limited [38; 53]. The synthesized Krytox-PEG copolymer enabled the formation of a stable primary emulsion (W_1 /PFC) compared to primary emulsions prepared using the unmodified Krytox. This is likely due to the presence of the hydrophilic PEG group that stabilizes the W_1 /PFC interface [54]. The use of a non-ionic hydrophilic group minimizes potential interactions between the surfactant and charged therapeutic agents, such as proteins, which could lose biological activity while encapsulated in the W_1 phase [55]. Similarly structured Krytox-PEG copolymers have displayed favorable biocompatibility properties when used to encapsulate mammalian cells or small multicellular organisms within aqueous microcompartments surrounded by PFC [38; 56].

The PFC layer separating the payload containing W_1 phase from the exterior

W_2 phase serves a dual purpose. First, the PFC acts as a diffusion barrier, thereby preventing the inward or outward diffusion of material, such as the payload, from the W_1 phase; this is clearly seen, for example, in Fig. 4.3 and with the calculated fluxes for F1 and F2. The minimization of payload diffusion from the emulsion is important in order to couple payload release with ADV of the emulsion. Since the viscosities of PFP (0.64 mPa·s) and PFH (1.11 mPa·s) are close to that of saline (i.e. W_1 phase), the barrier property of the PFC phase is likely attributed to the hydrophobic and lipophobic properties of the PFC [16] and not caused by any restriction in payload diffusion due to the PFC viscosity [41]. Second, the PFC phase vaporizes upon ADV, thereby releasing the W_1 phase into the W_2 phase. Since the ADV threshold scales inversely with degree of PFC superheat when the degree of superheat is negative [42], low boiling point liquids should be used as the vaporizable phase of the emulsion in order to minimize the acoustic energy required for ADV to occur at normal body temperature. Straight-chain PFCs, such as PFP, meet this boiling point requirement along with being biocompatible and inert [16]. Previous studies with PFC droplets [42] and PFC droplets containing an oil layer [18; 19] demonstrated an increase in mean droplet size as the boiling point, and hence viscosity, of the PFC phase increased. An increase in the dispersed phase viscosity is known to cause an increase in particle size [57]. Since F1 and F2 - composed of PFP and PFH - respectively, possessed mean diameters that were not statistically different, this may imply that the volume fraction of PFC within each globule is relatively small such that the globule viscosities of F1 and F2 are similar.

Currently, the primary clinical use of thrombin is topical hemostasis [58]. The intravascular use of thrombin has been limited to procedures where thrombin is administered via a catheter, as in the treatment of pseudoaneurysms [36; 37], due to the risk of mortality associated with extensive intravascular clotting. The encapsulation of thrombin within a PFC emulsion and its subsequent release

upon ADV could enable the targeted formation of thrombi within the vasculature. Additionally, due to the short (< 15 s) half-life of thrombin in human plasma [59], a colloidal thrombin formulation could increase the stability of the administered thrombin [60–62].

Thrombin activity, as measured via the ACT assay, was maintained during all emulsification steps except in the case of T2 (sonication followed by shaking). Structural changes, denaturation, and loss of activity can occur when proteins are exposed to US [63] or high shear rates [64]. Thus, sonication (under chilled conditions) may have rendered the thrombin more susceptible to denaturation during shaking, where a temperature increase and high shear stresses were generated. Interestingly, the reverse processing conditions were not harsh enough to reduce the thrombin activity. In addition, thrombin activity was impacted by the presence of high levels of the synthesized, Krytox-PEG copolymer (Fig. 4.5). In this study, Pluronic F-68, a polymer with known antithrombotic properties [45; 46], did not alter the ACT in the presence of thrombin. Pluronic F-68 can become embedded into the cell membrane of platelets, thereby inhibiting platelet aggregation by sterically hindering interactions between platelets and lowering interfacial tension [45]. Due to the structural similarities between the Krytox-PEG copolymer and Pluronic F-68, it is possible that the mechanism causing an inhibition in platelet aggregation is similar in both cases. When the emulsions with high Krytox-PEG copolymer concentrations were washed in triplicate (via centrifugation), the obtained ACTs were not statistically different from the control case. This observation, combined with the statistically constant droplet diameter and number density across the range of Krytox-PEG copolymers tested, suggest that excess copolymer was present when the concentration exceeded 0.05 mg/mL blood.

The thrombin emulsions displayed higher percent encapsulations than the fluorescein emulsions. This may be due to the smaller osmotic pressure difference

across the W_1/W_2 phases of the thrombin emulsion. Large differences in osmotic pressure can cause the rapid breakdown of double emulsions to simple emulsions (i.e. PFC/W) [65]. Despite the stable retention of thrombin within the emulsions over a 1-hour period, some thrombin was released from the emulsions in the absence of US during the ACT measurements (Fig. 4.6). However, due to the high loading of thrombin within the emulsions (417 IU/mL), the release of a small amount of thrombin could alter the ACT (Figs. 4.4 and 4.6). This release could have been facilitated by the movement of the magnet over the glass beads in the ACT tube, thereby grinding the droplets. *In vitro* studies have indicated that less than 0.1 IU/mL thrombin is required to trigger the onset of clot formation whereas the concentration of free thrombin during a coagulation reaction ranges from less than 0.1 IU/mL to greater than 11.5-57.5 IU/mL [66]. Comparatively, the normal concentration of prothrombin (factor II), the inactive precursor of thrombin, is approximately 1.3 IU/mL in adult humans [67]. As seen in Fig. 4.6 and Table 4.2, T3 displayed the largest and smallest ACT values before and after ADV, respectively. Thrombin was most highly retained in T3 before ADV, whereas ADV caused a ten-fold increase in the amount of thrombin released (Table 4.3). Due to a larger mean diameter of T3 (27.4 μm) relative to the other thrombin formulations, T3 is most amenable to intraarterial administration, similar to double emulsions utilized in the treatment of hepatocellular carcinoma [68].

The effect of ADV on protein stability, specifically proteins released from PFC emulsions via ADV, is currently unknown. Previous work [42] demonstrated that ADV can occur independently of inertial cavitation, a mechanism that can induce molecular damage. The volume percent of droplets vaporized (Table 4.2) was larger than the percent of thrombin released estimated using the concentrations in Table 4.3. For example, 28.7% (by volume) of T4 was vaporized as a result of ADV, but only 2.4% of the thrombin was released based on the measured ACT. As seen in Fig.

4.4, the ACT levels off for thrombin concentrations higher than 10 IU/mL; thus the ACT cannot be used to calculate high thrombin concentrations, such as that which would be obtained theoretically if complete thrombin release from the emulsion were to occur (46.3 IU/mL). Even with this consideration, the large difference between the volume percent of droplets vaporized and the percent of thrombin released could indicate that ADV is inactivating the thrombin, especially considering the rapid consumption of PFC observed during ADV [43]. Precipitated thrombin - an indicator of thrombin inactivation - was not seen with T3 after ADV, despite the complete vaporization of the emulsion; due to the partial vaporization of the other formulations, it was not possible to observe precipitated thrombin. Previous studies [17] focusing on the release of a small molecular weight compound (304.2 g/mol) via ADV did not demonstrate molecular inactivation due to ADV. Large molecules, such as thrombin (~ 36000 g/mol), can experience broken chemical bonds due to the shear forces generated by the rapid motion of solvent following cavitation collapse [69]. Additionally, as seen for T2 (Fig. 4.6), ADV generated additional inactivation of thrombin that had already been partially inactivated, which causes the ACT to increase after droplet vaporization. The investigation of acoustic parameters that would maximize thrombin release but minimize the apparent thrombin inactivation are beyond the scope of this work.

4.5 Conclusions

PFC double emulsions can serve as carriers for water-soluble therapeutic agents. These emulsions can be vaporized using US, thereby releasing the encapsulated agent from the emulsions via ADV. The use of a Kyttox-PEG copolymer, which was found to have antithrombotic properties at higher concentrations, enabled the stable formation of the primary emulsion. Both fluorescein and thrombin were highly retained in the emulsions; ADV caused a statistically significant increase in

fluorescein and thrombin release. The results also suggest that thrombin inactivation may be occurring as a result of the ADV process. Future studies are focused on understanding this inactivation, especially as it relates to ADV and inertial cavitation, and demonstrating the synergisms of ADV and drug delivery *in vivo*.

4.6 Acknowledgments

The authors would like to thank Dr. Xia Shao (Department of Nuclear Medicine, University of Michigan, Ann Arbor, MI) for assistance with the Krytox-PEG copolymer synthesis and Dr. Kim Ives (Department of Radiology, University of Michigan, Ann Arbor, MI) for assistance in acquiring blood. This work was supported in part by NIH grant 5R01EB000281.

REFERENCES

- [1] P. A. Dayton, S. Zhao, S. H. Bloch, P. Schumann, K. Penrose, T. O. Matsunaga, R. Zutshi, A. Doinikov, and K. W. Ferrara, "Application of ultrasound to selectively localize nanodroplets for targeted imaging and therapy," *Molecular Imaging*, vol. 5, pp. 160–174, July 2006.
- [2] S. Ganta, H. Devalapally, A. Shahiwala, and M. Amiji, "A review of stimuli-responsive nanocarriers for drug and gene delivery," *Journal of Controlled Release*, vol. 126, no. 3, pp. 187–204, 2008.
- [3] S. T. Laing, H. Kim, J. A. Kopechek, D. Parikh, S. Huang, M. E. Klegerman, C. K. Holland, and D. D. McPherson, "Ultrasound-mediated delivery of echogenic immunoliposomes to porcine vascular smooth muscle cells *in vivo*," *Journal of Liposome Research*, vol. 20, no. 2, pp. 160–167, 2010.
- [4] N. Rapoport, Z. Gao, and A. Kennedy, "Multifunctional nanoparticles for combining ultrasonic tumor imaging and targeted chemotherapy," *Journal of the National Cancer Institute*, vol. 99, no. 14, pp. 1095–1106, 2007.
- [5] E. C. Unger, T. Porter, W. Culp, R. LaBell, T. Matsunaga, and R. Zutshi, "Therapeutic applications of lipid-coated microbubbles," *Advanced Drug Delivery Reviews*, vol. 56, no. 9, pp. 1291–1314, 2004.
- [6] J. Eisenbrey, O. M. Burnstein, R. Kambhamptai, F. Forsberg, J. Liu, and M. Wheatley, "Development and optimization of doxorubicin loaded poly(lactic acid) contrast agent for ultrasound directed drug delivery," *Journal of Controlled Release*, vol. 143, no. 1, pp. 38–44, 2010.
- [7] I. Lentacker, B. Geers, J. Demeester, S. C. D. Smedt, and N. N. Sanders, "Design and evaluation of doxorubicin-containing microbubbles for ultrasound-triggered doxorubicin delivery: cytotoxicity and mechanisms involved," *Molecular Therapy*, vol. 18, no. 1, pp. 101–108, 2010.
- [8] H. Liang, J. Tang, and M. Halliwell, "Sonoporation, drug delivery, and gene therapy," *Proceedings of the Institution of Mechanical Engineers Part H - Journal of Engineering in Medicine*, vol. 224, no. H2, pp. 343–361, 2010.
- [9] J. L. Ren, C. S. Xu, Z. Y. Zhou, Y. Zhang, X. S. Li, Y. Y. Zheng, H. T. Ran, and Z. G. Wang, "A novel ultrasound microbubble carrying gene and Tat

- peptide: preparation and characterization,” *Academic Radiology*, vol. 16, no. 12, pp. 1457–1465, 2009.
- [10] S. Datta, C. C. Coussios, A. Y. Ammi, T. D. Mast, G. M. de Courten-Myers, and C. K. Holland, “Ultrasound-enhanced thrombolysis using Definity as a cavitation nucleation agent,” *Ultrasound in Medicine and Biology*, vol. 34, no. 9, pp. 1421–1433, 2008.
- [11] F.-Y. Yang, S.-H. Liu, F.-M. Ho, and C.-H. Chang, “Effect of ultrasound contrast agent dose on the disruption of focused-ultrasound-induced blood-brain barrier disruption,” *Journal of the Acoustical Society of America*, vol. 126, no. 6, pp. 3344–3349, 2009.
- [12] P. A. Dayton and K. W. Ferrara, “Targeted imaging using ultrasound,” *Journal of Magnetic Resonance Imaging*, vol. 16, no. 4, pp. 362–377, 2002.
- [13] S. Hernot and A. L. Klibanov, “Microbubbles in ultrasound-triggered drug and gene delivery,” *Advanced Drug Delivery Reviews*, vol. 60, no. 10, pp. 1153–1166, 2008.
- [14] S. Tinkov, R. Bekerredjian, G. Winter, and C. Coester, “Microbubbles as ultrasound triggered drug carriers,” *Journal of Pharmaceutical Sciences*, vol. 98, no. 6, pp. 1935–1961, 2009.
- [15] R. Diaz-Lopez, N. Tsapis, and E. Fattal, “Liquid perfluorocarbons as contrast agents for ultrasonography and ^{19}F -MRI,” *Pharmaceutical Research*, vol. 27, no. 1, pp. 1–16, 2010.
- [16] J. G. Riess, “Oxygen carriers (“blood substitutes”) - raison d’etre, chemistry, and some physiology,” *Chemical Reviews*, vol. 101, no. 9, pp. 2797–2919, 2001.
- [17] M. L. Fabiilli, K. J. Haworth, I. E. Sebastian, O. D. Kripfgans, P. L. Carson, and J. B. Fowlkes, “Delivery of chlorambucil using an acoustically-triggered, perfluoropentane emulsion,” *Ultrasound in Medicine and Biology*, vol. 36, no. 8, pp. 1364–1375, 2010.
- [18] J. Y. Fang, C. F. Hung, M. H. Liao, and C. C. Chien, “A study of the formulation design of acoustically active lipospheres as carriers for drug delivery,” *European Journal of Pharmaceutics and Biopharmaceutics*, vol. 67, no. 1, pp. 67–75, 2007.
- [19] J. Y. Fang, C. F. Hung, S. C. Hua, and T. L. Hwang, “Acoustically active perfluorocarbon nanoemulsions as drug delivery carriers for camptothecin: drug release and cytotoxicity against cancer cells,” *Ultrasonics*, vol. 49, no. 1, pp. 39–46, 2009.
- [20] T. L. Hwang, Y. J. Lin, C. H. Chi, T. H. Huang, and J. Y. Fang, “Development and evaluation of perfluorocarbon nanobubbles for apomorphine delivery,” *Journal of Pharmaceutical Sciences*, vol. 98, no. 10, pp. 3735–3747, 2009.

- [21] R. E. Apfel, “Activatable infusible dispersions containing drops of a superheated liquid for methods of therapy and diagnosis,” Patent 5,840,276, Apfel Enterprises, Inc., November 1998.
- [22] T. Giesecke and K. Hynynen, “Ultrasound-mediated cavitation thresholds of liquid perfluorocarbon droplets *in vitro*,” *Ultrasound in Medicine and Biology*, vol. 29, no. 9, pp. 1359–1365, 2003.
- [23] O. D. Kripfgans, J. B. Fowlkes, D. L. Miller, O. P. Eldevik, and P. L. Carson, “Acoustic droplet vaporization for therapeutic and diagnostic applications,” *Ultrasound in Medicine and Biology*, vol. 26, no. 7, pp. 1177–1189, 2000.
- [24] K.-I. Kawabata, N. Sugita, H. Yoshikawa, T. Azuma, and S.-I. Umemura, “Nanoparticles with multiple perfluorocarbons for controllable ultrasonically induced phase shifting,” *Japanese Journal of Applied Physics*, vol. 44, no. 6B, pp. 4548–4552, 2005.
- [25] N. Y. Rapoport, A. M. Kennedy, J. E. Shea, C. L. Scaife, and K.-H. Nam, “Controlled and targeted tumor chemotherapy by ultrasound-activated nanoemulsions/microbubbles,” *Journal of Controlled Release*, vol. 138, no. 2, pp. 268–276, 2009.
- [26] O. D. Kripfgans, J. B. Fowlkes, M. Woydt, O. P. Eldevik, and P. L. Carson, “*In vivo* droplet vaporization for occlusion therapy and phase aberration correction,” *IEEE Transactions on Ultrasonics, Ferroelectrics, and Frequency Control*, vol. 49, no. 2, pp. 726–738, 2002.
- [27] O. D. Kripfgans, C. M. Orifici, P. L. Carson, K. A. Ives, O. P. Eldevik, and J. B. Fowlkes, “Acoustic droplet vaporization for temporal and spatial control of tissue occlusion: a kidney study,” *IEEE Transactions on Ultrasonics, Ferroelectrics, and Frequency Control*, vol. 52, pp. 1101–1110, July 2005.
- [28] M. Zhang, M. L. Fabiilli, K. J. Haworth, J. B. Fowlkes, O. D. Kripfgans, W. Roberts, K. A. Ives, and P. L. Carson, “Initial investigation of acoustic droplet vaporization for occlusion in canine kidney,” *Ultrasound in Medicine and Biology*, vol. 36, no. 10, pp. 1691–1703, 2010.
- [29] K. Arima, K. Yamakado, H. Kinbara, A. Nakatsuka, K. Takeda, and Y. Sugimura, “Percutaneous radiofrequency ablation with transarterial embolization is useful for treatment of stage 1 renal cell carcinoma with surgical risk: results at 2-year mean follow up,” *International Journal of Urology*, vol. 14, no. 7, pp. 585–590, 2007.
- [30] F. Wu, Z. Wang, W. Chen, J. Zou, J. Bai, H. Zhu, K. Li, C. Jin, F. Xie, and H. Su, “Advanced hepatocellular carcinoma: treatment with high-intensity focused ultrasound ablation combined with transcatheter arterial embolization,” *Radiology*, vol. 235, no. 2, pp. 659–667, 2005.

- [31] P. Charbonnet, J. Toman, L. Buhler, B. Vermeulen, P. Morel, C. Becker, and F. Terrier, "Treatment of gastrointestinal hemorrhage," *Abdominal Imaging*, vol. 30, no. 6, pp. 719–726, 2005.
- [32] A. Petroianu, "Arterial embolization for hemorrhage caused by hepatic arterial injury," *Digestive Diseases and Sciences*, vol. 52, no. 10, pp. 2478–2481, 2007.
- [33] G. Debrun, V. Aletich, J. Ausman, F. Charbel, and M. Dujovny, "Embolization of the nidus of brain arteriovenous malformations with n-butyl cyanoacrylate," *Neurosurgery*, vol. 40, no. 1, pp. 112–120, 1997.
- [34] W. Taki, Y. Yonekawa, H. Iwata, A. Uno, K. Yamashita, and H. Amemiya, "A new liquid material for embolization of arteriovenous-malformations," *American Journal of Neuroradiology*, vol. 11, no. 1, pp. 163–168, 1990.
- [35] K. Yamashita, W. Taki, H. Iwata, and H. Kikuchi, "A cationic polymer, Eudragit-E as a new liquid embolic material for arteriovenous malformations," *Neuroradiology*, vol. 38, no. Suppl 1, pp. S151–S156, 1996.
- [36] K. Krueger, M. Zaehring, D. Strohe, H. Struetzer, J. Boecker, and K. Lackner, "Postcatheterization pseudoaneurysm: results of US-guided percutaneous thrombin injection in 240 patients," *Radiology*, vol. 236, no. 3, pp. 1104–1110, 2005.
- [37] E. K. Paulson, D. H. Sheafor, M. A. Kliever, R. C. Nelson, L. B. Eisenberg, M. W. Sebastian, and M. H. Sketch, "Treatment of iatrogenic femoral arterial pseudoaneurysms: comparison of US-guided thrombin injection with compression repair," *Radiology*, vol. 215, no. 2, pp. 403–408, 2000.
- [38] C. Holtze, A. Rowat, J. Aggresti, J. Hutchinson, F. Angile, C. Schmitz, S. Koster, H. Duan, K. Humphry, R. Scanga, J. Johnson, D. Pisignano, and D. Weitz, "Biocompatible surfactants for water-in-fluorocarbon emulsions," *Lab on a Chip*, vol. 8, no. 10, pp. 1632–1639, 2008.
- [39] C. Tonelli, A. D. Meo, S. Fontana, and A. Russo, "Perfluoropolyether functional oligomers: unusual reactivity in organic chemistry," *Journal of Fluorine Chemistry*, vol. 118, no. 1-2, pp. 107–121, 2002.
- [40] S. Zhu, W. F. Edmonds, M. A. Hillmyer, and T. P. Lodge, "Synthesis and self-assembly of highly incompatible polybutadiene-poly(hexafluoropropylene oxide) diblock copolymers," *Journal of Polymer Science Part B - Polymer Physics*, vol. 43, no. 24, pp. 3685–3694, 2005.
- [41] A. Benichou and A. Aserin, "Recent developments in O/W/O multiple emulsions," in *Multiple emulsions: technology and applications* (A. Aserin, ed.), Hoboken, NJ: Wiley-Interscience, 2008.

- [42] M. L. Fabiilli, K. J. Haworth, N. H. Fakhri, O. D. Kripfgans, P. L. Carson, and J. B. Fowlkes, "The role of inertial cavitation in acoustic droplet vaporization," *IEEE Transactions on Ultrasonics, Ferroelectrics, and Frequency Control*, vol. 56, no. 5, pp. 1006–1017, 2009.
- [43] O. D. Kripfgans, M. L. Fabiilli, P. L. Carson, and J. B. Fowlkes, "On the acoustic vaporization of micrometer-sized droplets," *Journal of the Acoustical Society of America*, vol. 116, no. 1, pp. 272–281, 2004.
- [44] J. Gibson, S. Rees, T. McManus, and W. Scheitlin, "A citrate-phosphate-dextrose solution for the preservation of human blood," *American Journal of Clinical Pathology*, vol. 28, no. 6, pp. 569–578, 1957.
- [45] C. Edwards, S. Heptinstall, and K. Lowe, "Pluronic F-68 inhibits agonist-induced platelet aggregation in whole human blood in vitro," *Artificial cells, blood substitutes, and immobilization biotechnology*, vol. 26, no. 5, pp. 441–447, 1998.
- [46] S. M. Moghimi and A. C. Hunter, "Poloxamers and poloxamines in nanoparticle engineering and experimental medicine," *Trends in Biotechnology*, vol. 18, no. 10, pp. 412–420, 2000.
- [47] A. Florence and D. Whitehill, "The formulation and stability of multiple emulsions," *International Journal of Pharmaceutics*, vol. 11, no. 4, pp. 277–308, 1982.
- [48] S. Matsumoto, Y. Kita, and D. Yonezawa, "An attempt at preparing water-in-oil-in-water multiple-phase emulsions," *Journal of Colloid and Interface Science*, vol. 57, no. 2, pp. 353–361, 1976.
- [49] X. Zhang, X. Liu, D. Gu, W. Zhou, T. Xie, and Y. Mo, "Rheological models for xanthan gum," *Journal of Food Engineering*, vol. 27, no. 2, pp. 203–209, 1996.
- [50] S. D. Putney, "Encapsulation of proteins for improved delivery," *Current Opinion in Chemical Biology*, vol. 2, no. 4, pp. 548–552, 1998.
- [51] S. L. Borgne and M. Graber, "Amidase activity and thermal stability of human thrombin," *Applied Biochemistry and Biotechnology*, vol. 48, no. 2, pp. 125–135, 1994.
- [52] M. V. Papadopoulou, M. Ji, and W. D. Bloomer, "NLCQ-1, a novel hypoxic cytotoxin: potentiation of melphalan, cisDDP and cyclophosphamide *in vivo*," *International Journal of Radiation Oncology Biology Physics*, vol. 42, no. 4, pp. 775–779, 1998.
- [53] H. M. Courrier, T. F. Vandamme, and M. P. Krafft, "Reverse water-in-fluorocarbon emulsions and microemulsions obtained with a fluorinated surfactant," *Colloids and Surfaces A: Physicochemical and Engineering Aspects*, vol. 244, no. 1-3, pp. 141–148, 2004.

- [54] S. Jeon, J. Lee, J. Andrade, and P. de Gennes, "Protein-surface interactions in the presence of polyethylene oxide," *Journal of Colloid and Interface Science*, vol. 142, no. 1, pp. 149–158, 1991.
- [55] L. S. Roach, H. Song, and R. F. Ismagilov, "Controlling nonspecific protein adsorption in a plug-based microfluidic system by controlling interfacial chemistry using fluorinated-phase surfactants," *Analytical Chemistry*, vol. 77, no. 3, pp. 785–796, 2005.
- [56] J. Clausell-Tormos, D. Lieber, J.-C. Baret, A. El-Harrak, O. J. Miller, L. Frenz, J. Blouwolff, K. J. Humphry, S. Koster, H. Duan, C. Holtze, D. A. Weitz, A. D. Griffiths, and C. A. Merten, "Droplet-based microfluidic platforms for the encapsulation and screening of mammalian cells and multicellular organisms," *Chemistry and Biology*, vol. 15, no. 5, pp. 427–437, 2008.
- [57] M. Jumaa and B. W. Möller, "The effect of oil components and homogenization conditions on the physicochemical properties and stability of parenteral fat emulsions," *International Journal of Pharmaceutics*, vol. 163, no. 1, pp. 81–89, 1998.
- [58] R. L. Lundblad, R. A. Bradshaw, D. Gabriel, T. L. Ortel, J. Lawson, and K. G. Mann, "A review of the therapeutic uses of thrombin," *Thrombosis and Haemostasis*, vol. 91, no. 5, pp. 851–860, 2004.
- [59] J. Jesty, "The kinetics of inhibition of α -thrombin in human plasma," *The Journal of Biological Chemistry*, vol. 261, no. 22, pp. 10313–10318, 1986.
- [60] T. Chandy, G. S. Das, R. F. Wilson, and G. H. Rao, "Development of polylactide microspheres for protein encapsulation and delivery," *Journal of Applied Polymer Science*, vol. 86, no. 5, pp. 1285–1295, 2002.
- [61] O. Ziv, T. Lublin-Tennenbaum, and S. Margel, "Synthesis and characterization of thrombin conjugated γ -Fe₂O₃ magnetic nanoparticles for hemostasis," *Advanced Engineering Materials*, vol. 11, no. 12, pp. B251–B260, 2009.
- [62] O. Ziv-Polat, M. Topaz, T. Brosh, and S. Margel, "Enhancement of incisional wound healing by thrombin conjugated iron oxide nanoparticles," *Biomaterials*, vol. 31, no. 4, pp. 741–747, 2010.
- [63] C. Marchioni, E. Riccardi, S. Spinelli, F. dell'Unto, P. Grimaldi, A. Bedini, C. Giliberti, L. Giuliani, R. Palomba, and A. C. Castellano, "Structural changes induced in proteins by therapeutic ultrasounds," *Ultrasonics*, vol. 49, no. 6-7, pp. 569–576, 2009.
- [64] A. Oliva, A. Santovena, J. Farina, and M. Llabres, "Effect of high shear rate on stability of proteins: kinetic study," *Journal of Pharmaceutical and Biomedical Analysis*, vol. 33, no. 2, pp. 145–155, 2003.

- [65] J. Jiao and D. J. Burgess, "Multiple emulsion stability: pressure balance and interfacial film strength," in *Multiple emulsions: technology and applications* (A. Aserin, ed.), Hoboken, NJ: Wiley-Interscience, 2008.
- [66] A. S. Wolberg, "Thrombin generation and fibrin clot structure," *Blood Reviews*, vol. 21, no. 3, pp. 131–142, 2007.
- [67] M. Andrew, B. Paes, R. Milner, M. Johnston, L. Mitchell, D. M. Tollefsen, and P. Powers, "Development of the human coagulation system in the full-term infant," *Blood*, vol. 70, no. 1, pp. 165–172, 1987.
- [68] S. Higashi, N. Tabata, K.-H. Kono, Y. Maeda, M. Shimizu, T. Nakashima, and T. Setoguchi, "Size of lipid microdroplets effects results of hepatic arterial chemotherapy with an anticancer agent in water-in-oil-in-water emulsion to hepatocellular carcinoma," *The Journal of Pharmacology and Experimental Therapeutics*, vol. 289, no. 2, pp. 816–819, 1999.
- [69] M. Taghizadeh and T. Asadpour, "Effect of molecular weight on the ultrasonic degradation of poly(vinyl-pyrrolidone)," *Ultrasonics Sonochemistry*, vol. 16, no. 2, pp. 280–286, 2009.

CHAPTER V

Conclusions and Future Work

5.1 Introduction

The work presented in chapters II through IV contributes to the development of acoustic droplet vaporization (ADV) as a drug delivery mechanism. Compared to vascular occlusion, the most extensively studied therapeutic application of ADV [1–3], the use of ADV in drug delivery, which was initially proposed by Apfel [4], is relatively new. Previous studies dealing with ADV and drug delivery have focused on the formulation of drug-laden perfluorocarbon (PFC) emulsions [5–7]. However, only limited efforts were concentrated on bridging the knowledge gap between pharmaceutical and acoustical studies, especially interrelating the two fields. This dissertation begins to address some of the important connections between the two disciplines.

The two drug delivery applications highlighted in chapters III and IV display the potential of ADV to produce minimally invasive chemoembolization and sustained vascular occlusion, respectively. The use of PFC emulsions and ADV in drug delivery provides many therapeutic advantages and synergisms not afforded by the more widely studied microbubble delivery systems, thereby potentially increasing the realizability of targeted drug delivery using ADV. PFC emulsions possess a longer circulation half-life relative to microbubbles. Thus, the time available to perform an acoustically enabled, targeted intervention or procedure is longer. Furthermore,

systemic drug deposition due to colloidal dissolution is less of an issue with droplets than with microbubbles. Droplets can also be stably formulated with submicron diameters that can undergo extravasation within the leaky microvasculature of tumors [8; 9]. Localized ischemia caused by ADV-generated microbubbles can increase the residence time and potentially increase the absorption of drug within the targeted area. As will be discussed later, the delivery of prodrugs activated via hypoxia, itself generated by ADV, is another attractive option.

5.2 Experimental Conclusion

5.2.1 The Role of Inertial Cavitation in Acoustic Droplet Vaporization

Chapter II investigated the role of inertial cavitation (IC) in ADV via the measurement of the IC and ADV thresholds in an *in vitro* setup. A previous study demonstrated that IC nuclei (i.e. US contrast agent) can lower the ADV threshold [10]. Flowing droplets were exposed to pulsed ultrasound (US) from a focused, 3.5 MHz single element transducer. Simultaneously, broadband noise, characteristic of IC, was detected using a passive acoustic detector; ADV, detected as an increase in echogenicity, was simultaneously recorded using B-mode US. Bulk fluid, droplet, and acoustic parameters known to influence each threshold were explored.

In all tested cases, the ADV threshold occurred at a lower rarefactional pressure than the IC threshold, indicating that IC is not necessary to cause vaporization. The ADV thresholds were not statistically different when measured in gas saturated (170 mmHg O₂ or 106.5% O₂) and degassed (60 mmHg O₂ or 37.6% O₂) water, a finding that is consistent with previous results [1]. When measured in heparanized whole blood or water-glycerol mixtures, both thresholds increased relative to values obtained in water due to the increase in bulk fluid viscosity. Interestingly, whole blood and water-glycerol mixtures possess surface tensions that are lower than pure

water. Thus, the direct correlation between the IC threshold and viscosity, and not surface tension, suggests that the IC nuclei were not submicron in size [11] and likely the gas bubbles generated by ADV.

The mean droplet diameter and dispersed phase viscosity, for PFC-in-water (PFC/W) emulsions, were directly correlated across the homologous series of straight chain PFCs (C_5F_{12} , C_6F_{14} , C_8F_{18}). For negative degrees of superheat (i.e. the emulsion was not superheated), an inverse trend exists between both thresholds and the degree of superheat, which is defined as the difference between a given temperature and the boiling point of the PFC. The ADV and IC thresholds remained statistically constant for positive degrees of superheat. For droplets whose mean diameters were between 1 and 5 μm , the ADV threshold displayed an inverse correlation with mean diameter between 1 and 2.5 μm ; between 2.5 and 5.0 μm , the ADV threshold was relatively constant. Similarly, the IC threshold was constant across the entire range of mean droplet diameters (1 - 5 μm). There were no statistically significant differences in either threshold for droplets stabilized by bovine serum albumin (BSA) or lipids.

Concerning pulse repetition frequency (PRF), droplets exposed to a single US exposure displayed higher ADV and IC thresholds than droplets exposed to multiple exposures. Increasing the PRF for droplets already exposed to multiple exposures did not cause a change in either threshold. An inverse correlation existed between the IC threshold and the pulse length; the ADV threshold was constant for microsecond pulse lengths, which is consistent with previous results [10].

Overall, the results suggest that the nucleus for ADV is internal to a droplet and the IC nucleus is the bubble generated by ADV. The latter point is supported by an analytical model which estimates the minimum acoustic rarefactional pressures required to produce IC as a function of bubble size [11].

5.2.2 Delivery of Chlorambucil using an Acoustically-Triggered, Perfluoropentane Emulsion

In chapter III, *in vitro* studies were completed that demonstrated the ability of ADV to release an oil soluble drug encapsulated within an emulsion. The work focused on the delivery of a chemotherapy drug which, combined with the occlusive properties of ADV-generated microbubbles, could enable the development of non-invasive chemoembolization. A double emulsion (PFC-in-oil-in-water, PFC/O/W), suitable for intravenous administration, was formulated using soybean oil, perfluoropentane (PFP), and BSA as the shell. Chlorambucil (CHL), a lipophilic chemotherapy agent, was dissolved in the soybean oil. Optical studies indicated that the fraction of PFP per droplet increased as the droplet diameter increased. The ADV threshold of the dual phase droplets was higher, for a given mean diameter, compared to single phase droplets (i.e. PFP/W) studied in chapter II. However, when the mean diameter of the dual phase droplets was corrected for the oil layer, thereby enabling the estimation of the PFP core diameter, the ADV thresholds of the dual phase droplets were consistent with the thresholds obtained in chapter II.

A full factorial design of three parameters - droplets, CHL, and US - in two levels (with or without) - was completed in order to assess the cellular growth inhibition (GI) resulting from each combination. A 60-minute incubation with CHL-laden droplets (100 μ M) caused a 46.7% GI of Chinese hamster ovary (CHO) cells, compared to 83.3% GI obtained with cells exposed to the same concentration of CHL dissolved in dimethyl sulfoxide (DMSO). Thus, the cytotoxicity of CHL decreased upon its encapsulation and subsequent retention within the emulsion. Upon exposure to 6.3 MHz US, the CHL-laden droplets caused an 84.3% GI. Therefore, ADV significantly increased the GI and hence CHL exposure experienced by the cells. Comparatively, the ADV of sham droplets (i.e. without CHL) caused a 22.6% GI, which was likely due to the ADV process itself and the deplating of

cells by unvaporized droplets. All of these GI values reflect experiments where the droplets were not in direct contact with the cells during treatment. ADV of droplets in direct contact with CHO cells caused a 74.9% GI, a significant increase relative to the cases where the droplets were not in direct contact. This initial investigation into the cellular bioeffects of ADV revealed that the vaporization process could produce cell detachment or death *in vitro*, though the two phenomena were inseparable based on the methods used to calculate GI. The benefits of using an ADV-generated occlusion to increase the residence time of a chemotherapy agent within a tumor was seen by comparing the CHL concentration required to produce 50% GI for 15 minute (167 μM) and 60 minute (57 μM) exposures. Additionally, the mean CHO cell diameter was shown to correlate with CHL exposure.

The ADV efficiency (i.e. the fraction of droplets that vaporize) was shown to display a sigmoidal relationship as a function of droplet diameter, with a direct correlation occurring between 2 and 12 μm (see Fig. 3.9). This is consistent with the data obtained in chapter II (see Fig. 2.7) which displays an inverse relationship between ADV threshold and droplet diameter. Thus, it appears that droplets with a lower ADV threshold possess a higher ADV efficiency. Repeated US exposures were shown to increase the ADV efficiency for a given droplet diameter, though the incremental increase in efficiency was smaller as the number of exposures increased. This suggests that a constant fraction of remaining droplets vaporize per exposure.

5.2.3 Delivery of Water-Soluble Drugs using Acoustically-Triggered, Perfluorocarbon Double Emulsions

The utility of the ADV drug delivery formulation presented in chapter III was expanded in chapter IV to include the encapsulation of water-soluble compounds. A biocompatible, fluorophilic, triblock copolymer was synthesized which enabled the formation of water-in-PFC-in-water ($W_1/\text{PFC}/W_2$) double emulsions. The double emulsions in chapter IV, multiple water droplets surrounded by a globule of PFC,

were distinct in structure from the PFC/O/W emulsions in chapter III, a single PFC core surrounded by an oil layer. In the first series of studies, the retention of fluorescein in the W_1 phase was assessed using a Franz diffusion cell. The mass fluxes of fluorescein in PFP and perfluorohexane (PFH) emulsions, measured over 60 minutes, was 17% and 12%, respectively, relative to cases where the emulsions were exposed to 20 kHz US to generate ADV. Thus, the PFC layer within the double emulsion hindered the diffusion of fluorescein from the W_1 phase.

In the second series of experiments, thrombin - an enzyme involved in the coagulation of blood - was incorporated into the W_1 phase. The goal of this work was to study the potential of extending the duration of an ADV-generated embolization via the simultaneous generation of a clot within a targeted vessel. Different processing techniques were explored during the second emulsification step (i.e. emulsification of the primary emulsion to form the secondary emulsion) and thrombin release from the emulsions was assessed using the activated clotting time (ACT) assay. Thrombin inactivation was observed when the enzyme was subjected to sonication followed by shaking. Additionally, high concentrations of copolymer were noted to produce a substantial increase in the ACT, likely due to the interaction of the copolymer with platelets. Thrombin was stably retained in four out of five formulations tested. For three out of five formulations, the ACT of whole blood decreased in a statistically significant manner when incubated with thrombin-loaded emulsions exposed to 3.5 MHz US compared to emulsions not exposed to US. Thus, ADV was shown to increase the release of thrombin encapsulated within double emulsions. Furthermore, the formulations developed in chapter IV can be used in the development of PFC double emulsions containing other water-soluble compounds in diverse ADV applications.

5.3 Summary of Contributions

ADV can be used to trigger the release of lipophilic or hydrophilic drugs encapsulated within PFC double emulsions. The relationship between ADV and IC, a phenomenon which can affect the efficacy of ADV-triggered drug release, was also explored. Overall, the coupling of ADV-generated occlusion and ADV-triggered drug release may afford therapeutic advantages not available with other drug release and delivery mechanisms. The results from this dissertation are summarized below.

- ADV is a mechanism that is distinct from IC, with the ADV threshold occurring at a lower rarefactional pressure than the IC threshold for micron-sized droplets.
- *In vitro*, the ADV threshold is directly correlated with the viscosity of the fluid surrounding the droplets and inversely correlated with the degree of superheat (for negative degrees of superheat) and droplet diameter. The ADV threshold is independent of the gas saturation of the fluid surrounding the droplets, the shell stabilizing the droplets, degree of superheat (for positive degrees of superheat), PRF, and pulse width.
- The nucleus for ADV occurs within the droplet while the IC nucleus is likely the bubble generated by ADV.
- Stable, micron-sized double emulsions can be formulated with a PFC-in-oil-in-water or water-in-PFC-in-water structure.
- ADV can be used to significantly increase the release of oil or water-soluble compounds encapsulated within PFC double emulsions.
- ADV of droplets adjacent to adherent cells can cause cell detachment.
- The oil layer surrounding the PFC core in a PFC-in-oil-in-water emulsion does not significantly change the ADV threshold when compared to PFC

only droplets that possess the same diameter as the PFC core in the double emulsion.

- The ADV efficiency is directly correlated with droplet diameter.
- The copolymer synthesized to stabilize the primary emulsion of the water-in-PFC-in-water emulsion possesses anticoagulative properties.
- ADV can cause inactivation of macromolecules, such as thrombin, but not low molecular weight drugs such as chlorambucil.

5.4 Future Work

5.4.1 Optimization of PFC Loading in Emulsions

The emulsions studied in this dissertation are polydisperse in size, with coefficients of variance ranging from 50-100% for the droplet diameters. Upon intravascular administration, a droplet with a diameter larger than a capillary diameter can cause an embolization. For an intravenous injection of an emulsion, large droplets will get filtered by the pulmonary microvasculature upon entering the lungs. Figure 5.1 displays a normalized size distribution of capillary diameters in the human lung [12] and a probability function, based on the lung capillary distribution, that a particle of a given diameter will pass through the capillaries [13]. A particle with a diameter equal to the average capillary diameter ($6.5 \mu\text{m}$) has a lung passage probability equal to 0.5; correspondingly, particles whose diameters are smaller or larger than the average capillary diameter possess lung passage probabilities greater than or less than 0.5, respectively. Figure 5.1 also displays *in vivo* data from studies investigating the effect of particulate size on lung retention. The majority of these studies were conducted using non-degradable, non-deformable particles. Similar lung retention studies should be completed with PFC emulsions since the droplets are deformable and PFC excretion occurs in the lungs [14]. Lung retention studies, which are part of

a biodistribution study, can be accomplished via the imaging of radiolabeled droplets using positron emission tomography (PET). Initial PET studies were completed in rats by incorporating ^{18}F -fluorobenzoic acid hexadecyl ester into the BSA shell of PFP droplets [15]. Another option is the incorporation of the commonly used radiotracer ^{18}F -fluorodeoxyglucose (^{18}F -FDG) in the W_1 phase of a W_1 /PFC/ W_2 emulsion. Preliminary PET data obtained in rats, using the double emulsion, can be seen in Fig. 5.2.

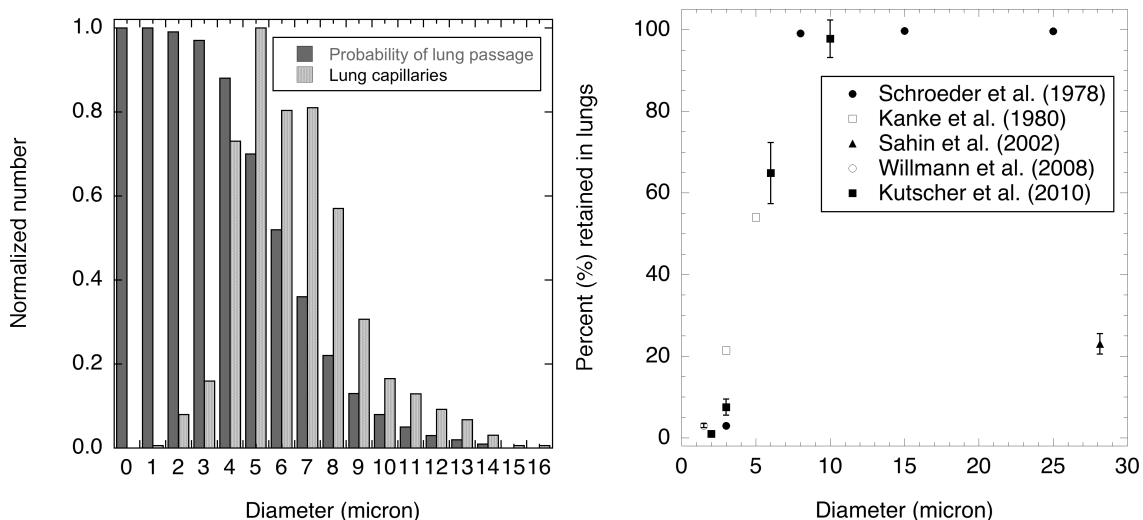


Figure 5.1: Left: Distribution of human lung capillaries [12] and the associated probability that a particle of a given diameter will pass through the capillaries [13]. Right: Percent of particles retained in the lungs, relative to the total number of particles injected, one-hour after intravenous administration of particles. Five different *in vivo* studies are shown: radiolabeled, polystyrene divinylbenzene microspheres in canines [16; 17]; radiolabeled, terbutaline sulfate loaded albumin microspheres in mice [18]; radiolabeled microbubbles in mice [19]; and fluorescent polystyrene microparticles in rats [20]. Since albumin microspheres can undergo biodegradation within the lungs due to the presence of proteolytic enzymes [18], the percent of albumin microspheres retained in the lungs is lower compared to non-degradable, non-deformable particles of similar sizes [16].

The number of pulmonary vessels occluded by large (i.e. not transpulmonary) droplets can be estimated using a representative distribution of BSA stabilized PFP droplets that were emulsified via shaking (Fig. 5.3). These droplets were used in chapter II and in recent *in vivo*, canine experiments [3], as well as in other works

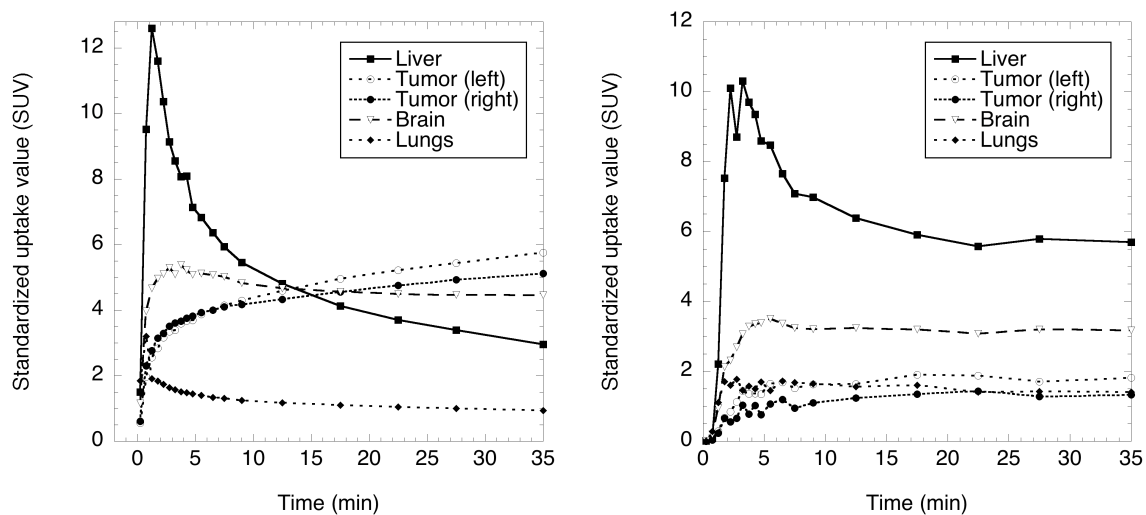


Figure 5.2: Time activity curves of standardized uptake values (SUV) for ^{18}F -FDG solution (left) and ^{18}F -FDG contained in the W_1 phase of a $W_1/\text{PFC}/W_2$ emulsion (right) post tail vein injection in Fischer 344 rats. PFP was used as the PFC phase. The rats were inoculated with 9L gliosarcoma tumors in the bilateral forearms. The sonicated emulsion displayed a similar size distribution as seen in Fig. 5.3. Greater uptake of ^{18}F -FDG occurs in both tumors and the brain with the ^{18}F -FDG solution, compared to the $W_1/\text{PFC}/W_2$ emulsion (see Table 5.2 for integrated SUV data) due to ^{18}F -FDG encapsulation within the droplets. Accumulation of droplets in the liver and minimal lung uptake are also evident.

[1; 2; 10; 21–24]. A single droplet dose administered in the aforementioned canine studies [3] was 10^8 - 10^9 droplets/kg, or approximately 3.0×10^9 - 10^{10} droplets/animal. Therefore, using the probability function in Fig. 5.1 and the droplet distribution in Fig. 5.3, as well as assuming a similar number and size distribution of pulmonary capillaries in a human (70 kg) and large dog (30 kg), 4% of the droplets will remain in the pulmonary capillaries after a single pass through the pulmonary circulation, which is equivalent to 1.2×10^8 - 10^9 droplets. As seen in Table 5.1, there are 2.8×10^{11} capillaries in the lung. Therefore, only 0.04-0.4% of lung capillaries are potentially occluded by a single droplet injection on first pass. Additionally, there are 3.0×10^6 - 10^7 droplets larger than $17 \mu\text{m}$, which as seen in Table 5.1, is the smallest diameter of a precapillary arteriole; comparatively, there are 3.0×10^8 precapillary arterioles present in the lungs (Table 5.1). Thus, the major impact of droplet occlusion in the lungs likely occurs at the precapillary arteriole levels since the number of droplets that could occlude at the capillary or distribution artery level is negligible relative to the number of respective vessels. Additionally, it becomes clearly evident that the vaporization of transpulmonary droplets on the venous side could cause additional pulmonary emboli due to the approximate five-fold increase in diameter when a droplet is converted into a gas bubble [22].

Table 5.1: Blood vessels in the adult human lung [25]. By comparison, the average number of alveoli in the adult human lung is 4.8×10^8 [26].

Type of vessel	Number of vessels	Diameter (μm)
Capillary	2.8×10^{11}	8-16
Precapillary arteriole	3.0×10^8	17-59
Distribution artery	4.0×10^6	60-100

Hence, the minimization of large (i.e. not transpulmonary) droplets is important to reduce the likelihood of pulmonary emboli and the pulmonary deposition of drugs contained in large diameter, PFC double emulsions. One method to decrease the fraction of large droplets is the use of sonication to create the PFC emulsion, as

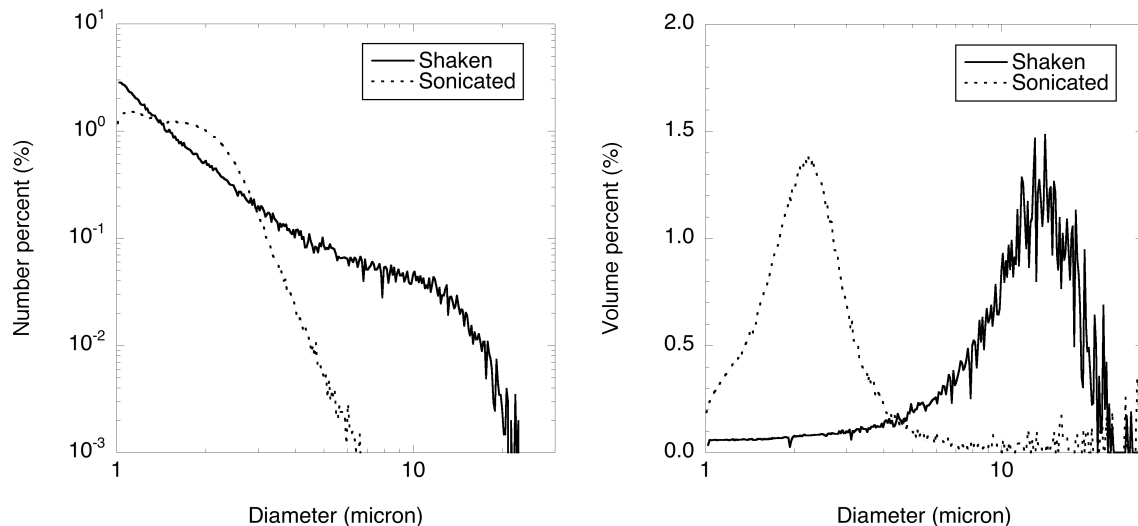


Figure 5.3: Number (left) and volume (right) weighted distributions of BSA stabilized PFP droplets. The emulsions are labeled according to the emulsification method used. The sonicated droplets possess a smaller mean diameter ($1.7 \mu\text{m}$ versus $2.0 \mu\text{m}$) and a lower fraction of droplets that are greater than $8 \mu\text{m}$ in diameter (0.01% versus 2.2% based on number or 4.5% versus 74.6% based on volume) compared to the shaken droplets.

seen in Fig. 5.3. Another method is to employ centrifugal separation. However, the minimization of small droplets, which are defined as droplets that are too small to undergo ADV (due to a negative degree of superheat) or droplets that produce gas bubbles that are too small to occlude a capillary, is also important for two reasons. First, as seen in chapters II and III, the ADV threshold and efficiency scale inversely and directly, respectively, with droplet diameter. Thus, small droplets are difficult to vaporize, requiring increased rarefactional pressures or cavitation-driven ADV at lower frequencies - both of which could cause vascular damage. If a small droplet does vaporize, then occlusion is only possible if the resulting bubble coalesces with other bubbles to form a larger bubble. Second, as will be discussed later, PFC droplets can cause systemic bioeffects, similar to other particulates. Therefore, the ideal PFC droplet distribution will be transpulmonary with minimal concentrations of small or large droplets (i.e. monodisperse). Additionally, depending on the desired effect (embolization versus drug release), the droplets should be large enough

that upon ADV, the resulting microbubbles can cause vascular embolization at the capillary level. It is currently unknown what droplet diameter satisfies these criteria, though insights can be obtained from the data in Fig. 5.1.

Monodispersed droplets can be produced using microfluidic channels fabricated from poly(dimethylsiloxane) (PDMS) [27], thereby optimizing the PFC loading for *in vivo* use. Figure 5.4 displays examples of these channels while Fig. 5.5 shows droplet distributions obtained from the microchannels. The use of monodisperse droplets should enable tighter control of the vaporization process since the ADV threshold and efficiency are dependent on the droplet diameter and potential minimization of the total number of droplets needed for a given application. Additionally, the placement of two T-junctions in series facilitates the production of double emulsions, thereby enabling control of both the internal and external droplet diameters [28]. One consideration is the production rate of droplets from microfluidic devices, which ranges from 10 Hz to 10 kHz [29]. For the previously mentioned canine experiment [3], it would take a single microchannel, operating at 10 kHz, 11.5 days to produce a single dose of 10^{10} droplets. Comparatively, the same number of polydisperse droplets is obtained via shaking or sonication in 45 s. Thus, it is clearly evident that the construction of microchannels in parallel should be completed in order to make this droplet production method more feasible.

5.4.2 PFC Emulsion Bioeffects

Closely related to the development of ideally sized PFC emulsions, the study of bioeffects associated with PFC emulsions used in ADV is also critically important. Most data on PFC bioeffects originate from two medical applications: liquid ventilation and blood substitutes [30]. The former application primarily utilizes neat (i.e. not emulsified) PFC whereas the latter uses emulsified PFC; thus, the focus of this discussion will be on the latter application.

Upon intravascular administration, PFC droplets undergo opsonization,

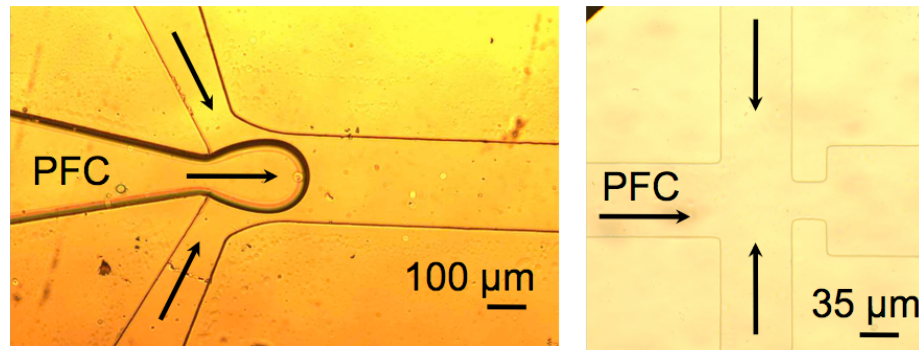


Figure 5.4: Micrographs of microfluidic channels, fabricated in PDMS using soft lithography, exhibiting two different flow focusing geometries. In each image, the PFC phase flows through the central channel while an aqueous solution of surfactant flows through two channels focused onto the PFC stream, thereby shearing droplets of PFC. Besides PDMS, which is hydrophobic, microchannels can be made using glass, which is hydrophilic, but can be made hydrophobic via siliconization or silanization [28].

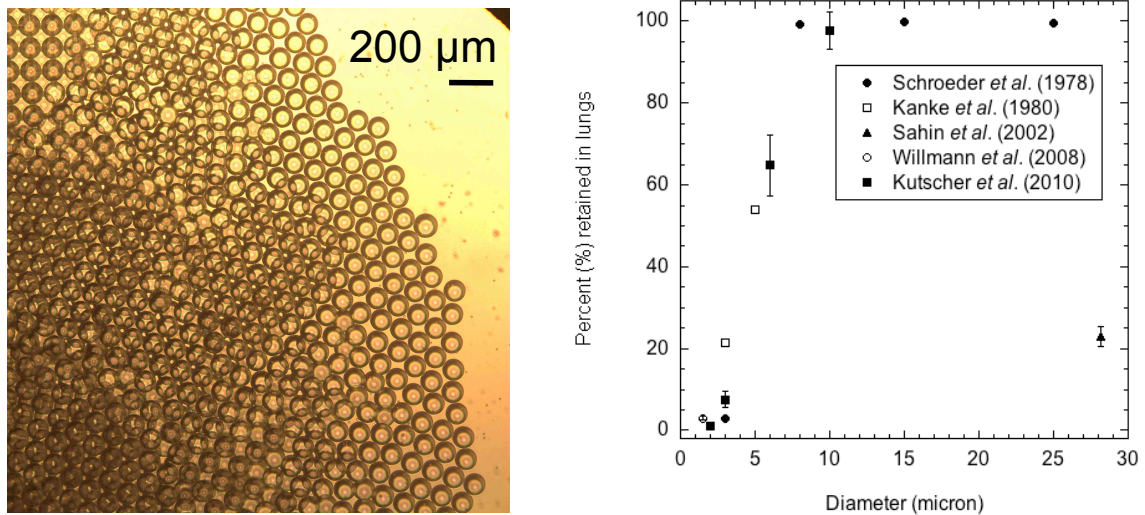


Figure 5.5: Left: Micrograph of monodispersed, BSA-stabilized PFH-in-water droplets obtained using the microchannel in Fig. 5.4 (left). Right: Number weighted distributions of BSA-stabilized PFH-in-water droplets produced using the microchannel geometry in Fig. 5.4 (right). The channel with a $20 \mu\text{m}$ orifice produced PFH droplets with a mean diameter of $13.2 \mu\text{m}$ and 5.8% coefficient of variance (CV) at a rate of 290 Hz. The channel with a $35 \mu\text{m}$ orifice produced PFH droplets with a mean diameter of $22.1 \mu\text{m}$ and 3.7% CV at a rate of 128 Hz. These distributions display the ability of microchannels to produce monodisperse droplets (i.e. low CV), though a smaller orifice is needed in order to produce droplets that are transpulmonary.

phagocytosis, and eventual removal from the blood via temporary storage in the reticuloendothelial system (RES). Figure 5.2 and Table 5.2 display the accumulation of PFP droplets in the liver post intravenous (IV) administration. Similar to other particulates, PFC emulsions can induce febrile-like reactions in certain species [31]. The severity of this response, which is due to the RES activation, is directly related to particle size [32]. Therefore, micron-sized PFC emulsion used for ADV applications could elucidate a stronger febrile response than the submicron PFC droplets used as blood substitutes. The febrile response associated with PFC emulsions administered for ADV therapies has currently not been investigated. Additionally, the minimization of particle size and narrowing of the particle size distribution can slow the RES uptake and experienced side effects [31; 33].

Table 5.2: Integrated standardized uptake value (SUV) data (0 - 35 minutes), from Fig. 5.2, for a solution of ^{18}F -FDG and ^{18}F -FDG encapsulated in the W_1 phase of a $W_1/\text{PFC}/W_2$ emulsion.

Tissue	Solution	Emulsion
Liver	169.1	217.8
Tumor (left)	164.0	56.9
Tumor (right)	153.5	41.2
Brain	160.9	109.6
Lungs	41.6	51.7

The stored PFCs - located primarily in the liver, spleen, and bone marrow - are transported via lipid carriers to the lungs for eventual excretion [14]. PFP (C_5F_{12} , 29°C boiling point), the most commonly used PFC in ADV applications, is excreted completely from the lungs within 2 hours after administration of a PFP contrast agent (i.e. microbubbles) in human subjects [34]. Compared to PFP (288 g/mol), PFCs used as blood substitutes possess molecular weights in the range of 460-520 g/mol [35]. As the molecular weight decreases, the vapor pressure tends to increase, which can cause pulmonary complications. Blood substitute studies using emulsified FX-80 ($\text{C}_8\text{F}_{16}\text{O}$, 3M Company), an azeotropic mixture of perfluorobutyltetrahydrofuran, highlight some PFC bioeffects. FX-80 has a vapor

pressure of 0.08 bar at 37°C, making it one of the most volatile PFCs studied as a blood substitute; comparatively, the vapor pressure of PFP is 1.4 bar at 37°C. Rats given IV injections of FX-80 emulsions displayed a rapid increase in respiration rate and bloated lungs [36; 37] as well as platelet agglutination [38]. Hyperinflated non-collapsible lungs (HNCL) was observed in some species, such as rabbits, with the severity of HNCL related to the vapor pressure of the administered PFC emulsion [39], though not all species are apparently susceptible to HNCL [40; 41]. The mechanism hypothesized to cause HNCL - pulmonary gas trapping (PGT) - is based on the formation of intra-alveolar microbubbles induced by the pulmonary elimination of PFC [42]. The PGT mechanism is supported by results from an *in vivo* study where rabbits were injected with neat perfluoroheptane (C₇F₁₆) [43]. The inhalation of PFC vapor, from the same chemical species as the PFC emulsion, has been found to reduce the effects of PGT *in vivo* [42].

The IV administration of PFP emulsions *in vivo* has been shown to eliminate cardiac arrhythmias, such as premature ventricular contractions, that were observed with intracardiac injections of droplets [3]. Figure 5.6 displays changes observed in the arterial blood gas concentrations (pO₂ and pCO₂), pH, and respiration rate in a canine that received multiple injections of PFP droplets. Similar trends were observed in canines after the IV injection of neat PFC liquid [44]. The incidence of HNCL in canines dosed with PFP emulsions has not been confirmed, though suspected in a recent study [3]. Thus, in order to mitigate lung effects and changes in blood chemistry associated with PFC emulsions, especially those containing PFCs with high vapor pressures, it is important to minimize the dose of PFC administered and especially the amount of PFC retained in the lungs. Therefore, the optimization of the PFC loading in the emulsion (discussed in the previous section) is closely linked to the minimization of systemic bioeffects associated with PFCs. Alternatively, the use of PFC in ventilation should be attempted in future *in vivo*

studies to determine if this can decrease the severity of PFC lung effects.

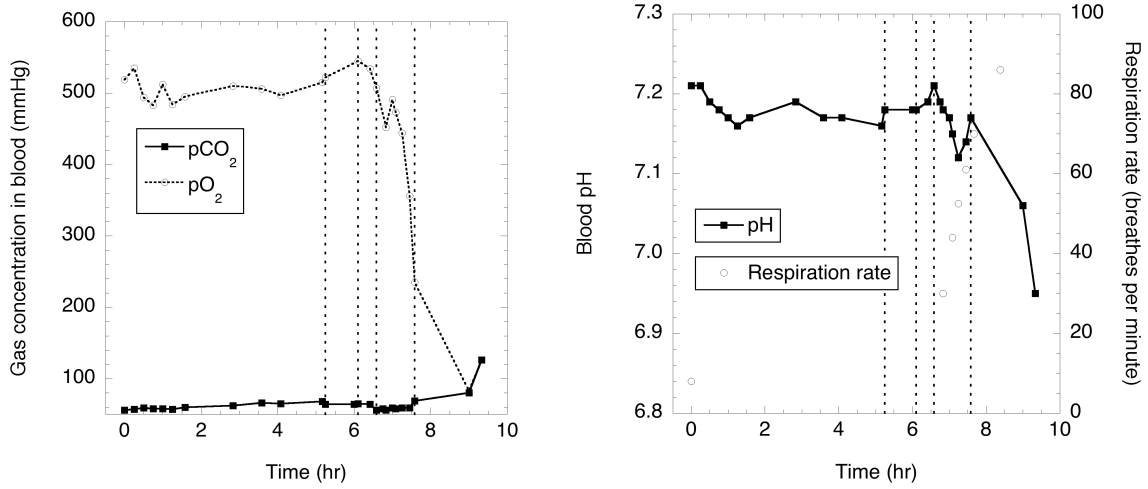


Figure 5.6: Arterial blood gas tensions (left) as well as arterial pH and respiration rate (right) in a canine (26 kg) before and after IV injections of lipid-stabilized, PFP droplets. Oxygen was used as the carrier of isoflurane, the inhaled anesthetic. A laparotomy was performed on the animal to expose the left kidney. Each injection, denoted by a vertical dotted line, contained 375 μL PFP and consisted of 2.4×10^{10} droplets (9.2×10^8 droplets/kg). ADV was performed in the renal artery subsequent to each injection. During the course of the experiment, the pO_2 and pH decreased and the pCO_2 and respiration rate increased in response to the injection of PFP droplets. Respiratory acidosis was suspected in this case. Based on the emulsion size distribution and the lung filtration function in Fig. 5.1 (left), 1% and 54% of the droplets by number and volume, respectively, are estimated to remain in the lung capillaries upon a single pass through the pulmonary circulation. This data is associated with a previously published study [3].

5.4.3 ADV Bioeffects

Unlike microbubble contrast agents and their interaction with US [45], the bioeffects related to the ADV process have not been studied extensively, especially the mechanisms of the ADV process which cause bioeffects. Bioeffects could be generated as a result of the various phases of the vaporization process: the droplet displacement prior to ADV at velocities up to 20 m/s [23], the rapid consumption of the liquid PFC during ADV, and the expansion of the resulting PFC bubble [46; 47]. Once the PFC bubble is created, it can undergo IC, a phenomenon that is known

to produce molecular or cellular damage due to the creation of fluid jets, extreme heating, and free radical generation upon bubble collapse. In chapter II, the IC threshold, measured at 3.5 MHz, increased over 1 MPa in whole blood, relative to the threshold in saline, due to the increase in solution viscosity. It is unclear whether these *in vitro* results will translate directly into the *in vivo* case. Overall, the types and magnitudes of bioeffects associated with ADV and ADV followed by IC should be investigated. Additionally, it was observed in chapter III that ADV of droplets resting on a layer of adherent cells can cause almost three-fold more cell detachment than ADV of droplets distal to the cell layer. In both cases, the viability of the detached cells, which could be determined using a dye exclusion (e.g. Trypan blue) or metabolic activity (e.g. MTT) assay, was not determined. Furthermore, it should be determined *in vivo* whether ADV of droplets adjacent to the endothelial lining of a blood vessel can cause endothelial cell detachment or alter vascular permeability via sonoporation.

Similar to results found with the cavitation of microbubble contrast agents, ADV can generate hemolysis [48], capillary ruptures, and petechial hemorrhages. Differences in vascular bioeffects may also occur depending on the location of ADV. For example, the generation of ADV in the feeder artery of an organ, as has been done in previous *in vivo* experiments [2; 3] could generate different effects than ADV within the capillary bed of an organ. Vasconstriction, which has been reported in US studies with [49; 50] and without microbubble contrast agents [51], has also been anecdotally observed in ADV studies. The level to which vasoconstriction contributes to the vascular embolization observed in *in vivo* studies is unknown. Vascular bioeffects associated with ADV could be potentially beneficial in certain therapeutic applications such as in blood-brain barrier disruption [52] or the sensitization of cancer cells to radiotherapy [53] - two applications where microbubble contrast agent disruption has shown to display synergistic properties.

As discussed previously, the vaporization of droplets on the venous side could cause a pulmonary embolism. Based on the PFP concentration in emulsions used for *in vivo* studies [1; 3; 23], 0.25 mL PFP per mL emulsion, the volume of PFP gas generated (assuming complete vaporization of the emulsion and the applicability of the ideal gas law) is 35 mL per mL of emulsion at 37°C. Deleterious respiratory effects have been observed *in vivo* when ADV occurs in large veins containing a substantial fraction of the return venous supply (ex. inferior vena cava), though the threshold (i.e. gas volume) at which this occurs is unknown. Thus, the use of a registered diagnostic US array and therapeutic US transducer enables the minimization of venous ADV via precise targeting.

5.4.4 The Mechanism of Drug Release during ADV

High speed microscopy has enabled the study of individual droplets (PFC/W) undergoing ADV [23; 46]. Similar studies focused on the ADV of PFC double emulsions should be undertaken in order to assess the effect of the secondary phase within the droplet. As seen in chapter III, the presence of an oil layer surrounding the PFC core in a PFC-in-oil-in-water (PFC/O/W) emulsion did not alter the ADV threshold significantly when correcting for the diameter of the PFC core. The ADV threshold was not measured for the W_1 /PFC/ W_2 emulsions studied in chapter IV. The presence of multiple W_1 droplets within the PFC globule, and thus many W_1 /PFC interfaces, may act as nucleation sites for ADV. It would be especially interesting to compare the ADV threshold of two, equally sized W_1 /PFC/ W_2 droplets - one containing multiple W_1 cores and the other containing a single W_1 core equal in volume to the multiple cores case. The latter droplet could be made using a microchannel system as previously described (see Fig. 5.4).

Presumably, upon ADV of a W_1 /PFC/ W_2 emulsion *in vivo*, the W_1 phase mixes with blood. However, the fate of the oil phase in a PFC/O/W or O/PFC/W emulsion after ADV is unknown. Clearly, the oil phase could be released and coalesce

into a single large droplet after ADV. However, due to the high concentration of albumin in serum (40-50 mg/mL) [54], it is possible that smaller oil droplets are dispersed by the ADV mechanism and subsequently stabilized by albumin. The fragmentation of microbubble contrast agents, containing an oil layer, has been studied using high-speed microscopy [55; 56]. These published works focus on microbubble collapse, a distinct mechanism from ADV, rather than the release of the oil phase. Thus, ADV studies that investigate the behavior of the oil phase after ADV, especially in solutions that contain concentrated surfactant (e.g. serum), should be completed. Similar studies could also determine the number and size of gas bubbles generated from the ADV of W_1 /PFC/ W_2 droplets. A balance exists between the ratio of the W_1 and PFC phases since sufficient PFC is needed to prevent the coalescence of the W_1 and W_2 phases. However, a large PFC to W_1 ratio reduces the payload capacity of each droplet. The size of the resulting PFC gas bubble produced from the ADV of a W_1 /PFC/ W_2 droplet is critical in determining whether this gas bubble is capable of occluding blood flow within a capillary.

Closely related to the study of the ADV mechanism is the impact of ADV on the stability of the subsequently released drug. In chapter III, ADV did not apparently cause molecular inactivation of CHL, a small molecular weight compound (304.2 g/mol), when released from a PFC/O/W emulsion. However, as seen in chapter IV, ADV did cause inactivation of thrombin (~ 36000 g/mol) when released from a W_1 /PFC/ W_2 emulsion. The structural changes induced in thrombin after ADV could be studied using infrared and circular dichroism spectroscopies [57]. The study could be expanded to include therapeutic molecules possessing a wide range of molecular weights, especially macromolecules like proteins, which are more sensitive to inactivation (i.e denaturation) using US. The monitoring of IC during the experiment, as was done in chapter II, would enable the determination of whether ADV alone, versus ADV followed by IC, can cause the same level or structural type

of inactivation. To minimize the molecular effects of cavitation, Tween 80, sucrose, and mannitol could be dissolved in the W_1 phase along with the protein-based therapeutic agent [58; 59]. Tween 80 can decrease the exposure of a solubilized protein to gas, which can induce denaturation. Sucrose can participate in hydrogen bonding, thereby preventing protein unfolding, and mannitol can scavenge any free radicals generated during cavitation.

5.4.5 Shell Modifications

As discussed previously, the intravascular administration of PFC emulsions can activate the RES and induce febrile conditions. The use of a pegylated surfactant, which contains polyethylene glycol (PEG) conjugated to the surfactant, can reduce these side-effects. PEG, a hydrophilic polymer, is non-toxic, safe, and has good biocompatibility [60]. The presence of PEG chains on the droplet surface can hinder blood protein absorption and uptake by the mononuclear phagocyte system, thereby creating stealth particles [61]. Thus, pegylated droplets would have a longer circulation time and greater stability against enzymatic attack and immunogenic recognition.

Active targeting of PFC emulsions can be achieved by conjugating a ligand, specific for a molecular target, to a surfactant or pegylated surfactant [62]. The spatial selectivity of ADV triggered drug release would be greatly enhanced by the ability to accumulate droplets on endothelial targets, such as vascular endothelial growth factor receptor (VEGFR), P-selectin, or intercellular adhesion molecule-1 (ICAM-1). Extravascular receptors could also be targeted by formulating targeted submicron droplets that, for example, could extravasate in the leaky vasculature of tumors due to the presence of large inter-endothelial gaps. Monoclonal antibodies have been widely used as targeting ligands in US contrast studies [19]; however, the species-dependence, immunogenicity, cost, adhesive kinetics, and size of monoclonal antibodies are potential drawbacks [63]. Thus, other types of ligands, such as

peptides, have been studied [64]. One common coupling chemistry used to conjugate a targeting ligand to the surface of a microbubble or droplet is (strept)avidin-biotin [63], with biotinylated lipids and biotinylation kits commercially available. Despite the flexibility and strength of this coupling, it is unlikely to be used in a clinical setting due to the immunogenicity of (strept)avidin [65; 66]. Alternatives to (strept)avidin-biotin coupling include the covalent attachment of a ligand via thioether or amide bonding.

5.4.6 Further Formulation Studies

The success of an ADV application such as drug delivery or embolotherapy relies fundamentally on the ability to vaporize PFC droplets with a high degree of efficiency and in a controlled manner. As shown in chapter II, the ADV threshold is inversely related to the degree of superheat for negative degrees of superheat. Additionally, the ADV efficiency was shown to scale directly with droplet diameter in chapter III. Therefore, the ability to modulate the vaporizability of a PFC emulsion is critically important. A few chemical approaches are now presented.

Figure 5.7 displays the vaporization temperature (T_b) of PFP droplets, as a function of droplet diameter (d), derived from combining the Laplace pressure and Antoine equations (Eq. 5.1) where σ is the interfacial tension; P_o is the pressure external to the droplet; and A , B , and C are the Antoine equation parameters for PFP. For example, at normal body temperature (37°C), a droplet with a diameter larger than 6.4 μm is superheated when the surface tension is 50 mN/m. Thus, for polydisperse droplet populations as those used in chapters II-IV, not all droplets are superheated, which is further supported by the ADV threshold and efficiency results from chapters II and III. One option is to increase the degree of superheat of the dispersed PFC phase, thereby lowering the diameter above which the droplets are superheated, by using a lower boiling point fluorocarbon such as perfluorobutane (PFB, C_4F_{10} , -1.7°C boiling point) or 1H-nonafluorobutane (H-PFB, C_4HF_9 , 14°C

boiling point). For example, PFB droplets with surface tensions of 30 mN/m and 50 mN/m are superheated at normal body temperature when the droplet diameters are larger than $0.43 \mu\text{m}$ and $0.72 \mu\text{m}$, respectively. Alternatively, mixtures of PFP, PFB, and H-PFB can be used to adjust the ADV threshold and efficiency [4; 67]. The second option is to use different surface active agents, which possess high critical micelle concentrations, that significantly lower the interfacial tension between PFP and the continuous aqueous phase. As seen in Fig. 5.7, cetyl trimethyl ammonium bromide (CTAB) lowers the interfacial tension of PFP to 10.4 mN/m [68], which lowers the diameter above which PFP droplets are superheated to $1.3 \mu\text{m}$. These strategies could be used in the development of submicron-sized PFC emulsions in order to minimize the amount of acoustic energy needed to vaporize these droplets.

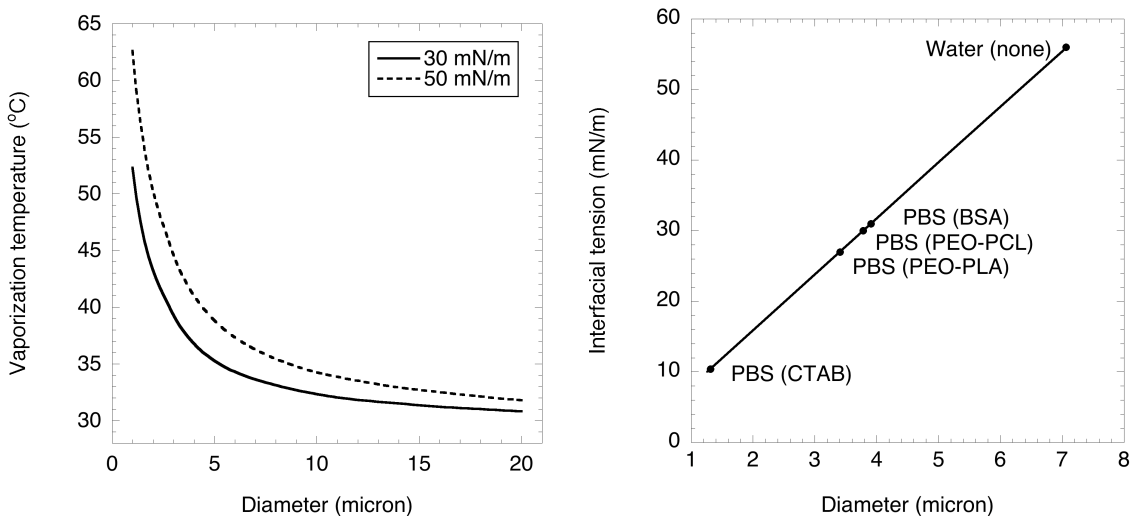


Figure 5.7: Left: The vaporization temperature of PFP droplets, as a function of droplet diameter, for two surface tension values, 30 mN/m and 50 mN/m [8]. Right: The surface tension required to stabilize PFP droplets at 37°C as a function of droplet diameter. At a given surface tension, droplets whose diameters lie to the right of the line are superheated. Individual data points represent interfacial tensions of PFP against water or phosphate buffered saline (PBS) [68]. The type of surfactant used is indicated in parentheses: BSA, polyethylene oxide-*co*-poly- ϵ -caprolactone (PEO-PCL), polyethylene oxide-*co*-polylactic acid (PEO-PLA), and cetyl trimethyl ammonium bromide (CTAB). The interfacial tension was measured at a surfactant concentration greater than critical micelle concentration for each surfactant type.

$$T_b = \frac{B}{A - \log_{10}\left(\frac{4\sigma}{d} + P_o\right)} - C \quad (5.1)$$

The stability of PFC double emulsions, with regards to decreasing the burst release and outward diffusion of encapsulated materials, can be potentially improved by using other shell materials. Figure 5.8 and Table 5.3 display *in vitro* data relating to formulation studies, complementary to the work in chapter III, exploring the effect of lipid versus BSA shells on the encapsulation of CHL in PFC-in-oil-in-water emulsions. Cholesterol was incorporated into the lipid shell, thereby increasing the shell rigidity, in an attempt to increase the stability of the emulsion, drug loading, and drug retention [69]. Polymeric shells, such as poly(lactic-co-glycol acid) (PLGA), have been used to generate PFC microcapsules and nanocapsules, via a modified solvent emulsion/evaporation method, with enhanced stability relative to other types of shells [70–72]. Currently, these capsules have been made using higher boiling point PFCs (>56°C), though not with PFP due to the use of methylene chloride (40°C boiling point) during the processing, which has a boiling point close to PFP (29°C).

Table 5.3: The composition and characterization of CHL loading in various PFP-in-oil-in-water emulsions. The mean (n = 3 vials) and standard deviation of each value is presented. The CHL loading was obtained using high performance liquid chromatography (see chapter III for method). The percent of CHL encapsulated within the emulsion dispersed phase (i.e. encapsulation %) was determined using ultrafiltration [73]. For the lipid stabilized emulsions, the CHL loading was substantially lower than the BSA-stabilized droplets. Micrographs of the lipid and BSA stabilized droplets confirmed a much thicker oil phase for the latter type of emulsion.

Emulsifier		Cholesterol (wt%)	Mean diameter (μm)	CHL		Encapsulation (%)
Type	mg/mL			mg/mL	pg/droplet	
BSA	4	0	3.06 \pm 0.21	3.12 \pm 0.01	7.68 \pm 0.75	97.7 \pm 2.3
Lipid	10	0	2.41 \pm 0.08	0.67 \pm 0.10	0.46 \pm 0.07	98.4 \pm 0.1
Lipid	10	10	2.36 \pm 0.07	0.85 \pm 0.09	0.61 \pm 0.06	98.7 \pm 0.2
Lipid	20	0	2.21 \pm 0.02	0.93 \pm 0.02	0.40 \pm 0.01	96.5 \pm 0.1
Lipid	20	10	2.27 \pm 0.11	0.92 \pm 0.01	0.41 \pm 0.01	98.1 \pm 0.5
Lipid	20	20	1.91 \pm 0.05	1.15 \pm 0.05	0.32 \pm 0.03	97.8 \pm 0.8
Lipid	20	50	1.96 \pm 0.16	1.40 \pm 0.04	0.27 \pm 0.02	97.0 \pm 0.2

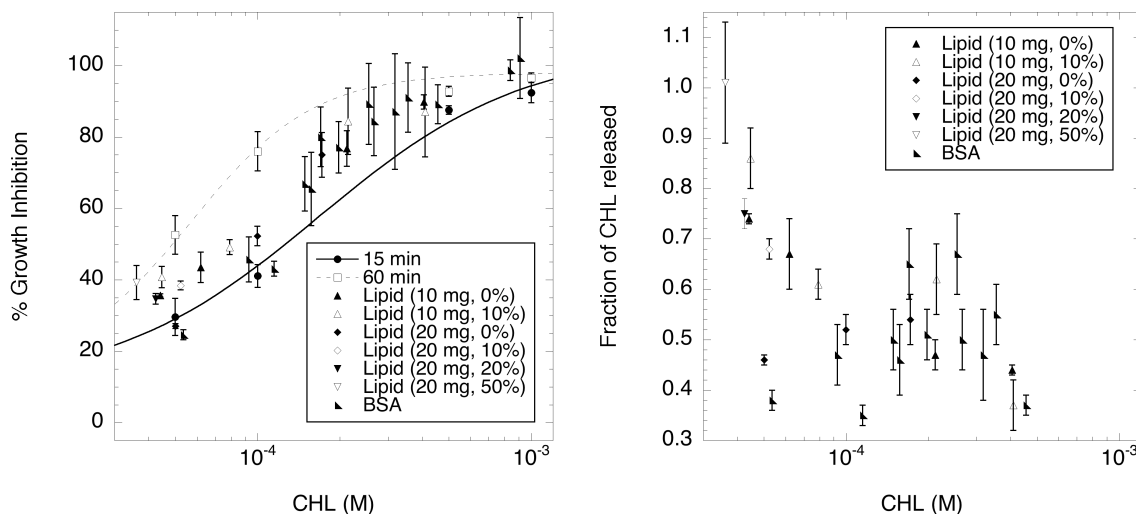


Figure 5.8: Left: The cytotoxicity of different CHL emulsion formulations (PFP-in-oil-in-water) on Chinese hamster ovary cells at various concentrations for 60 minute exposures. The data is overlaid onto the cytotoxicity results obtained from CHL in DMSO for 15 and 60 minute exposures (Fig. 3.6). Lipid droplets were prepared using a modified thin-film method using different ratios of L- α -phosphatidylcholine and cholesterol. The amount of total lipids per mL of emulsion, as well as the percent of lipids that is cholesterol, is indicated in the parentheses. BSA stabilized droplets, used in chapter III, are displayed as well. Right: The data from the left plot is expressed as the fraction of CHL released, based on estimating the amount of CHL released, from the %GI, using the CHL in DMSO data (Fig. 3.6). This drug release is due to CHL partitioning outward from the soybean oil. For both the left and right plots, each data point is the average of six wells from three independent experiments. Additionally, error bars are standard deviations of the means.

5.4.7 *In vivo* Demonstration

Currently, *in vivo* demonstrations of US-triggered drug release from PFC emulsions has been limited to a small animal model [8; 74]. Additionally, the aforementioned studies use submicron-sized droplets, where ADV is solely used to release the encapsulated drug from the emulsion. This dissertation proposes the use of ADV to simultaneously deliver an encapsulated drug and to generate vascular embolization. Some hypothesized synergisms of ADV-triggered drug delivery and embolization include: 1) greater drug absorption within targeted tissue due to the prolonged residence time caused by ischemia and 2) the activation of hypoxia-activated prodrugs (discussed later) due to extended ischemia. Additionally, ADV could increase the ability of a released agent to penetrate further into a solid tumor; typically, anticancer drugs only penetrate 3-5 cell diameters from a blood vessel [75; 76]. None of these synergisms have been tested *in vivo*. The ability to generate vascular occlusion has been demonstrated *in vivo* in both small [2] and large animal [3] models, though the relationship between the duration of the occlusion and other experimental parameters (injected droplet dose, acoustic exposure, etc.) is unclear. Prior publications have shown that longer duration embolizations can be achieved with emulsions administered intraarterially versus intravenously due to the lack of first pass lung filtration in the former route [2; 3].

Previous studies in rats have anecdotally demonstrated that ADV can be used to generate ischemia and hypoxia via PET imaging of $^{15}\text{O-H}_2\text{O}$ and ^{18}F -fluoroazomycin arabinoside (^{18}F -FAZA), respectively. These studies should be continued, in order to produce statistically significant results, using the previously mentioned radiotracers or using orthogonal measurement techniques for ischemia (e.g. Doppler US) and hypoxia (e.g. oxygen electrodes). The hypothesis that ADV-generated ischemia can increase drug absorption within targeted tissue can be tested by measuring the amount of drug present in an organ/tumor using conventional (e.g. high performance

liquid chromatography) or radiolabeled methods. The completion of additional PET studies, as seen in Fig. 5.2, would greatly enhance the understanding of the biodistribution and pharmacokinetics of PFC emulsions used for ADV.

5.4.8 Delivery of Prodrugs

Areas of hypoxia, which can be found in some tumors, rarely occur in normal tissue [77]. Unlike the chronic or diffusion-limited hypoxia occurring in tumors, acute or perfusion-limited hypoxia can occur via the temporary arrest of blood flow, as in the case of an ADV-generated embolization. Hypoxia can be used to activate prodrugs, such as the chemotherapeutic agents tirapazamine or NLCQ-1 [78], which are otherwise non-toxic in normoxic tissues. Both of the aforementioned drugs are substrates for intracellular one-electron reductases, which convert the prodrug into a free radical [79]. The free radical is either cytotoxic itself or can undergo further metabolism to become cytotoxic. In normoxic tissue, the free radical reacts rapidly with oxygen to regenerate the initial prodrug. In hypoxic tissue, the free radical accumulates.

The release of a hypoxia-triggered prodrug, encapsulated within a PFC emulsion, via ADV is an elegant example of the potential synergisms of ADV-triggered drug release and embolization. ADV can be used to increase the level or homogeneity of hypoxia within a tumor, or to generate hypoxia within another organ for the activation of another type of prodrug. The simultaneous release of a chemical embolic agent, as was demonstrated in chapter IV, could be used to extend the duration of the embolization, possibly resulting in a greater level of hypoxia. Clearly, the ability of an ADV-generated embolization to generate sufficient levels of acute hypoxia to activate a hypoxia-triggered prodrug needs to be tested and demonstrated *in vivo*. Ultimately, the clinical realizability of the proposed therapy relies on elucidating the relationship between emulsion properties (e.g. droplet diameter, concentration, etc.), therapeutic acoustic parameters (e.g. frequency, pulse repetition rate, etc.), and *in*

vivo properties (e.g. blood vessel flow rate, vascular geometry, etc.) to the eventual *in vivo* performance (e.g. ischemia, hypoxia, drug delivery, etc.).

5.5 Acknowledgments

The authors would like to thank Drs. Morand Piert and Phillip Sherman (Department of Nuclear Medicine, University of Michigan, Ann Arbor, MI) for assistance with the PET experiments and David Li (Department of Biomedical Engineering, University of Michigan, Ann Arbor, MI) for the design and fabrication of the microfluidic channels. This work was supported in part by NIH grant 5R01EB000281.

REFERENCES

- [1] O. D. Kripfgans, J. B. Fowlkes, M. Woydt, O. P. Eldevik, and P. L. Carson, “*In vivo* droplet vaporization for occlusion therapy and phase aberration correction,” *IEEE Transactions on Ultrasonics, Ferroelectrics, and Frequency Control*, vol. 49, no. 2, pp. 726–738, 2002.
- [2] O. D. Kripfgans, C. M. Orifici, P. L. Carson, K. A. Ives, O. P. Eldevik, and J. B. Fowlkes, “Acoustic droplet vaporization for temporal and spatial control of tissue occlusion: a kidney study,” *IEEE Transactions on Ultrasonics, Ferroelectrics, and Frequency Control*, vol. 52, pp. 1101–1110, July 2005.
- [3] M. Zhang, M. L. Fabiilli, K. J. Haworth, J. B. Fowlkes, O. D. Kripfgans, W. Roberts, K. A. Ives, and P. L. Carson, “Initial investigation of acoustic droplet vaporization for occlusion in canine kidney,” *Ultrasound in Medicine and Biology*, vol. 36, no. 10, pp. 1691–1703, 2010.
- [4] R. E. Apfel, “Activatable infusible dispersions containing drops of a superheated liquid for methods of therapy and diagnosis,” Patent 5,840,276, Apfel Enterprises, Inc., November 1998.
- [5] J. Y. Fang, C. F. Hung, M. H. Liao, and C. C. Chien, “A study of the formulation design of acoustically active lipospheres as carriers for drug delivery,” *European Journal of Pharmaceutics and Biopharmaceutics*, vol. 67, no. 1, pp. 67–75, 2007.
- [6] J. Y. Fang, C. F. Hung, S. C. Hua, and T. L. Hwang, “Acoustically active perfluorocarbon nanoemulsions as drug delivery carriers for camptothecin: drug release and cytotoxicity against cancer cells,” *Ultrasonics*, vol. 49, no. 1, pp. 39–46, 2009.
- [7] T. L. Hwang, Y. J. Lin, C. H. Chi, T. H. Huang, and J. Y. Fang, “Development and evaluation of perfluorocarbon nanobubbles for apomorphine delivery,” *Journal of Pharmaceutical Sciences*, vol. 98, no. 10, pp. 3735–3747, 2009.
- [8] N. Y. Rapoport, A. M. Kennedy, J. E. Shea, C. L. Scaife, and K.-H. Nam, “Controlled and targeted tumor chemotherapy by ultrasound-activated nanoemulsions/microbubbles,” *Journal of Controlled Release*, vol. 138, no. 2, pp. 268–276, 2009.

- [9] N. Rapoport, A. M. Kennedy, J. E. Shea, C. L. Scaife, and K.-H. Nam, "Ultrasonic nanotherapy of pancreatic cancer: lessons from ultrasound imaging," *Molecular Pharmaceutics*, vol. 7, no. 1, pp. 22–31, 2010.
- [10] A. H. Lo, O. D. Kripfgans, P. L. Carson, E. D. Rothman, and J. B. Fowlkes, "Acoustic droplet vaporization: effects of pulse duration and contrast agent," *IEEE Transactions on Ultrasonics, Ferroelectrics, and Frequency Control*, vol. 54, pp. 933–946, May 2007.
- [11] C. K. Holland and R. E. Apfel, "An improved theory for the prediction of microcavitation thresholds," *IEEE Transactions on Ultrasonics, Ferroelectrics, and Frequency Control*, vol. 36, pp. 204–208, March 1989.
- [12] J. C. Hogg, "Neutrophil kinetics and lung injury," *Physiological Reviews*, vol. 67, pp. 1249–1295, October 1987.
- [13] N. de Jong, F. J. ten Cate, W. B. Vletter, and J. R. T. C. Roelandt, "Quantification of transpulmonary echocontrast effects," *Ultrasound in Medicine and Biology*, vol. 19, no. 4, pp. 279–288, 1993.
- [14] J. G. Riess, "Oxygen carriers ("blood substitutes") - raison d'être, chemistry, and some physiology," *Chemical Reviews*, vol. 101, no. 9, pp. 2797–2919, 2001.
- [15] X. Shao, A. Lo, and J. B. Fowlkes, "¹⁸F-labeled droplets and biodistribution," *Society of Nuclear Medicine Annual Meeting*, 2007.
- [16] H. Schroeder, G. H. Simmons, and P. P. DeLuca, "Distribution of radiolabeled subdivisible microspheres after intravenous administration in beagle dogs," *Journal of Pharmaceutical Sciences*, vol. 67, no. 4, pp. 504–507, 1978.
- [17] M. Kanke, G. H. Simmons, D. L. Weiss, B. A. Bivins, and P. P. DeLuca, "Clearance of ¹⁴¹Ce-labeled microspheres from blood and distribution in specific organs following intravenous and intraarterial administration in beagle dogs," *Journal of Pharmaceutical Sciences*, vol. 69, no. 7, pp. 755–762, 1980.
- [18] S. Sahin, H. Selek, G. Ponchel, M. T. Ercan, M. Sargon, A. A. Hincal, and H. S. Kas, "Preparation, characterization and *in vivo* distribution of terbutaline sulfate loaded albumin microspheres," *Journal of Controlled Release*, vol. 82, no. 2-3, pp. 345–358, 2002.
- [19] J. K. Willmann, Z. Cheng, C. Davis, A. M. Lutz, M. K. Schipper, C. H. Nielsen, and S. S. Gambhir, "Targeted microbubbles for imaging tumor angiogenesis: assessment of whole-body biodistribution with dynamic micro-PET in mice," *Radiology*, vol. 249, no. 1, pp. 212–219, 2008.
- [20] H. L. Kutscher, P. Chao, M. Deshmukh, Y. Singh, P. Hu, L. B. Joseph, D. C. Reimer, S. Stein, D. L. Laskin, and P. J. Sinko, "Threshold size for optimal passive pulmonary targeting and retention of rigid microparticles in rats," *Journal of Controlled Release*, vol. 143, no. 1, pp. 31–37, 2010.

- [21] K. J. Haworth, J. B. Fowlkes, P. L. Carson, and O. D. Kripfgans, “Towards aberration correction of transcranial ultrasound using acoustic droplet vaporization,” *Ultrasound in Medicine and Biology*, vol. 34, pp. 435–445, March 2008.
- [22] O. D. Kripfgans, J. B. Fowlkes, D. L. Miller, O. P. Eldevik, and P. L. Carson, “Acoustic droplet vaporization for therapeutic and diagnostic applications,” *Ultrasound in Medicine and Biology*, vol. 26, no. 7, pp. 1177–1189, 2000.
- [23] O. D. Kripfgans, M. L. Fabiilli, P. L. Carson, and J. B. Fowlkes, “On the acoustic vaporization of micrometer-sized droplets,” *Journal of the Acoustical Society of America*, vol. 116, no. 1, pp. 272–281, 2004.
- [24] A. H. Lo, O. D. Kripfgans, P. L. Carson, and J. B. Fowlkes, “Spatial control of gas bubbles and their effects on acoustic fields,” *Ultrasound in Medicine and Biology*, vol. 32, no. 1, pp. 95–106, 2006.
- [25] M. A. Davis, “Particulate radiopharmaceuticals for pulmonary studies,” in *Radiopharmaceuticals* (G. Subramanian, ed.), pp. 267–281, New York: Society of Nuclear Medicine, 1975.
- [26] M. Ochs, J. R. Nyengaard, A. Jung, L. Knudsen, M. Voigt, T. Wahlers, J. Richter, and H. J. G. Gundersen, “The number of alveoli in the human lung,” *American Journal of Respiratory and Critical Care Medicine*, vol. 169, no. 1, pp. 120–124, 2004.
- [27] S. L. Anna, N. Bontoux, and H. A. Stone, “Formation of dispersions using “flow focusing” in microchannels,” *Applied Physics Letters*, vol. 82, no. 3, pp. 364–366, 2003.
- [28] T. Nisisako, S. Okushima, and T. Torii, “Controlled formulation of monodisperse double emulsions in a multiple-phase microfluidic system,” *Soft Matter*, vol. 1, no. 1, pp. 23–27, 2005.
- [29] S. Y. Teh, R. Lin, L.-H. Hung, and A. P. Lee, “Droplet microfluidics,” *Lab on a Chip*, vol. 8, no. 2, pp. 198–220, 2008.
- [30] M. P. Krafft, A. Chittofrati, and J. G. Riess, “Emulsions and microemulsions with a fluorocarbon phase,” *Current Opinion in Colloid and Interface Science*, vol. 8, no. 3, pp. 251–258, 2003.
- [31] S. Flaim, D. Hazard, J. Hogan, and R. Peters, “Characterization and mechanism of side-effects of Oxygent HT (highly concentrated fluorocarbon emulsion) in swine,” *Artificial Cells, Blood Substitutes, and Immobilization Biotechnology*, vol. 22, no. 4, pp. 1511–1515, 1994.
- [32] P. Keipert, S. Otto, S. Flaim, J. Weers, E. Schutt, T. Pelura, D. Klein, and T. Yaksh, “Influence of perflubron emulsion particle size on blood half-life and febrile response in rats,” *Artificial Cells, Blood Substitutes, and Immobilization Biotechnology*, vol. 22, no. 4, pp. 1169–1174, 1994.

- [33] J. Senior, J. C. Crawley, and G. Gregoriadis, "Tissue distribution of liposomes exhibiting long half-lives in the circulation after intravenous injection," *Biochimica et Biophysica Acta*, vol. 839, no. 1, pp. 1–8, 1985.
- [34] J.-M. Correas, A. R. Mueter, E. Singlas, D. R. Kessler, D. Worah, and S. C. Quay, "Human pharmacokinetics of a perfluorocarbon ultrasound contrast agent evaluated with gas chromatography," *Ultrasound in Medicine and Biology*, vol. 27, no. 4, pp. 565–570, 2001.
- [35] J. G. Riess, "Reassessment of criteria for the selection of perfluorochemicals for 2nd generation blood substitutes - analysis of structure property relationships," *Artificial Organs*, vol. 8, no. 1, pp. 44–56, 1984.
- [36] R. P. Geyer, "Whole animal perfusion with fluorocarbon dispersions," *Federation Proceedings*, vol. 29, no. 5, pp. 1758–1763, 1970.
- [37] H. A. Sloviter and T. Kamimoto, "Erythrocyte substitute for perfusion of brain," *Nature*, vol. 216, no. 5114, pp. 458–460, 1967.
- [38] H. A. Sloviter, H. Yamada, and S. Ogoshi, "Some effects of intravenously administered dispersed fluorochemicals in animals," *Federation Proceedings*, vol. 29, no. 5, pp. 1755–1757, 1970.
- [39] L. C. Clark, R. E. Hoffmann, and S. L. Davis, "Response of the rabbit lung as a criterion of safety for fluorocarbon breathing and blood substitutes," *Biomaterials, Artificial Cells, and Immobilization Biotechnology*, vol. 20, no. 2-4, pp. 1085–1099, 1992.
- [40] S. F. Flaim, "Pharmacokinetics and side effects of perfluorocarbon-based blood substitutes," *Artificial Cells, Blood Substitutes, and Immobilization Biotechnology*, vol. 22, no. 4, pp. 1043–1054, 1994.
- [41] T. Leakakos, E. Schutt, J. Calvin, D. Smith, J. Bradley, C. Strnat, U. del Balzo, D. Hazard, S. Otto, T. Fields, P. Keipert, D. Klein, and S. Flaim, "Pulmonary gas trapping differences among animal species in response to intravenous infusion of perfluorocarbon emulsions," *Artificial Cells, Blood Substitutes, and Immobilization Biotechnology*, vol. 22, no. 4, pp. 1199–1204, 1994.
- [42] E. Schutt, P. Barber, T. Fields, S. Flaim, J. Horodniak, P. Keipert, R. Kinner, L. Kornburst, T. Leakakos, T. Pelura, J. Weers, R. Houmes, and B. Lachmann, "Proposed mechanism of pulmonary gas trapping (PGT) following intravenous perfluorocarbon emulsion administration," *Artificial Cells, Blood Substitutes, and Immobilization Biotechnology*, vol. 22, no. 4, pp. 1205–1214, 1994.
- [43] B. Canaud, P. Aljama, C. Tielemans, V. Gasparovic, A. Gutierrez, and F. Locatelli, "Pathochemical toxicity of perfluorocarbon-5070, a liquid test performance fluid previously used in dialyzer manufacturing, confirmed in animal experiment," *Journal of the American Society of Nephrology*, vol. 16, no. 6, pp. 1819–1823, 2005.

- [44] D. J. Sass, R. A. V. Dyke, E. H. Wood, S. A. Johnson, and P. Didisheim, "Gas embolism due to intravenous FC 80 liquid fluorocarbon," *Journal of Applied Physiology*, vol. 40, no. 5, pp. 745–751, 1976.
- [45] D. L. Miller, M. A. Averkiou, A. A. Brayman, E. C. Everbach, C. K. Holland, J. H. Wible, and J. Wu, "Bioeffects considerations for diagnostic ultrasound contrast agents," *Journal of Ultrasound in Medicine*, vol. 27, no. 4, pp. 611–632, 2008.
- [46] K. J. Haworth and O. D. Kripfgans, "Initial growth and coalescence of acoustically vaporized perfluorocarbon microdroplets," *IEEE International Ultrasonics Symposium Proceedings*, pp. 623–626, 2008.
- [47] A. Qamar, Z. Z. Wong, J. B. Fowlkes, and J. L. Bull, "Dynamics of acoustic droplet vaporization in gas embolotherapy," *Applied Physics Letters*, vol. 96, no. 14, 2010.
- [48] D. L. Miller, O. D. Kripfgans, J. B. Fowlkes, and P. L. Carson, "Cavitation nucleation agents for nonthermal ultrasound therapy," *Journal of the Acoustical Society of America*, vol. 107, no. 6, pp. 3480–3486, 2000.
- [49] H. Chen, A. A. Brayman, and T. J. Matula, "Microbubble dynamics in microvessels: Observations of microvessel dilation, invagination and rupture," *IEEE Ultrasonics Symposium*, vol. 1-4, pp. 1163–1166, 2008.
- [50] T. Hirokawa, R. Karshafian, C. J. Pavlin, and P. N. Burns, "Insonation of the eye in the presence of microbubbles - preliminary study of the duration and degree of vascular bioeffects - work in progress," *Journal of Ultrasound in Medicine*, vol. 26, no. 6, pp. 731–738, 2007.
- [51] K. Hynynen, A. H. Chung, V. Colucci, and F. A. Jolesz, "Potential adverse effects of high-intensity focused ultrasound exposure on blood vessels *in vivo*," *Ultrasound in Medicine and Biology*, vol. 22, no. 2, pp. 193–201, 1996.
- [52] N. Vykhodtseva, N. McDannold, and K. Hynynen, "Progress and problems in the application of focused ultrasound for blood-brain barrier disruption," *Ultrasonics*, vol. 48, no. 4, pp. 279–296, 2008.
- [53] R. Karshafian, A. Giles, P. N. Burns, and G. J. Czarnota, "Ultrasound-activated microbubbles as novel enhancers of radiotherapy in leukemia cells *in vitro*," *IEEE Ultrasonics Symposium*, vol. 1-4, pp. 1792–1794, 2009.
- [54] A. T. Høstmark, S. E. Tomten, and J. E. Berg, "Serum albumin and blood pressure: a population-based, cross-sectional study," *Journal of Hypertension*, vol. 23, no. 4, pp. 725–730, 2005.
- [55] K. Kooiman, M. R. Bohmer, M. Emmer, H. J. Vos, C. Chlon, W. T. Shi, C. S. Hall, S. H. de Winter, K. Schroen, M. Versluis, N. de Jong, and A. van Wamel, "Oil-filled polymeric microcapsules for ultrasound-mediated delivery of

- lipophilic drugs,” *Journal of Controlled Release*, vol. 133, no. 2, pp. 109–118, 2009.
- [56] D. J. May, J. S. Allen, and K. W. Ferrara, “Dynamics and fragmentation of thick-shelled microbubbles,” *IEEE Transactions on Ultrasonics, Ferroelectrics, and Frequency Control*, vol. 49, no. 10, pp. 1400–1410, 2002.
- [57] C. Marchioni, E. Riccardi, S. Spinelli, F. dell’Unto, P. Grimaldi, A. Bedini, C. Giliberti, L. Giuliani, R. Palomba, and A. C. Castellano, “Structural changes induced in proteins by therapeutic ultrasounds,” *Ultrasonics*, vol. 49, no. 6-7, pp. 569–576, 2009.
- [58] S. D. Putney, “Encapsulation of proteins for improved delivery,” *Current Opinion in Chemical Biology*, vol. 2, no. 4, pp. 548–552, 1998.
- [59] Z. M. Tian, M. X. Wan, S. P. Wang, and J. Q. Kang, “Effects of ultrasound and additives on the function and structure of trypsin,” *Ultrasonics Sonochemistry*, vol. 11, no. 6, pp. 399–404, 2004.
- [60] J. M. Harris and R. B. Chess, “Effect of pegylation on pharmaceuticals,” *Nature Reviews Drug Discovery*, vol. 2, no. 3, pp. 214–221, 2003.
- [61] D. E. Owens and N. A. Peppas, “Opsonization, biodistribution, and pharmacokinetics of polymeric nanoparticles,” *International Journal of Pharmaceutics*, vol. 307, no. 1, pp. 93–102, 2006.
- [62] S. H. Bloch, P. A. Dayton, and K. W. Ferrara, “Targeted imaging using ultrasound contrast agents,” *IEEE Engineering in Medicine and Biology Magazine*, vol. 23, no. 5, pp. 18–29, 2004.
- [63] P. A. Dayton and J. J. Rychak, “Molecular ultrasound imaging using microbubble contrast agents,” *Frontiers in Bioscience*, vol. 12, pp. 5124–5142, 2007.
- [64] R. Pillai, E. Marinelli, H. Fan, P. Nanjappan, B. Song, M. von Wronski, S. Cherkaoui, I. Tardy, S. Pochon, M. Schneider, A. Nunn, and R. Swenson, “A phospholipid-PEG2000 conjugate of a vascular endothelial growth factor receptor 2 (VEGFR2)-targeting heterodimer peptide for contrast-enhanced ultrasound imaging of angiogenesis,” *Bioconjugate Chemistry*, vol. 21, no. 3, pp. 556–562, 2010.
- [65] P. Caliceti, M. Chinol, M. Roldo, F. M. Veronese, A. Semezato, S. Salmaso, and G. Paganelli, “Poly(ethylene glycol)-avidin bioconjugates: suitable candidates for tumor pretargeting,” *Journal of Controlled Release*, vol. 83, no. 1, pp. 97–108, 2002.
- [66] A. L. Klibanov, “Microbubble contrast agents - targeted ultrasound imaging and ultrasound-assisted drug-delivery applications,” *Investigative Radiology*, vol. 41, no. 3, pp. 354–362, 2006.

- [67] K.-I. Kawabata, N. Sugita, H. Yoshikawa, T. Azuma, and S.-I. Umemura, “Nanoparticles with multiple perfluorocarbons for controllable ultrasonically induced phase shifting,” *Japanese Journal of Applied Physics*, vol. 44, no. 6B, pp. 4548–4552, 2005.
- [68] M. A. Kandadai, P. Mohan, G. Lin, A. Butterfield, M. Skliar, and J. J. Magda, “Comparison of surfactants used to prepare aqueous perfluoropentane emulsions for pharmaceutical applications,” *Langmuir*, vol. 26, no. 7, pp. 4655–4660, 2010.
- [69] R. Patlolla and V. Vobalaboina, “Pharmacokinetics and tissue distribution of etoposide delivered in parenteral emulsion,” *Journal of Pharmaceutical Sciences*, vol. 94, no. 2, pp. 437–445, 2005.
- [70] J. Bauer, M. Zähres, A. Zeller mann, M. Kirsch, F. Petrat, H. de Groot, and C. Mayer, “Perfluorocarbon-filled poly(lactide-co-glycolide) nano- and microcapsules as artificial oxygen carriers for blood substitutes: a physico-chemical assessment,” *Journal of Microencapsulation*, vol. 27, no. 2, pp. 122–132, 2010.
- [71] J. Huang, J. S. Xu, and R. X. Xu, “Heat-sensitive microbubbles for intraoperative assessment of cancer ablation margins,” *Biomaterials*, vol. 31, no. 6, pp. 1278–1286, 2010.
- [72] E. Pisani, N. Tsapis, J. Paris, V. Nicolas, L. Cattel, and E. Fattal, “Polymeric nano/microcapsules of liquid perfluorocarbons for ultrasonic imaging: physical characterization,” *Langmuir*, vol. 22, no. 9, pp. 4397–4402, 2006.
- [73] S. Ganta, J. W. Paxton, B. C. Baguley, and S. Garg, “Pharmacokinetics and pharmacodynamics of chlorambucil delivered in parenteral emulsion,” *International Journal of Pharmaceutics*, vol. 360, pp. 115–121, 2008.
- [74] N. Rapoport, Z. Gao, and A. Kennedy, “Multifunctional nanoparticles for combining ultrasonic tumor imaging and targeted chemotherapy,” *Journal of the National Cancer Institute*, vol. 99, no. 14, pp. 1095–1106, 2007.
- [75] T. W. Hambley, “Is anticancer drug development heading in the right direction?,” *Cancer Research*, vol. 69, no. 4, pp. 1259–1262, 2009.
- [76] A. I. Minchinton and I. F. Tannock, “Drug penetration in solid tumors,” *Nature Reviews Cancer*, vol. 6, no. 8, pp. 583–592, 2006.
- [77] B. Movsas, J. D. Chapman, A. L. Hanlon, E. M. Horwitz, R. E. Greenberg, C. Stobbe, G. E. Hanks, and A. Pollack, “Hypoxic prostate/muscle pO₂ ratio predicts for biochemical failure in patients with prostate cancer: preliminary findings,” *Urology*, vol. 60, no. 4, pp. 634–639, 2002.
- [78] S. McKeown, R. Cowen, and K. Williams, “Bioreductive drugs: from concept to clinic,” *Clinical Oncology*, vol. 19, no. 1, pp. 427–442, 2007.

- [79] J. M. Brown and W. R. Wilson, “Exploiting tumour hypoxia in cancer treatment,” *Nature Reviews Cancer*, vol. 4, pp. 437–447, 2004.